Developing a non-invasive approach for the treatment of pathological tremor



Beatriz Silveira de Arruda

A thesis submitted for the degree of

Doctor of Philosophy

Nuffield Department of Clinical Neurosciences

MRC Brain Network Dynamics Unit

Oxford University & Green Templeton College

January 2024

i) Declaration

I, Beatriz Silveira de Arruda, confirm that the work presented in this thesis is my own. Where information has been derived from other sources, I confirm that this has been indicated in the thesis.

Signed:……Beatriz Silveira de Arruda……..

Date:……12 January 2024……..

ii) Acknowledgements

First and foremost, I extend my heartfelt thanks to my academic guides at Oxford. To Peter Brown, who mentored me in my initial year, laying the foundation for my journey; Hayriye Cagnan, whose supervision from my second year onwards was instrumental, and whose ideas and previous work formed the basis of this thesis; Tim Denison, for his generous provision of resources and a supportive lab environment; and Huiling Tan, whose continuous kindness and management of my funding were greatly appreciated.

My deep gratitude goes to Hayriye and Tim for their frequent, enlightening discussions, collective wisdom and support that helped me navigate through a DPhil journey filled with unexpected challenges over the past three years. Their shared commitment to making neurotechnology accessible to a broader demographic inspired me and strongly resonated with my own motivations for pursuing my studies at Oxford.

I am especially grateful to Mo Benjaber, a role model engineer and compassionate mentor. His guidance was pivotal in the successful completion of the engineering aspects of my project. My gratitude extends to everyone in the laboratories of my supervisors, particularly John Fleming, Mayela Zamora, Alek Pogosyan, Diogo Soriano, Tim West, Ali Kavoosi, and Raveen Kariyawasam for their invaluable help and insights at various stages of my journey.

I must also express my profound gratitude to the seventeen people with Parkinson's disease who participated in our studies, entrusting us with their time and experiences.

Beyond the DPhil, I encountered mentors who not only offered professional opportunities but also shared the joy of music with me. My sincere thanks to Ana Domingos, for her inspirational guidance, teaching opportunities, and invaluable

insights into academia and beyond. Equally, to Vitor Lopes dos Santos, whose support was crucial in charting my path post-Oxford.

In Oxford, I was fortunate to form wonderful communities that became a home. To my salsa band, particularly Femi, Joe, and Meli, to my capoeira group, led by my dear *mestre* Sereno, as well as to my friends Adam, Sylvia, and everyone else who contributed to my time in Oxford being truly enjoyable—thank you for being there through many seasons.

I am grateful to the mentors and friends I met at Brown University and in the Nicolelis laboratories. There, I discovered my passion for neuroengineering and received the foundational knowledge and experiences that paved my way to Oxford.

My gratitude also extends back to friends in my homeland, Brazil. To Aline, for her continuous support, clever sociological discussions, and online companionship through the most challenging points of the DPhil journey, to Laurinha, for so many years of unwavering friendship, cheerfulness, and support, and to Vera, for illuminating my path with her guidance.

Finally, to my family: my dear sister, Júlia Louise, and aunt, Sandra, for their love and support through my journey. To my father, Nilton, whose caring presence transcended my physical distance over the past years. And to my mother, Mônica, my role model as an inspiring and compassionate teacher, who instilled in me a curiosity about the world and, through much sacrifice, ensured a strong educational foundation—everything you went through made it possible for me to be where I am today.

iii) Abstract

Tremor is the most common movement disorder and a prevalent symptom in neurological conditions such as Parkinson's disease (PD). Given the limitations of medication, which often carries significant side effects and may not effectively treat tremor, and the limited availability of surgical treatments such as deep brain stimulation, there is a pressing clinical need for non-invasive therapeutic alternatives. This thesis investigates the potential of phase-locked peripheral electrical stimulation, delivered non-invasively to a nerve in the wrist, in modulating Parkinsonian rest tremor. Our initial investigations involved individuals with PD using a large, non-portable pilot system. The findings highlighted the high variability of tremor, characterised by distinct oscillation patterns within individuals. We discovered significant instantaneous changes in tremor severity, particularly when these distinct tremor modes were considered. Depending on the participant-specific stimulation phases, tremor could be significantly suppressed or amplified. Additionally, the variability in tremor patterns presented challenges in accurate phase tracking due to shifts in the axis of maximum tremor excursion and changes in tremor centre frequency. In response to these challenges, we developed a portable and adaptable version of the system, designed to account for these dynamic changes in tremor characteristics. The in-house built device, along with its on-board adaptable phase tracker, underwent rigorous bench testing for verification. Subsequently, the system was validated in a clinical setting with individuals with PD. Although the device's performance was validated and it proved to be a robust research tool, the tremor suppression achieved, while significant, was modest. This thesis demonstrates the potential of non-invasive phase-locked peripheral electrical stimulation in tremor management, particularly in PD. It underscores the need for adaptable and patient-specific treatment strategies and paves the way for future research in non-invasive tremor suppression techniques.

iv) Contents

i) Declaration ..... **ii**

ii) Acknowledgements ..... **iii**

iii) Abstract ..... **v**

iv) Contents ..... **vi**

v) List of figures ..... **xi**

vi) List of tables ..... **xiv**

vii) Abbreviations ..... **xvi**

viii) Publications ..... **xvii**

1. General introduction **1**

1.1. Pathological tremor disorders **1**

1.2. Conventional tremor treatments **3**

1.2.1. Pharmacological approaches 4

1.2.2. Surgical approaches 5

1.3. Non-invasive tremor treatments **7**

1.3.1. Vibratory stimulation 7

1.3.2. Functional electrical stimulation 8

1.3.3. Sub-motor threshold electrical stimulation 9

1.4. Phasic stimulation and brain rhythms modulation **10**

1.5. Wrist nerve circuitry and connectivity **11**

1.6. Thesis objectives **13**

2. Identifying and modulating distinct tremor states through peripheral nerve stimulation in Parkinsonian rest tremor **15**

2.1. Background **16**

2.2. Materials and methods ... **18**
2.2.1. Cohort ... 18
2.2.2. Data acquisition ... 20
2.2.3. Without stimulation condition ... 23
2.2.4. Peripheral nerve stimulation ... 23
2.2.5. Data processing and analysis ... 24
2.2.6. Tremor oscillation patterns ... 26
2.2.7. Phase-amplitude profiles ... 29
2.2.8. Re-aligned phase-amplitude profiles ... 30
2.3. Results ... **31**
2.3.1. Tremor oscillation patterns ... 31
2.3.2. Differences between Tremor Oscillation Patterns ... 34
2.3.3. Phase-specific response to peripheral stimulation ... 34
2.3.4. Angle of stimulation ... 38
2.4. Discussion ... **42**
2.4.1. Multiple tremor oscillators ... 42
2.4.2. Contextual factors shape tremor dynamics ... 43
2.4.3. Phase-dependent modulation of tremor ... 45
2.4.4. Limitations of the current study ... 46
2.4.5. Challenges and future directions ... 47
2.5. Conclusions ... **48**
3. Design of an adaptable, phase-tracking peripheral device ... **49**
3.1. Background and system requirements ... **49**
3.1.1. Design requirements ... 50
3.1.2. Phase estimation methods ... 56
Zero Crossings ... 56
Hilbert transform ... 58
State-space models ... 60
3.2. Physical design ... **63**
3.2.1. Hardware ... 63
3.2.2. Enclosure ... 66

3.3. Software design 68
3.3.1. Overview 68
3.3.2. Phase estimation algorithm 69
3.3.3. Adaptive strategy accounting for tremor's variability 73
3.3.4. Pre-processing 77
3.3.5. Calculation of change in tremor severity 78
3.3.6. Triggering stimulation 80
3.3.7. Data saving 83
3.3.8. User interface 84
3.4. Verification procedure 84
3.4.1. Offline, MATLAB-based algorithm characterisation 84
3.4.2. Vibration plate tests 86
3.4.3. Experimenter wearing the device 90
3.5. Verification results 92
3.5.1. Offline, MATLAB-based algorithm characterisation 92
3.5.2. Vibration plate tests 96
On-board and reference accelerometers comparisons 96
On-board and offline, MATLAB-based phase-tracker performance comparisons 98
3.5.3. Experimenter wearing the device 103
3.6. Discussion 110
3.6.1. Summary system characteristics against design requirements 110
3.6.2. Phase tracker verification 111
3.6.3. Adaptive strategy 112
3.6.4. Limitations of the current system 114
3.6.5. Future directions 116
3.7. Conclusion 116
4. Validation of an in-house built wrist-worn system for phase-locked peripheral nerve stimulation in people with Parkinson's disease 118
4.1. Introduction 118
4.2. Materials and methods 120
4.2.1. Cohort 120
4.2.2. Data acquisition equipment 121

4.2.3. Testing protocol 122
4.2.3. Data processing and analysis 124
4.2.4. Phase estimation algorithm's performance 125
4.2.5. Adaptation to changes in the tremor dominant axis and centre frequency 126
4.2.6. Random search stimulation state-amplitude response profiles 127
Bonferroni-corrected confidence limits 128
4.2.7. Continuous stimulation effects 129
4.3. Results 130
4.3.1. Phase estimation algorithm performance 130
4.3.2. Adaptation to changes in the tremor dominant axis and centre frequency 135
4.3.3. Random search stimulation state-amplitude response profiles 138
4.3.4. Exploring an example of significant change in tremor 142
4.3.5. Continuous stimulation at the most suppressive state 144
4.3.6. Participant feedback 148
4.4. Discussion 148
4.4.1. Phase estimation algorithm validation 149
4.4.2. Adaptive strategy assessment 150
4.4.3. Changes in tremor severity upon phasic and non-phasic stimulation 151
4.4.4. Limitations and challenges of this study 152
4.4.5. Future directions 154
4.5. Conclusion 154
5. General discussion 156

5.1. Summarised outcomes 156
5.2. Tremor modulation by peripheral nerve stimulation 157
5.3. Limitations 160
5.3.1. Peripheral nerve electrical stimulation 160
5.3.2. Study design and execution 162
5.3.3. Wrist-worn system design 165
5.4. Avenues for future research 167
5.4.1. Potential explorations with the current system 167
5.4.2. Considerations for at-home use 168

5.5. Concluding remarks **169**
6. References **171**

Appendix **1**

A.1. Pilot study's supplementary information **1**
A.1.1. Supplementary methods 1
Tremor oscillation patterns 1
Tremor oscillation patterns and phase-amplitude profiles 1
A.1.2. Supplementary results 2
A.2. Wrist worn system's envelope characterisation **6**
A.3. Wrist-worn system's user interface **7**

v) List of figures

Figure 1.1. A representation of the ulnar, median, and radial nerves in the wrist and hand, along with their corresponding dermatomes 12

Figure 2.1: A representation of one study participant's posture and the placement of the triaxial accelerometer, peripheral stimulation device, and EMG surface electrodes on the upper limb 23

Figure 2.2: Data collection and analysis pipeline 26

Figure 2.3: An example of how cluster representation in serial 5-second periods changes over time in the signals without stimulation 34

Figure 2.4: Example phase-amplitude profiles for one study participant 37

Figure 2.5: Fisher-corrected correlation between and within clusters 38

Figure 2.6: Rose plots indicating the number of phase bins for which there was significant tremor suppression or significant tremor amplification at each of the 12 equally spaced stimulation phases 39

Figure 2.7: Probabilities of changes in tremor severity at each phase bin for real versus surrogate data 41

Figure 3.1: Zero crossings of a signal and its differentiation 58

Figure 3.2: Example signals and their respective Hilbert-derived phase estimates 60

Figure 3.3: Block diagram showing hardware components of the wrist-worn system 66

Figure 3.4: The circular-shaped printed circuit board 67

Figure 3.5: The wrist-worn system's 3D enclosure design 68

Figure 3.6: The rotating analytic signal in a two-dimensional space 71

Figure 3.7: Phase tracking algorithm core operations 74

Figure 3.8: Self-tuning strategy to select the dominant signal axis and centre frequency best corresponding to those of the tremor 77

Figure 3.9: Dominant axis selection in example signals 78

Figure 3.10: Block diagram of the data pre-processing stream 79

Figure 3.11: Block diagram representing the operations to calculate the tremor envelope and subsequent change in tremor severity for each stimulation state presentation 81

Figure 3.12: Example sinewave and its estimated phase sampled at the wrist-worn device's accelerometer sampling rate 83

Figure 3.13: The experimenter wearing the fully assembled system on their wrist and the three axes orientation considered during the test and analysis 92

Figure 3.14: Example algorithm performance for band- and high-pass filtered oscillations centred at 5 Hz against the phases derived from the Hilbert transform 94

Figure 3.15: Example start-up phase error observed in a pure 5 Hz sinusoidal wave, as well as in band- and high-pass filtered signals 95

Figure 3.16: Mean and standard deviation of the absolute value of the difference between input and estimated signals 96

Figure 3.17: Example correlation versus lag plots for all three axes of both sensors 98

Figure 3.18: On-board and offline moving averaged-based selection of the dominant axis for tests with a vibration plate 100

Figure 3.19: On-board and offline error signal-based selection of the centre frequency for tests with a vibration plate 102

Figure 3.20: Phase error time courses for during the random search condition for tests with a vibration plate 103

Figure 3.21: Exact (in blue) and target (in red) stimulation phases during the random search condition, covering six target phases presented in random order, for tests with a vibration plate 104

Figure 3.22: On-board and offline moving averaged-based selection of the dominant axis for tests with an experimenter wearing the device 105

Figure 3.23: On-board and offline error signal-based selection of the centre frequency for tests with an experimenter wearing the device 107

Figure 3.24: Phase error time courses for each study participant during the random search condition for tests with an experimenter wearing the device 108

Figure 3.25: Exact (in blue) and target (in red) stimulation phases during the random search condition, covering six target phases presented in random order, for tests with an experimenter wearing the device 109

Figure 4.1: Experimental protocol recording stages 125

Figure 4.2: Exact (in blue) and target (in red) stimulation phases during the random search condition for all study participants, covering six target phases presented in random order 133

Figure 4.3: Phase error time courses for each study participant during the random search condition 134

Figure 4.4: Example 10-second segments obtained during the random search condition 135

Figure 4.5: Dominant axis selection as performed by the wrist-worn system (online) and in MATLAB (offline) during the random search condition for all study participants 137

Figure 4.6: Centre frequency selection as performed by the wrist-worn system (online) and in MATLAB (offline) during the random search condition 138

Figure 4.7: Scatter plots illustrating the change in tremor severity at each trial 140

Figure 4.8: Stimulation state-amplitude profiles showing the median change in tremor severity per state 142

Figure 4.9: Tremor envelope time courses obtained during the random search for P3 144

Figure 4.10: Tremor envelope during the continuous stimulation setting for the most frequently tracked dominant axis of each study participant 148

Figure A.1: On-board envelope comparison A-7

vi) List of tables

Table 2.1: Individual study participant information and their summary 21

Table 2.2: Summary of number of instances with significant changes in tremor severity 38

Table 2.3: Statistical comparison between real and surrogate probabilities of change in tremor 42

Table 3.1: User needs informing the design of the wrist-worn system 55

Table 3.2: Risk mitigations for the wrist-worn system investigational use on people with Parkinson's disease 56

Table 3.3: Acceptable phase error margin within which stimulation was triggered for each target centre frequency considered 84

Table 3.4: Error defined the phases calculated using the Hilbert transform and the MATLAB-based phase estimation algorithm 93

Table 3.5: Correlation between each of the three axes recorded with the on-board accelerometer and the reference device 98

Table 3.6: Signal-to-noise ratio for each axis of both the on-board and reference sensors 99

Table 3.7: Mean and standard deviation of the instantaneous frequency and phase error at each recording segment considered for tests with a vibration plate 101

Table 3.8: Mean and standard deviation of the instantaneous frequency and phase error at each recording segment considered for tests with an experimenter wearing the device 108

Table 3.9: Accelerometer signals and phase error summary at distinct tremor amplitudes 110

Table 3.10: A comparison of the minimum quantitative requirements against the performance achieved by the phase tracking algorithm and wrist-worn device 112

Table 4.1: Individual study participants' characteristics 122

Table 4.2: Phase errors for each study participant during random search and continuous stimulation conditions 132

Table 4.3: Number of stimulation trials presented with each axis tracked as dominant for each study participant 141

Table 4.4: Summary envelope metrics during distinct continuous stimulation segments 146

Table 4.5: The percentage of segments during the continuous stimulation condition that remained below the baseline envelope's median amplitude for both the final 1-minute of stimulation and the entire 10 minutes of stimulation 147

Table 4.6: Participant responses on the 5-point Likert scale questionnaire 149

Table 5.1: Summary of key thesis objectives and experimental chapters' results 158

Table A.1: Phase bins (in degrees) in which significant tremor suppression occurred for each phase-amplitude profile A-3

Table A.2: Phase bins (in degrees) in which significant tremor amplification occurred for each phase-amplitude profile A-5

vii) Abbreviations

ABS: acrylic butadiene styrene

AD: analogue-to-digital

CLI: command line interface

DBS: deep brain stimulation

EMG: electromyography

ET: essential tremor

FES: functional electrical stimulation

FDR: false discovery rate

GPi: globus pallidus pars interna

LED: light emitting diode

PCA: principal component analysis

PCB: printed circuit board

PD: Parkinson's disease

PPI: patient and public involvement

RGB: red-green-blue

SNc: substantia nigra pars compacta

SNR: signal-to-noise ratio

STN: subthalamic nucleus

TENS: transcutaneous electrical nerve stimulation

TOP: tremor oscillation pattern

TTL: transistor-transistor logic

viii) Publications

Publication incorporated into this thesis:

Arruda, B. S., Reis, C., Sermon, J. J., Pogosyan, A., Brown, P., & Cagnan, H. (2021). Identifying and modulating distinct tremor states through peripheral nerve stimulation in Parkinsonian rest tremor. Journal of NeuroEngineering and Rehabilitation, 18(179). doi: 10.1186/s12984-021-00973-6

Other publication during the DPhil:

Reis, C., Arruda, B. S., Pogosyan, A., Brown, P., & Cagnan, H. (2021). Essential tremor amplitude modulation by median nerve stimulation. Scientific Reports, 11(1), 1–10. doi: 10.1038/s41598-021-96660-6

1. General introduction

This thesis investigates peripheral electrical stimulation as a non-invasive treatment for Parkinsonian rest tremor. The emphasis is on delivering phase-locked stimulation, synchronised with accelerometer-recorded tremor signals, to a nerve in the wrist. In this chapter, we explore the nature of pathological tremor disorders, examine both conventional and non-invasive treatment approaches for Parkinsonian tremor, discuss the significance of phasic stimulation, and provide an overview about wrist nerves. The chapter concludes by outlining the contents and primary objectives of this thesis.

1.1. Pathological tremor disorders

Pathological tremor is defined as involuntary, rhythmic movements that are oscillatory in nature, fluctuating around a central plane, and involve at least one part of the body (Bhatia et al., 2018; Lenka & Jankovic, 2021; Louis, 2019). These movements often present significant physical and social challenges for affected individuals. People with pathological tremor experience considerable interference in daily activities, with involuntary shaking affecting tasks ranging from simple actions such as writing and eating to more complex activities, potentially impacting their work capability (Louis et al., 2001; Louis & Machado, 2015; Mo & Priefer, 2021). This can lead to psychosocial consequences, as individuals with tremor may experience fear or embarrassment about their difficulties in performing routine tasks independently, or face unwanted attention or judgment due to their tremor (Gerbasi et al., 2022; Mo & Priefer, 2021; Monin et al., 2017; O'Suilleabhain et al., 2023).

Tremor is a common symptom in various neurological disorders, with Parkinson's disease (PD) and essential tremor (ET) being among the most prevalent. ET occurs in about 1% of the global population, with its prevalence increasing with age and reaching approximately 6% in people aged 65 years and over (Louis & Ferreira, 2010; Louis & McCreary, 2021). PD is the second most common neurodegenerative disorder after Alzheimer's disease, affecting 0.3% of people worldwide and 1% of those aged above 60 years (de Lau & Breteler, 2006). As the global population ages, it is expected that these movement disorders will become more prevalent (Dorsey et al., 2007).

The precise cause of ET remains under investigation, but it is believed to be associated with abnormalities in circuits in the cerebellum and in the cerebello-thalamo-cortical pathway, leading to pathological oscillations and postural and kinetic tremor—ET's main symptom (Deuschl, Wenzelburger, et al., 2000; Deuschl & Elble, 2009). This condition may also feature non-motor symptoms such as hearing loss, anxiety, and cognitive difficulties (Shalash et al., 2021). In contrast, PD presents with a broader spectrum of symptoms and has a better-defined pathophysiology.

PD is characterised by the progressive loss of dopaminergic neurons, predominantly in the substantia nigra pars compacta (SNc) of the midbrain (Jankovic, 2008). The SNc cells are an integral part of the neural circuits involving the basal ganglia, deep brain structures that play a key role in controlling voluntary movements (Yamada et al., 2016). These structures project to the thalamus, which then connects to the motor cortex. According to the classical model of basal ganglia circuits, there are two main pathways: the direct pathway, which facilitates movement, and the indirect pathway, which inhibits movement. SNc cells activate the direct pathway and suppress the indirect pathway (Calabresi et al., 2014).

The loss of these cells results in excessive inhibition of the thalamic neurons projecting to the motor cortex, leading to a range of symptoms (Obeso et al., 2009). These include the four cardinal Parkinsonian symptoms—tremor, bradykinesia (or slowness of movement), rigidity (muscle stiffness), and postural instability (Jankovic, 2008; Lenka & Jankovic, 2021). Additionally, gait difficulties frequently occur, including freezing of gait, festination (unwillingly adopting a running pace), and reduced step length (Obeso et al., 2017). Individuals with PD also commonly experience sleep disturbances, such as REM sleep disorder, autonomic dysfunction, psychiatric illnesses such as anxiety and depression, and cognitive impairments including dementia and memory deficits (Poewe et al., 2017; Riboldi et al., 2022).

The most common symptom of PD is involuntary shaking of the limbs when at rest, known as resting tremor, affecting over 75% of individuals with the condition (Deuschl, Wenzelburger, et al., 2000; Martin et al., 1973). In addition, action tremor, which occurs during voluntary movement, is experienced by approximately 60% of people with PD (Heusinkveld et al., 2018). Tremor is not only one of the most visibly noticeable symptoms of PD but often the first symptom that prompts individuals to seek medical attention (Heusinkveld et al., 2018).

1.2. Conventional tremor treatments

Treatment for PD primarily focuses on alleviating symptoms rather than addressing the root causes of neural degeneration, as these remain elusive, and currently, no treatment has been proven to reverse neuronal loss (Kalia & Lang, 2015). Therapeutic interventions commonly employed in clinical practice include both pharmacological and surgical approaches. These methods directly interface with brain networks linked with pathological oscillations underlying tremor and other symptoms of the disease. Further description of these approaches is provided below.

1.2.1. Pharmacological approaches

Pharmacological treatments for PD commonly aim to increase dopamine levels in the brain, thereby compensating for the loss of dopaminergic neurons in the SNc. The most prevalent treatment for PD, applicable at all stages of the disease, is Levodopa—a dopamine precursor that is converted into dopamine in the brain. Levodopa is typically combined with Carbidopa, which inhibits peripheral conversion of dopamine, thereby enhancing its central nervous system availability (Hauser et al., 2018; Tambasco et al., 2018).

However, long-term use of Levodopa can lead to the development of dyskinesias, characterised by excessive and involuntary movements (Bezard et al., 2001; Fahn, 1989; Turcano et al., 2018). Levodopa is also associated with other adverse effects, including nausea, dizziness, and psychiatric symptoms (Fahn, 1989). Aiming at delaying Levodopa introduction or enhancing its effects, dopamine agonists are frequently prescribed, particularly in the early stages of PD or for younger people (Stowe et al., 2008). While effective, these treatments are associated with side effects such as sleep disturbances, hallucinations, and impulse control disorders (Baker et al., 2009; Mohammad et al., 2021).

Additional medications used in PD management include monoamine oxidase-B inhibitors, which serve for mild symptom control in early-stage PD or as adjunct therapy in advanced stages, and catechol-O-methyl transferase inhibitors, which prolong Levodopa's effects (Fabbri et al., 2022; Schapira, 2011). Anticholinergics are primarily employed for tremor control, while Amantadine is administered for dyskinesia management (Paz & Murer, 2021; Rascol et al., 2021).

Each class of medication has its own profile of side effects, ranging from gastrointestinal disturbances to cognitive and neuropsychiatric symptoms. This requires person-specific treatment plans with careful monitoring. Despite these pharmacological efforts, medication efficacy in PD is limited. Notably, although tremor is the most common symptom, it responds less effectively to dopaminergic medications than other symptoms such as bradykinesia and rigidity (Fishman, 2008; Rodriguez-Oroz et al., 2009).

ET, in turn, is commonly managed, as a first-line treatment, with anticonvulsants (Primidone) and beta-blockers (Propranolol). These medications primarily aim to reduce the involuntary shaking that characterises this condition. However, the effectiveness of these pharmacological approaches is limited, with only half of the patients experiencing significant tremor suppression. Additionally, these medications are associated with potential side effects. Propranolol can cause fatigue, dizziness, bradycardia (slow heart rate), and gastrointestinal issues, while Primidone produces drowsiness, dizziness, nausea, and ataxia (Louis et al., 2010; Ondo, 2016).

1.2.2. Surgical approaches

Surgical intervention offers an alternative to medication for targeting the disrupted brain networks in pathological tremor. One such surgical approach, pallidotomy, involves lesioning the globus pallidus pars interna (GPi). Under normal physiological conditions, the GPi exerts an inhibitory effect on the thalamic nuclei that relay signals to the motor cortex (Alkhani & Lozano, 2001). The aim of resecting this brain region is to alleviate this inhibition, thereby reducing movement restrictions typical in PD. Another surgical method is thalamotomy, which entails the ablation of part of the thalamus. This approach is based on the hypothesis that the thalamus may serve as a potential site for central oscillators driving tremor (Perry & Lenz, 1998).

Surgery targeting thalamic nuclei can also be used to treat severe cases of ET (Elble et al., 2018). However, it is important to note that these lesion-based approaches are irreversible and may be associated with side effects, including gait disturbances, ataxia (lack of coordination), paraesthesia (abnormal sensations), dysgeusia (altered taste), and hemiparesis (half-body weakness) (Paff et al., 2021).

Deep brain stimulation (DBS) is another surgical approach, often preferred over irreversible ablative procedures. DBS involves the implantation of electrodes in the brain to deliver high-frequency electrical stimulation. Typically, they target either the GPi or the subthalamic nucleus (STN) for PD treatment, and the ventrolateral thalamus in ET (Cagnan et al., 2019; Krauss et al., 2021). Recognised as a highly effective therapeutic intervention, DBS offers long-term improvements in motor function, including the alleviation of tremor symptoms (Limousin & Foltynie, 2019). However, candidates for DBS surgery are subject to strict selection criteria (Cagnan et al., 2019; Pollak, 2013).

Despite its effectiveness, DBS is an invasive procedure that requires neurosurgery and the long-term use of an implantable device, making it a costly option. The provider costs for DBS can exceed US$ 130,000 (Stroupe et al., 2014). Access to trained clinical teams for DBS programming and surgery, as well as to specialised centres, is limited, often resulting in long waiting lists for the procedure (Abosch et al., 2013). These logistical challenges, compounded with the high cost of DBS, significantly restrict its availability (Cagnan et al., 2019). Worldwide, less than 2% of eligible PD patients undergo this surgery (Kestenbaum et al., 2015; Zhang et al., 2020). Furthermore, geographic and socioeconomic disparities resulting from the unequal distribution of resources worldwide further impede global access to DBS. For instance, in the African continent, DBS was available in only five out of 54 countries as of recent

studies, and it remains unaffordable for most patients due to the frequent lack of health insurance coverage in those regions (Hamid et al., 2021; Memon et al., 2023).

1.3. Non-invasive tremor treatments

Given the side effects and diminishing effectiveness over time of pharmacological treatments for tremor, coupled with the limited availability and accessibility of DBS, there is a growing clinical interest in non-invasive therapeutic options. These approaches could be more widely accessible, providing relief for pathological tremor without the drawbacks associated with invasive procedures. Specifically, methods that interact directly with the trembling limb show promise for development into wearable devices. Such wearables could offer practical, user-friendly treatment solutions, potentially improving the quality of life for a broad range of individuals affected by tremor disorders. Some of these novel approaches are described below.

1.3.1. Vibratory stimulation

One such approach is vibratory stimulation, as exemplified by the Emma Watch (Microsoft, Inc)—a wristband equipped with vibratory motors designed to alleviate action tremor in individuals with PD. The underlying mechanism is believed to involve vibrations that alter the sensory feedback received by the brain. This alteration could potentially disrupt the brain networks associated with tremor by stimulating the proprioceptive system. Enhancing proprioception might increase awareness of body position and movement, potentially improving motor control (Macerollo et al., 2018; MacErollo et al., 2020; Pacheco et al., 2023).

Initial explorations into the efficacy of vibratory stimulation suggested visually observable and subjectively reported improvements in motor performance among a small sample of individuals with PD tremor (Macerollo et al., 2018; MacErollo et al., 2020; Pacheco et al., 2023). However, the specific impact of this technology on rest tremor has not been extensively quantified. More in-depth research is needed to establish its effectiveness and potential as a non-invasive treatment option for tremor.

1.3.2. Functional electrical stimulation

Functional electrical stimulation (FES) represents another non-invasive strategy in the management of tremor. FES involves delivering peripheral stimulation above the motor threshold, either by concurrently stimulating a pair of antagonist muscles to increase joint impedance in the tremulous limb or by applying out-of-phase stimulation to muscles involved in the tremor (Dideriksen et al., 2017; Lora-Millan et al., 2021). This approach was initially explored in the early 1990s, applying closed-loop, out-of-phase stimulation of tremorgenic muscles in the arm to directly counteract the tremor (Javidan et al., 1992; Prochazka et al., 1992). In an early trial involving 10 individuals with various types of tremor (including ET, PD, and cerebellar tremor), this method achieved an average tremor suppression of 58.1%.

Despite these promising results, FES has not been widely adopted in clinical practice. The practical implementation of FES poses significant challenges, such as the need for precise timing and muscle selectivity in stimulation. Furthermore, this approach can lead to incomplete and unpredictable tremor suppression, muscle fatigue, and discomfort. These limitations have hindered its transition into clinical practice, as evidenced by studies conducted over the years (Dideriksen et al., 2017; Dosen et al., 2015; Hao et al., 2017; Javidan et al., 1992; Maneski et al., 2011; Prochazka et al., 1992).

1.3.3. Sub-motor threshold electrical stimulation

Sub-motor threshold stimulation, increasingly investigated for its therapeutic potential in tremor treatment, activates afferent pathways without inducing muscle contractions. This approach, which typically avoids the muscle fatigue associated with FES, is likely more comfortable due to lower amplitude currents (Lora-Millan et al., 2021). Technologies using this method often target wrist nerves, as electrical stimulation of the median nerve in the wrist has been shown to evoke activity in the human thalamus and STN—crucial components of the central tremor network and common DBS targets (Brittain et al., 2015; Hanajima et al., 2004; Nowacki et al., 2023).

Peripheral stimulation might disrupt tremor-related brain networks by evoking afferent activity, or alternatively, it could interfere with tremor signal transmission at the spinal level (Hao et al., 2017; Isaacson et al., 2020; Kim et al., 2022; Pahwa et al., 2019; Reis et al., 2021).

The Cala kIQ (Cala Health, Inc) wrist-worn device, developed for ET, alternates high-frequency stimulation between the radial and median nerves (Isaacson et al., 2020; Lin et al., 2018; Pahwa et al., 2019). A clinical trial reported a 49% improvement in tasks with this device, surpassing the 27% in a sham condition (Pahwa et al., 2019). Subsequently, a larger home-use study found tremor suppression in 92% of users, with more than half experiencing at least a 50% reduction (Isaacson et al., 2020).

In PD, a study showed over 60% tremor suppression with radial nerve stimulation (Hao et al., 2017). Additionally, research into ET has focused on parameter optimisation for personalised therapy. Phase-specific stimulation at the median nerve showed significant modulation of tremor, particularly considering instantaneous changes (Reis et al., 2021). Another study found that higher amplitude tremor in ET was

more effectively suppressed with higher amplitude, out-of-phase stimulation (Kim et al., 2022). The potential of parameter-optimised peripheral nerve stimulation in PD tremor remains unexplored.

1.4. Phasic stimulation and brain rhythms modulation

Phase-specific stimulation emerges as a novel and versatile strategy in tremor treatment, applicable to both invasive and non-invasive methodologies. This technique, focused on delivering stimulation at specific phases within an oscillatory cycle, targets particular brain waves or accelerometer-recorded tremor signals. The primary goal is to modulate brain rhythms by aligning the stimulation precisely with the oscillation's timing, aiming to alter its pathological patterns (Escobar Sanabria et al., 2020; Holt et al., 2016, 2019; McNamara et al., 2022; Peles et al., 2020).

Computational modelling suggests that beta oscillations (15-30 Hz), which are abnormally prolonged and synchronised in PD, can be effectively disrupted at certain phases (Azodi-Avval & Gharabaghi, 2015; Holt et al., 2016). In invasive treatments such as DBS, phase-locking to these beta oscillations has shown promise. One study, for instance, reported up to a 40% reduction in these waves' amplitude in PD patients when DBS was synchronised with patient-specific beta oscillation phases (Holt et al., 2019). Another study explored DBS synchronised with accelerometer-recorded tremor signals in patients with essential and dystonic tremor, achieving up to 87% tremor reduction (Cagnan et al., 2017). Furthermore, non-invasive approaches, such as transcranial alternating current stimulation over the motor cortex, have also shown potential, averaging 50% tremor suppression in PD patients (Brittain et al., 2013).

One significant benefit of phase-locked stimulation is its lower energy requirement compared to continuous, non-phasic stimulation, potentially reducing

side effects and improving comfort (Cagnan et al., 2017). However, the optimisation process to identify the most effective patient-specific phase and real-time estimation of the targeted oscillation's phase can be computationally demanding and should be carefully weighed against potential therapeutic benefits of phasic vs. open-loop constant high-frequency stimulation.

The principles of phase-locked stimulation may also be relevant to therapies applied peripherally, such as to nerves on the tremulous limb rather than the brain. The underlying mechanism suggests that thalamic neurons, which fire at specific instances during limb acceleration in tremor, could be influenced by phase-locked median nerve stimulation. This raises the possibility that such peripheral stimulation might impact the central oscillators driving Parkinsonian tremor (Brodkey et al., 2004; Milosevic et al., 2018). Preliminary findings in essential tremor patients using phase-locked wrist nerve stimulation indicate promise for this technique's broader application (Kim et al., 2022; Reis et al., 2021). However, the specific impact of phase-locked peripheral nerve stimulation on Parkinsonian tremor or its related central oscillators remains an unexplored avenue.

1.5. Wrist nerve circuitry and connectivity

In tremor treatment strategies that apply peripheral electrical stimulation, the selection of target nerves in the upper limb must be carefully considered. The human wrist is innervated by three primary nerves: the radial, median, and ulnar nerves, each containing sensory and motor fibres crucial for hand movement and sensation. These nerves originate from the brachial plexus, formed by the convergence of lower cervical and upper thoracic branches of spinal nerves (Okwumabua et al., 2023). *Figure 1.1* illustrates the location of these nerves in the wrist and hand, along with the dermatomes they innervate.

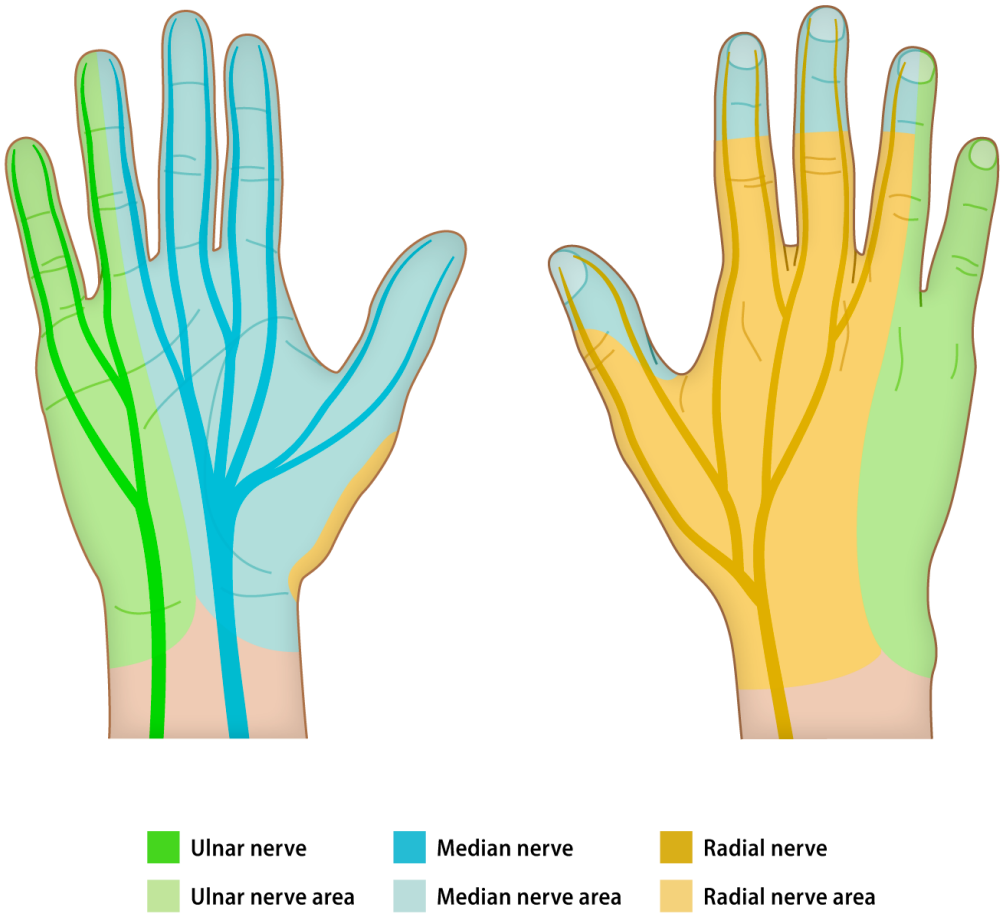


Figure 1.1: A representation of the ulnar, median, and radial nerves in the wrist and hand, along with their corresponding dermatomes.

The radial nerve, running along the thumb side of the forearm, is essential for coordinated hand movement, extending the wrist and fingers, and provides sensory input to the dorsum of the hand, affecting areas from the thumb to the third finger. The median nerve, renowned for its passage through the carpal tunnel, is responsible for controlling thumb base muscles and providing sensation to the thumb, index, long, and part of the ring finger. This nerve is often a focal point in carpal tunnel syndrome

discussions due to its unique anatomical pathway. The ulnar nerve, traversing along the palm side where the little finger is located, facilitates movement and sensation in the little and part of the ring finger and also contributes to various wrist movements, underscoring its role in intricate hand motions (Okwumabua et al., 2023; Wynter & Dissabandara, 2018)

Previous studies on peripheral nerve stimulation for tremor treatment have targeted the radial nerve alone, the median nerve alone, combinations of the median and radial nerves, or the median and ulnar nerves (Isaacson et al., 2020; Kim et al., 2020, 2022; Pahwa et al., 2019; Pascual-Valdunciel et al., 2021; Reis et al., 2021). The median nerve, in particular, emerges as a promising target for two reasons. First, its superficial location and course through the carpal tunnel make it a precise and consistent target, further facilitated by commercially available wristbands, often used in medical procedures including assessments for carpal tunnel syndrome (Meyer et al., 2018; Reis et al., 2021). In turn, a home-use study alternating stimulation between the radial and median nerves, likely aiming to enhance comfort during prolonged stimulation, employed a custom-designed wristband (Isaacson et al., 2020). Second, median nerve stimulation has been demonstrated to evoke activity in central tremor network regions, namely the thalamus and STN (Hanajima et al., 2004; Nowacki et al., 2023).

1.6. Thesis objectives

The overarching aim of this thesis is to contribute to the field of pathological tremor treatment by investigating the effects of phase-locked peripheral electrical stimulation at the median nerve on Parkinsonian rest tremor. Given the current gap in and clinical need for non-invasive therapeutic approaches for Parkinsonian tremor, this research is particularly timely and relevant.

Our objectives are structured as follows:

(i) **Exploring phasic stimulation effects:** to explore the potential of phase-locked peripheral nerve stimulation at the wrist in modulating Parkinsonian rest tremor. This approach has not yet been trialled for Parkinsonian tremor, making our investigation a pioneering effort in this area.

(ii) **System design and development:** to design, develop and verify a portable, wrist-worn system capable of delivering non-invasive stimulation. This system is unique in its ability to adapt to the variability of tremor when estimating phase.

(iii) **In-clinic system validation**: to evaluate the performance of this system and assess its feasibility as a therapeutic intervention in individuals with PD. This includes comparing the effects of phase-locked stimulation to those of open-loop stimulation on tremor.

To achieve these objectives, the thesis is organised into three experimental chapters, each of them containing a description of their specific methods. *Chapter 2* introduces a pilot study utilising a large, non-portable system to investigate the effects of phase-locked peripheral electrical stimulation on tremor. This study primarily examines the variability in tremor, as evidenced by changes in tremor oscillation patterns. *Chapter 3* details the development process of our novel portable phase-tracking system. This system is designed to trigger peripheral nerve stimulation while accommodating the variability inherent in tremor dynamics during phase tracking. *Chapter 4* presents an in-clinic feasibility study that tests the newly developed system in individuals experiencing Parkinsonian rest tremor, providing critical insights into its practical application.

2. Identifying and modulating distinct tremor states through peripheral nerve stimulation in Parkinsonian rest tremor

This chapter explores the potential of peripheral nerve stimulation in modulating Parkinsonian rest tremor. We investigated the effects of phase-locked median nerve stimulation in a group of ten individuals with Parkinson's disease, focusing on the most tremulous hand. Our approach involved delivering brief, non-invasive electrical pulses, synchronised with the phase of limb acceleration along the axis with the greatest tremor-related movement. The findings revealed significant changes in upper-limb tremor patterns, with the ability to both reduce (-36%) and amplify (117%) tremor through phasic stimulation. The chapter further discusses the variability of tremor patterns within the same limb, suggesting the necessity for ongoing adjustments in stimulation parameters to achieve consistent tremor suppression. The results underscore the potential of phase-locked peripheral nerve stimulation as a viable approach for mitigating Parkinsonian rest tremor, while also highlighting the complexity of tremor dynamics and the need for adaptable stimulation strategies. The research outlined in this chapter was presented at an international conference and published as a journal article.

Conference poster: *Arruda, B. S., Reis, C., Pogosyan, A., Brown, P., Cagnan, H., July 2020, Identifying distinct tremor states in Parkinsonian rest tremor. In 2020 42nd Annual International Conference of the IEEE Engineering in Medicine and Biology Society (EMBC), held online.*

Journal article: *Arruda, B. S., Reis, C., Sermon, J. J., Pogosyan, A., Brown, P., Cagnan, H. (2021). Identifying and modulating distinct tremor states through peripheral nerve stimulation in Parkinsonian rest tremor. Journal of NeuroEngineering and Rehabilitation, 18(179). doi: 10.1186/s12984-021-00973-6*

2.1. Background

Approximately 70% of the people with Parkinson's disease (PD) exhibit involuntary shaking of their limbs when resting (Deuschl, Wenzelburger, et al., 2000). Involuntary shaking of the limbs, also known as tremor, can dominate PD, and yet responds less well to dopaminergic medications than bradykinesia and rigidity (Fishman, 2008; Rodriguez-Oroz et al., 2009). Deep brain stimulation (DBS) can provide striking tremor relief however this surgical intervention is invasive and subject to strict selection criteria, which can limit the number of people benefiting to approximately 2% (Cagnan et al., 2019; Pollak, 2013). As a result, there has been growing interest in non-invasive therapies for tremor in PD. Therapies directly interfacing with the limb rather than cranial stimulation (Brittain et al., 2013; Saifee et al., 2016) are more tractable and have focused on occluding tremor by stimulation of antagonist muscles or suppressing tremor by stimulation of sensory afferents. However, these approaches can lead to incomplete and unpredictable tremor suppression, muscle fatigue and discomfort, and have not entered in to clinical practice (Dideriksen et al., 2017; Dosen et al., 2015; Hao et al., 2017; Javidan et al., 1992; Maneski et al., 2011; Prochazka et al., 1992). Vibratory stimulation is another non-invasive approach, which has been shown to improve motor performance in people with PD; however, its impact specifically on rest tremor has not been quantified extensively (Macerollo et al., 2018; MacErollo et al., 2020; Pacheco et al., 2023).

It has recently been demonstrated that brain rhythms can be modulated using phase-locked stimulation (Escobar Sanabria et al., 2020; Holt et al., 2016, 2019; McNamara et al., 2022; Peles et al., 2020). This stimulation strategy aims to selectively enhance or reduce a rhythm depending on the precise stimulation timing with respect to the target rhythm. In the case of tremor, phase-locked stimulation has been trialled in the form of cranial or deep brain stimulation locked to peripheral tremor, which

significantly modulated tremor severity (Brittain et al., 2013; Cagnan et al., 2019; Moll & Engel, 2017; Saifee et al., 2016). Previous research suggests that delivering stimulation to the median nerve can cause neural spiking in the thalamic nuclei, which overlap with regions implicated in tremor in PD and commonly used as surgical targets for DBS (Hanajima et al., 2004; Maendly et al., 1981; Milosevic et al., 2018; Ohye & Narabayashi, 1979; Vitek et al., 1994). Critically, thalamic neurons fire at specific moments of limb acceleration during tremor, raising the possibility that median nerve stimulation phase-locked to limb acceleration could potentially impact the central oscillators underpinning Parkinsonian tremor (Brodkey et al., 2004; Milosevic et al., 2018).

An important consideration for developing peripheral nerve stimulation-based treatments is the relationship between central tremor oscillators and the peripheral manifestation of tremor. Currently, it is believed that resting tremor in PD is generated by independent central oscillators separately representing each limb. Several studies of multi-limb tremor recordings indicate that tremor in different limbs is largely uncorrelated, while being correlated within a limb (Alberts et al., 1969; Ben-Pazi et al., 2001; Hurtado et al., 2000; P. E. O'Suilleabhain & Matsumoto, 1998; Raethjen et al., 2000). Nevertheless, the strength of coherence within a limb is seldom specified and significant coherence is absent in about 20% or more of instances (Hurtado et al., 2000; Raethjen et al., 2000). In a small sample of people with PD, the mean coherence between the axes of an accelerometer placed on a tremulous limb was 0.72 and the coherence between signals obtained from accelerometers placed on different regions of the same limb was only 0.56 (Ben-Pazi et al., 2001). There are two possible explanations for these observations: (i) coupling within a limb-specific central tremor oscillator drops in and out over time, or (ii) multiple central tremor oscillators contribute to rest tremor even within the same limb, perhaps with one or more dominating at any particular time.

Studies of the coherence between microelectrode recordings within the globus pallidus or subthalamic nucleus (STN) and electromyography (EMG) in people with PD provide evidence for the former (Hurtado et al., 1999, 2005), whereas the presence of spatially distinct pockets of coherence with tremor within the STN and ventral thalamus raises the possibility of multiple competing central oscillators (Pedrosa et al., 2012; Reck et al., 2009). The nature of the central representation of tremor is important for the insights it may afford into motor control and development of novel therapeutic interventions such as phase-locked stimulation (Cagnan et al., 2017; Holt et al., 2019; Peles et al., 2020). Afferent feedback is also critical in tremor pathophysiology. As the basal ganglia circuits involved in tremor are topographically arranged it is likely that the effects of afferent feedback will also be topographically limited (Crutcher & DeLong, 1984; DeLong et al., 1985; Kaneda et al., 2002; Romanelli et al., 2004; Theodosopoulos et al., 2003).

Here we test two major hypotheses which are interlinked; that the amplitude of PD rest tremor in the hand can be modulated by phase-locked stimulation of a peripheral nerve supplying the hand, and that tremor in the hand can involve multiple oscillators. To this end, we electrically stimulated the median nerve at the wrist in people with Parkinsonian rest tremor to show that tremor amplitude modulation can be achieved with phase-locked stimulation, provided that the existence of multiple oscillators is taken into account.

2.2. Materials and methods

2.2.1. Cohort

We recruited 14 people with PD who displayed upper-limb tremor at rest. This study received approval from the Health and Social Care Research Ethics Committee A

(HSC REC A) of the Health Research Authority, National Health Service (NHS, UK), in accordance with the Declaration of Helsinki (reference number: 19/NI/0009). All participants provided informed consent before participating in the tests. All participants were recruited by an advert placed with an advocacy group for people with PD. Study participants were assessed by an experienced movement disorders expert at the time of study (Peter Brown). This led to the exclusion of one person in whom the diagnosis of dystonia and one in whom the diagnosis of psychogenic tremor was made. Two further participants were excluded; one because tremor was minimal and confined to the little finger and one because hand tremor was confounded by tremor transmitted from the legs. Thus, we analysed data from 10 participants (Hoehn and Yahr Scale stages I and II). Eight out of 10 of the participants regularly took medication for PD and five of these eight participants omitted their last medication dose prior to the experiment. The three participants who chose not to omit their medication dose reported that their upper-limb tremor was unaffected by medication and exhibited upper-limb tremor at rest at the time of the study, as assessed by the movement disorders expert. *Table 2.1* summarises participant information.

Participant	1	2	3	4	5	6	7	8	9	10	Mean
Age [years]	75	64	55	56	75	63	62	75	57	73	65.5
Gender	Female	Female	Male	Male	Male	Female	Male	Female	Female	Female	-
Arm tested	Left	Right	Right	Right	Right	Right	Right	Left	Right	Right	-
Parkinson's disease medication state	On	On, skipped last dose	Off	On, skipped last dose	Off	On, skipped last dose	On, skipped last dose	On	On, skipped last dose	On	-
Likert scale assessment	Strongly agree	Strongly agree	Agree	Strongly agree	Strongly agree	Strongly agree	Strongly agree	Strongly agree	Strongly agree	Strongly agree	-
Tremor amplitude (mean ± SD) [m/s^2]	3.9±2.9	6.2±2.4	3.0±2.2	15.9±3.2	0.7±0.4	4.7±1.6	0.4±0.2	2.0±0.6	7.3±2.7	8.1±3.1	5.2
Peak tremor frequency [Hz]	5	4	5	5	5	5	5	5	5	6	5

Table 2.1: Individual study participant information and their summary. *Note stimulation sensation was assessed using the following Likert scale: "The stimulation was easily tolerated: A) Strongly disagree; B) Disagree; C) Neither agree nor disagree; D) Agree; E) Strongly agree".*

2.2.2. Data acquisition

Resting tremor was recorded in two conditions (i) without stimulation and (ii) during peripheral nerve stimulation, while study participants were sitting. Participants were asked to avoid voluntary movements during the recording. A triaxial accelerometer (ACL300 Biometrics Ltd) was fixed to the dorsum of the most tremulous hand using surgical tape and tremor was recorded with the hand hanging over the side of the chair which supported the forearm. The forearm was placed on the armrest of the chair such that it was supported up to the wrist (*Figure 2.1A*). In this position, the tremulous hand was hanging over the front of the armrest and could move without

obstruction. The accelerometer signal was amplified (K800 Biometrics Ltd) and recorded by an analogue-to-digital (AD) converter (Power1401, Cambridge Electronics Design) at a sampling rate of 10417 Hz. This sampling rate was chosen for phase estimation accuracy since it utilised an algorithm based on zero-crossings of the band-pass filtered accelerometer signal (see *Section 2.2.4—Peripheral nerve stimulation*) (Cagnan et al., 2017). A wristband containing a peripheral stimulation device was also attached to the study participant's wrist. EMGs were recorded from the abductor pollicis brevis, forearm finger flexors, and forearm finger extensors of the most tremulous arm using surface electrodes and an amplifier (D360 8 Channel Patient Amplifier, Digitimer) connected to an AD converter (Power1401, Cambridge Electronics Design). Good quality continuous EMGs (as assessed visually) were acquired from 9 out of 10 participants. One participant's EMG signals were not utilised in the analysis due to recording issues. Seven surface electrodes were attached to the participant's arm for EMG recordings (one pair for each muscle, plus the ground electrode), each electrode weighing 1 gram, the accelerometer, attached to the dorsum of the most tremulous hand, weighed 10 grams, and the electrical stimulation device, attached to the wrist, weighed 16 grams. *Figure 2.1* shows the placement of the accelerometer, peripheral stimulation device, and EMG surface electrodes on the participant's upper limb.

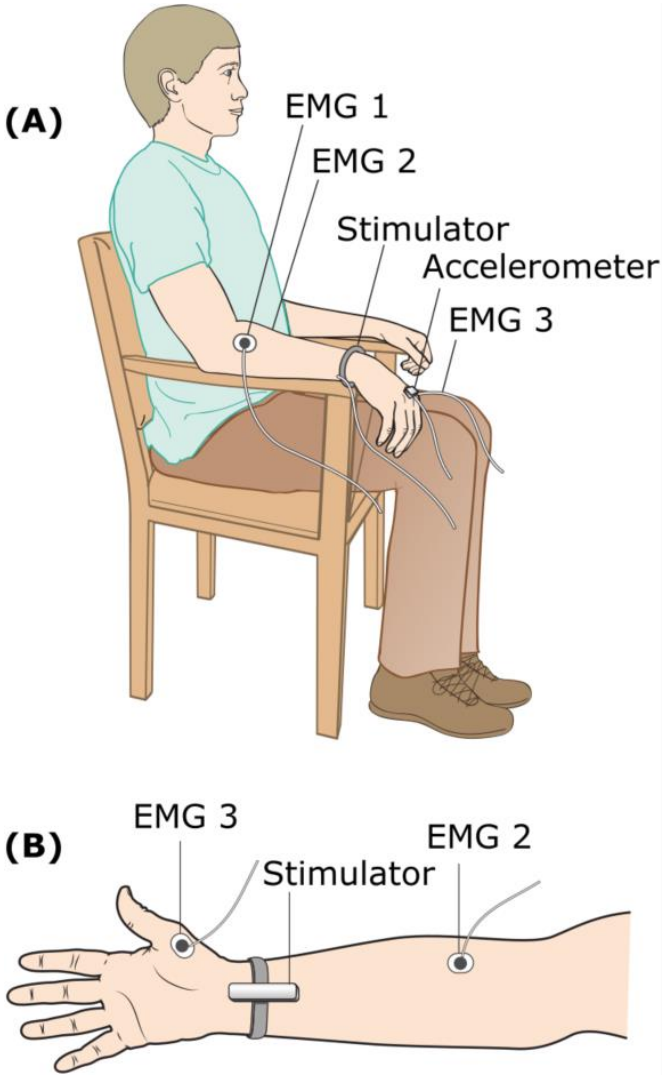


Figure 2.1: A representation of one study participant's posture and the placement of the triaxial accelerometer, peripheral stimulation device, and EMG surface electrodes on the upper limb. *(A) Study participant sitting on a chair, with the hand hanging over the armrest of the chair which supported the forearm. A triaxial accelerometer was placed on the dorsum of the most tremulous hand, a wristband containing a peripheral stimulation device was attached to wrist, targeting the median nerve, and EMG surface electrodes were placed on the participant's hand and forearm. EMG 1 recorded signals from the forearm finger extensor; EMG 2, from the forearm finger flexor; and EMG 3, from the abductor pollicis brevis. (B) View of the ventral surface*

of the study participant's forearm and hand, showing the placement of the electrical stimulation device and EMG 2 and 3 surface electrodes.

2.2.3. Without stimulation condition

The recordings made in the without stimulation condition lasted on average 5.7 ± 1.8 minutes (mean ± SD). Based on power spectral densities derived from the three accelerometer axes (Spike 2, Cambridge Electronic Design Limited), each participant's tremor frequency was identified as the frequency at which the power spectral density was the largest (2 to 8 Hz), and the dominant axis was identified as the one with the largest power spectral density at the participant's tremor frequency.

2.2.4. Peripheral nerve stimulation

Peripheral nerve stimulation amplitude was set to just below each participant's motor threshold, which was determined by gradually increasing the stimulation amplitude in steps of 0.5 mA from 2 mA until stimulation evoked a motor response (i.e. twitch of the thumb) and ranged from 4 to 14 mA (mean 6.8 ± SD 1.8 mA). The twitch of the thumb was used to verify that the stimulation electrode was properly placed over the median nerve, which innervates the abductor pollicis brevis. The dominant tremor axis identified in the without stimulation condition was band-pass filtered from 2 to 8 Hz (Digitimer NL125/6), and recorded with the AD converter (Power1401, Cambridge Electronics Design) at a sampling rate of 10417 Hz for online phase-estimation. Stimulation phase was estimated from the instantaneous zero crossings of this band-pass filtered signal and the average tremor frequency from the without stimulation condition. Once the desired phase of stimulation was detected, a pulse was sent to the

peripheral stimulator (Digitimer Constant Current Stimulator DS7A), closing the loop. Stimulation at a certain phase consisted of a burst of five pulses spaced at 7.7 ms. Stimulation was locked to one of 12 equally spaced phases from 0 to 330 degrees in the tremor cycle. Stimulation at each of the phases was presented for 5-second periods with a 1 second interval, and stimulation phase order was randomised between different blocks. Stimulation blocks, consisting of stimulation at 12 different phases, were repeated 11 to 16 times with 1-minute periods of rest in between. Stimulation sensation was assessed using the following Likert scale: "The stimulation was easily tolerated: A) Strongly disagree; B) Disagree; C) Neither agree nor disagree; D) Agree; E) Strongly agree". Study participants' responses are indicated in *Table 2.1*.

2.2.5. Data processing and analysis

Recordings were analysed using custom written scripts in MATLAB (The MathWorks, Inc.). Signals corresponding to the three accelerometer axes were down-sampled to 1000 Hz. The tremor frequency was derived from Welch's power spectral density using a window length of 1 second with no overlap for each condition (without stimulation and during peripheral nerve stimulation). Signals corresponding to each of the three accelerometer axes were band-pass filtered within ±2 Hz of the peak tremor frequency using a second order Butterworth filter—i.e. zero-phase, digital, forward and backward filter (*Figure 2.2*). EMG signals in contrast were high-pass filtered at 15 Hz using a second order Butterworth filter, following down-sampling to 1000 Hz. We then rectified each filtered EMG signal by taking its absolute value. Following rectification, we only considered the EMG signal components greater than 1 Hz. Only EMG signals from the without stimulation condition were used for analysis, as EMG data obtained during peripheral nerve stimulation was contaminated by stimulation artefacts.

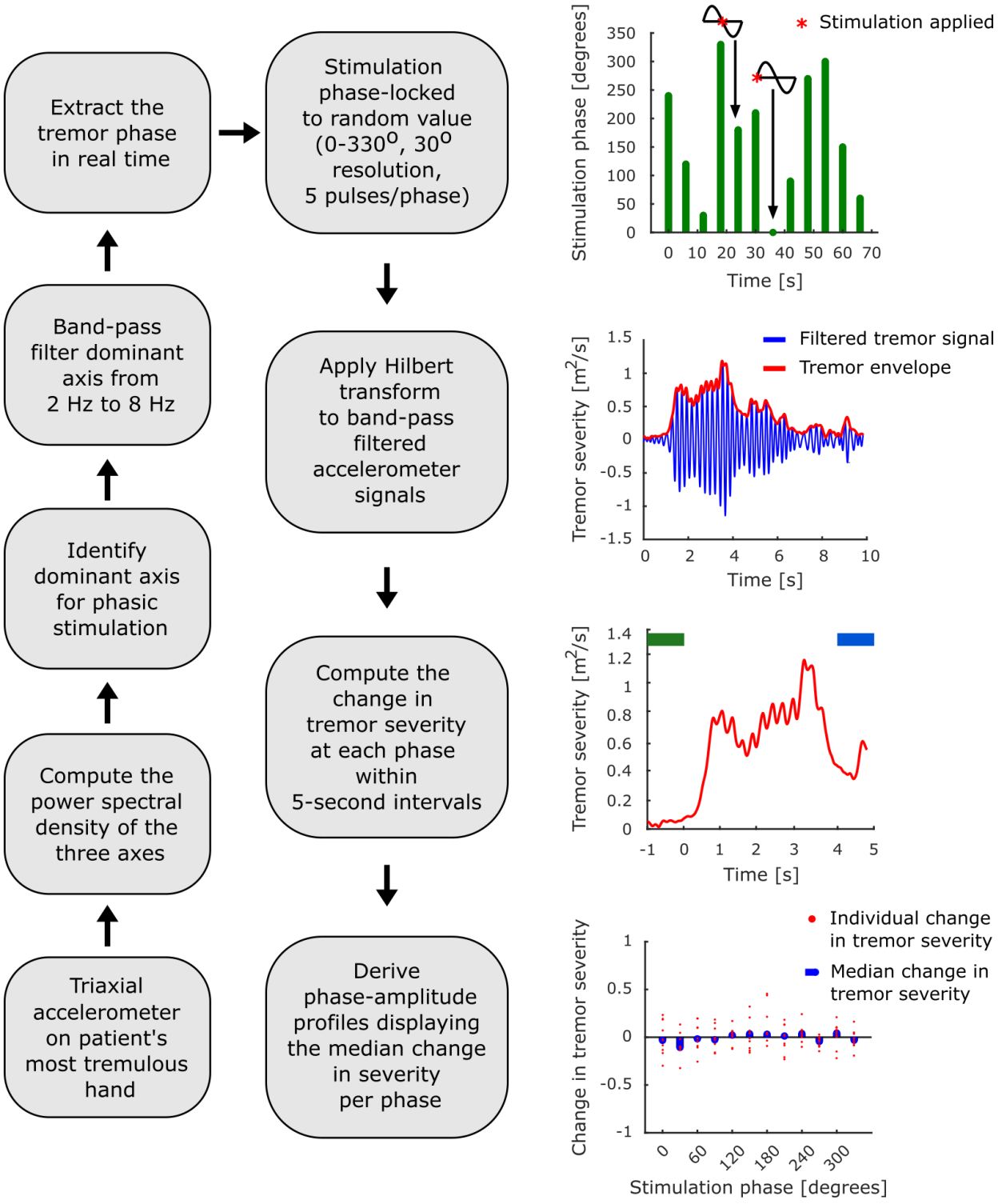

Triaxial accelerometer on patient's most tremulous hand
Compute the power spectral density of the three axes
Identify dominant axis for phasic stimulation
Band-pass filter dominant axis from 2 Hz to 8 Hz
Extract the tremor phase in real time
Stimulation phase-locked to random value (0-330°, 30° resolution, 5 pulses/phase)
Apply Hilbert transform to band-pass filtered accelerometer signals
Compute the change in tremor severity at each phase within 5-second intervals
Derive phase-amplitude profiles displaying the median change in severity per phase
Stimulation applied
Stimulation phase [degrees]
Time [s]
Filtered tremor signal
Tremor envelope
Tremor severity [m²/s]
Time [s]
Tremor severity [m²/s]
Time [s]
Individual change in tremor severity
Median change in tremor severity
Change in tremor severity
Stimulation phase [degrees]

Figure 2.2: Data collection and analysis pipeline. *Tremor signals were collected from the most tremulous hand using a triaxial accelerometer. The power spectral density of the three axes was computed, the dominant tremor axis was identified as the one with the largest peak at the frequency of the tremor and was subsequently band-pass filtered between 2 and 8 Hz. The tremor phase was extracted from the filtered signal in real time. Stimulation was phase-locked to one of 12 randomly assigned phases from 0 to 330 degrees with a 30-degree resolution. To evaluate the effect of phase-locked peripheral nerve stimulation, the Hilbert transform was applied to band-pass filtered accelerometer signals, from which change in tremor severity within 5-second epochs was computed by subtracting the average of the tremor envelope during the 1 second prior to stimulation onset (indicated in green) from the average envelope during the last 1 second (indicated in blue) and then dividing the result by the average of the 1 second prior to stimulation onset (indicated in green). The phase-amplitude profiles were derived as the medians for all the changes at a given phase.*

2.2.6. Tremor oscillation patterns

Initially we sought evidence for discrete tremor oscillation patterns (TOPs), representing different peripheral manifestations of tremor across time based on signals obtained from the three accelerometer axes. To this end, band-pass filtered tremor signals from the x, y and z accelerometer axes were subjected to principal component analysis (PCA) to derive the coefficients contributing to the first principal component. PCA was applied to signals from both conditions (i.e. without stimulation and during peripheral nerve stimulation) after signals from each condition were divided into 5-second segments. For the peripheral nerve stimulation condition, 5-second segments corresponded to instances when stimulation was delivered at one of the 12 specific phases. For the without stimulation condition, 5-second segments corresponded to

consecutive time segments without overlap. Following PCA, we concatenated the first principal component coefficients derived from both conditions (without stimulation and during peripheral nerve stimulation).

To determine whether there was more than one TOP across the recording, we subjected the concatenated first principal component coefficients of the tremor signals to cluster analysis based on Euclidean distances and inner squared distance seeking two clusters. We eliminated any clusters which contained less than 10% of the total number of segments obtained during the peripheral nerve stimulation condition from each study participant. Cluster silhouette values, which range from -1 and 1 and reflect how similar a point is to others in the same cluster with respect to points in other clusters, were used to characterise how well separated the clusters were. High scores would suggest that there was good cluster separation as the objects were better matched to their own cluster than to neighbouring clusters (Rousseeuw, 1987).

For the without stimulation condition, we computed the variance explained by each of the three principal components. In the cases in which the first principal component accounted for less than a median of 90% of the variance in the condition without stimulation, we also subjected the second principal component coefficients to the same cluster analysis, affording a maximum of four independent TOPs per recording (two from the first principal component coefficients and two from the second principal component coefficients).

To evaluate whether there were any physiological differences between TOPs, we computed for each study participant the median tremor amplitude envelope and frequency across 5-second segments of each cluster. The tremor amplitude was computed as the absolute value of the Hilbert transform, and the frequency was derived as the temporal rate of the instantaneous unwrapped phase, also obtained from the

Hilbert transform. Cluster division was based on the principal component coefficients derived from triaxial accelerometer signals recorded during the two experimental conditions (i.e. without stimulation and during peripheral nerve stimulation). EMG epochs were assigned to clusters according to the cluster analysis performed on the principal component coefficients of the simultaneously recorded accelerometer signals.

EMG-based cluster division was ruled out due to the unavailability of quality EMG data for one participant. Additionally, the EMG data could only be utilised in the condition without stimulation, as it was contaminated by artefacts during the stimulation condition. Consequently, only data from the condition without stimulation was considered for statistical comparison for both triaxial accelerometer and EMG signals, as it was not feasible to incorporate EMGs during stimulation due to the presence of artefacts. Furthermore, the absence of stimulation artefacts in the accelerometer data can be attributed to the physical separation between the stimulation electrodes and the accelerometer sensors. This minimised direct interference and ensured the integrity of the accelerometer recordings.

It should be noted that clusters which contained less than 10% of the total number of segments from the phase-locked stimulation condition were retained for this analysis since differences between TOPs were evaluated for the without stimulation condition only. For the cases in which more than one cluster was present, we performed a Wilcoxon signed-rank test between pairs of clusters within study participants. All cluster combinations within a participant were tested for participants with at least two clusters (19 degrees of freedom).

2.2.7. Phase-amplitude profiles

From the peripheral nerve stimulation condition, we obtained phase-amplitude profiles displaying the change in tremor severity as a function of the stimulation phase. These were derived solely from the triaxial accelerometer signals and separately for biomechanically defined clusters for each study participant and tremor axis. We defined the tremor severity as the tremor envelope, which in turn was computed as the absolute value of the Hilbert transform of the band-pass filtered signal corresponding to each of the three accelerometer axes. The change in tremor severity at each phase was computed for 5-second stimulation segments as the difference between the average severity during the last 1 second of stimulation (i.e. 4 to 5 seconds) and that during the 1 second prior to stimulation onset (i.e. -1 to 0 seconds), divided by the average severity during the 1 second prior to stimulation onset (*Figure 2.2*). This normalisation provides a comprehensive scale of stimulation effects where -1 indicates complete tremor suppression, 0 indicates no change in tremor and positive values indicate amplification of tremor. The median change in tremor severity for each of the 12 phases was then plotted, creating phase-amplitude profiles.

We determined whether stimulation delivered at a certain phase of limb acceleration significantly modulated tremor by comparing the change in tremor severity during peripheral nerve stimulation to spontaneous changes in tremor severity during the without stimulation condition. To this end, 50,000 5-second segments were drawn from the without stimulation condition, resulting in a distribution for changes in tremor severity without stimulation. It should be noted that some of these segments could partially overlap in time. PCA was applied to the 5-second segments forming the surrogate distribution, and the corresponding principal component coefficients were concatenated with those obtained from the peripheral nerve stimulation condition. The concatenated signals were subjected to cluster

analysis as outlined in the *Section 2.2.6—Tremor oscillation patterns*, allowing us to split the surrogate distribution according to TOPs.

Phase-amplitude profiles for each TOP were then compared to the surrogate distribution corresponding to the same cluster. We drew *n* random instances from the TOP-specific surrogate distribution where *n* was the average number of trials across the 12 phases, took the median across the *n* points, and repeated this process 1,000,000 times, creating a distribution with 1,000,000 points. We applied Bonferroni correction for 12 phase comparisons on this second distribution, thus generating the confidence intervals for the phase-amplitude profiles.

To explore the relationship between phase-amplitude profiles at the group level, we computed the average Fisher-transformed correlation between phase-amplitude profiles from different axes in the same cluster (for example, between axes x and y in cluster 1), and between the same axes across clusters (for example, between axis x in cluster 1 and axis x in cluster 2).

2.2.8. Re-aligned phase-amplitude profiles

The median change in tremor severity at each phase bin was classified as suppression when smaller than zero, as amplification when greater than zero, and as significant when it reached the Bonferroni-corrected confidence limits. Each phase amplitude profile, for each study participant, cluster, and axis, was realigned by mapping the point of minimum suppression or maximum amplification to 180 degrees. Subsequently, the number of instances of suppression or amplification at each phase was summed across phase amplitude profiles and normalised to a number between 0 and 1 by dividing the number of occurrences at each phase by that at 180 degrees.

For each study participant, cluster and tremor axis, we also generated surrogate phase-amplitude profiles by repeating the process to generate the distribution with 1,000,000 points (please refer to *Section 2.2.7—Phase-amplitude profiles*) and then drawing, 1,000 times, 12 random points from this distribution. These surrogate phase-amplitude profiles were realigned to the maximum and minimum change in tremor. We similarly classified each phase bin of the 1,000 surrogate phase-amplitude profiles as suppressive when the median change in tremor severity was smaller than zero and amplifying when greater than zero. We then realigned the profiles by mapping minimum suppression or maximum amplification to 180 degrees. We summed, per phase, study participant, cluster and axis, the number of instances with suppression or amplification across the 1,000 bins. We divided this sum by the number of bins, thus normalising the sum to a value between 0 and 1 reflecting the probability of seeing suppression or amplification at that phase. These probabilities were compared, with a two-sample t-test, to those derived from data recorded during peripheral nerve stimulation and corrected for multiple comparisons using the false discovery rate (FDR) procedure.

2.3. Results

2.3.1. Tremor oscillation patterns

We first aimed to identify switches in tremor oscillation patterns (TOPs) such as a switch from a predominant tremor in the x dimension (i.e. pronation-supination) to one in the z dimension (i.e. extension-flexion). In seven participants, the peripheral manifestation of tremor varied during the recording session and as a result we observed more than one TOP, indicated by the presence of more than one cluster delineating coefficients contributing to principal components of accelerometer recordings. Implicit in this result is that the dominant cluster (or clusters where the

second principal component was also considered) changed over time in these subjects exhibiting more than one cluster (*Appendix A.1*). *Figure 2.3* provides an example of how cluster representation in serial 5-second periods changes over time and includes the cluster label, the median tremor signal amplitude and the median rectified EMG envelope in each axis per 5-second period.

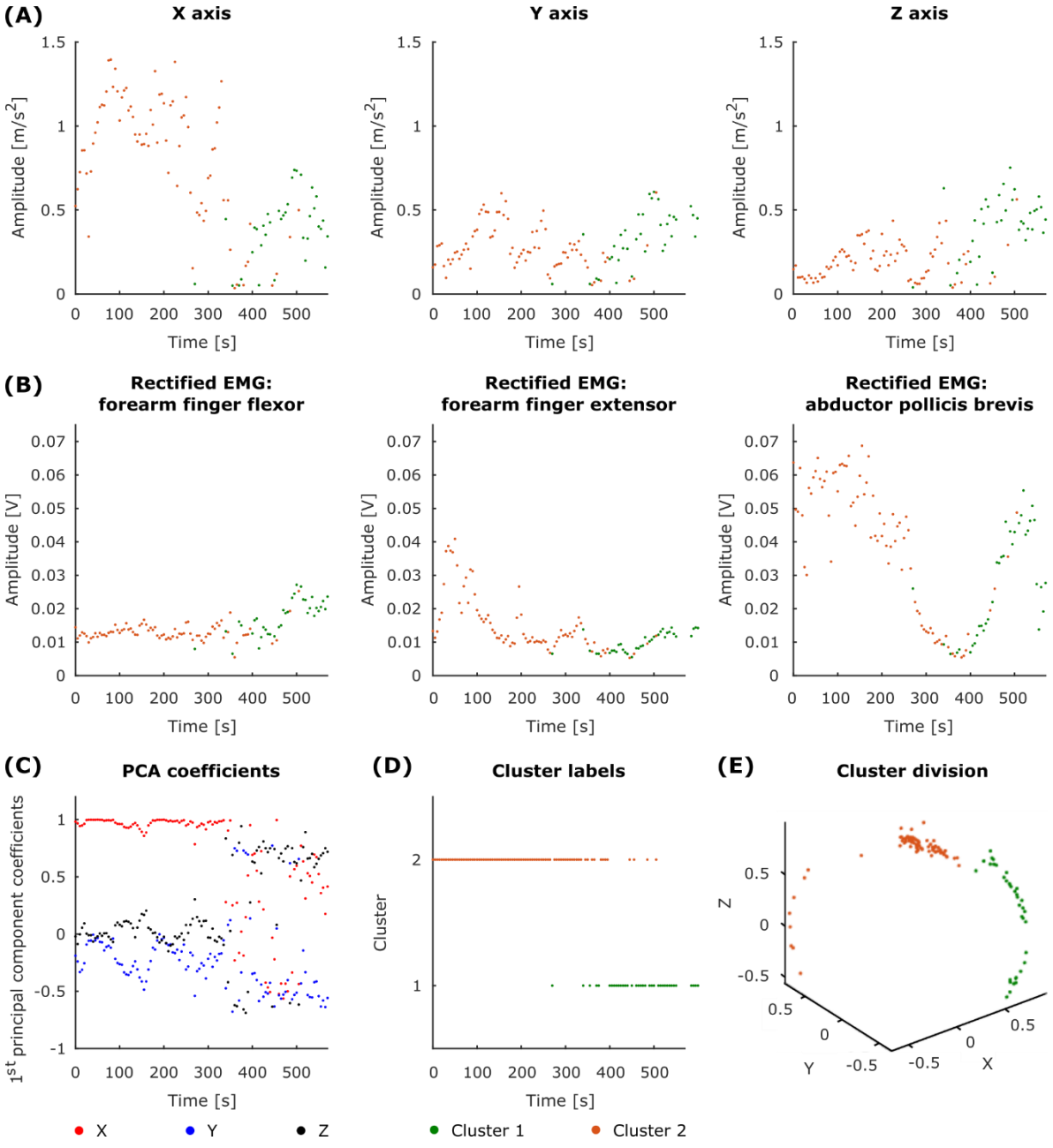


Figure 2.3: An example of how cluster representation in serial 5-second periods changes over time in the signals without stimulation. *(A) Dominant cluster label (orange or green) obtained from the first principal component coefficients is shown for the median accelerometer signal amplitude and (B) for the median rectified EMG in each channel per 5-second period. Movement predominantly occurring along the x-axis corresponds to pronation-supination,*

movement along the z-axis to flexion-extension, and movement along the y-axis to anteroposterior motions. (C) The first principal component coefficients corresponding to the three accelerometer axes. (D) The labels for the time segments assigned to each of the two clusters. (E) The corresponding three-dimensional cluster division from the first principal component coefficients.

2.3.2. Differences between tremor oscillation patterns

We next explored whether there were any physiological differences between clusters (i.e. TOPs) based on features of accelerometer and EMG recordings. Significant differences in tremor peak frequency and amplitude envelope were found for all three accelerometer axes ($p \leq 0.0003$ for all three axes, as given by the Wilcoxon signed-rank test applied to the absolute value of the difference in tremor amplitude and peak frequency across clusters). EMG peak frequency and amplitude envelope also showed significant differences between clusters ($p \leq 0.0003$ for all three muscles, as given by the Wilcoxon signed-rank test applied to the absolute value of the difference in EMG amplitude and peak frequency across clusters for the three muscles—abductor pollicis brevis, forearm finger flexors, and forearm finger extensor). It should be noted that the average duration of a cluster during the "without stimulation" condition was 214.8 ± 136.8 seconds (mean ± SD).

2.3.3. Phase-specific response to peripheral stimulation

Having confirmed that TOPs differ in frequency and amplitude, we next explored how phase-locked stimulation modulated tremor severity. *Figure 2.4* shows an example phase-amplitude profile derived for one participant. Stimulation significantly enhanced or reduced the instantaneous tremor severity depending on the stimulation timing. As

highlighted by this example, the most effective stimulation phase, indicated by the phase which induces changes in tremor amplitude beyond natural variability of tremor, was more consistent across different axes of the same cluster (TOP) vs. across clusters (i.e. cluster 1 suppressive phase of 330 degrees vs. cluster 2 suppressive phase of 120 degrees). At the group level, the correlation between axes in the same cluster was greater than that across clusters (*Figure 2.5*). The difference between the correlations within and between clusters was significant (p-value < 10^{-7} for a two-sample t-test). Those results underscore that, although the pattern of modulation differs between clusters from the same hand, within a cluster the pattern of modulation is relatively conserved across axes, providing additional evidence that clusters are meaningful in terms of a common representation.

At the group level, significant tremor suppression occurred across 12 bins in 12 phase-amplitude profiles for five out of 10 participants, and significant amplification across 16 bins in 12 plots from six participants. In total, 28 bins (1.7%) displayed significant change in tremor severity (*Table 2.2*). This number is eight times above the chance level for Bonferroni correction, which was used to determine the significance of different bins in the phase-amplitude profiles. On average, phase-locked median nerve stimulation was able to significantly amplify tremor by 117% ± 243% (mean ± SD) and suppress it by 36% ± 9% (mean ± SD).

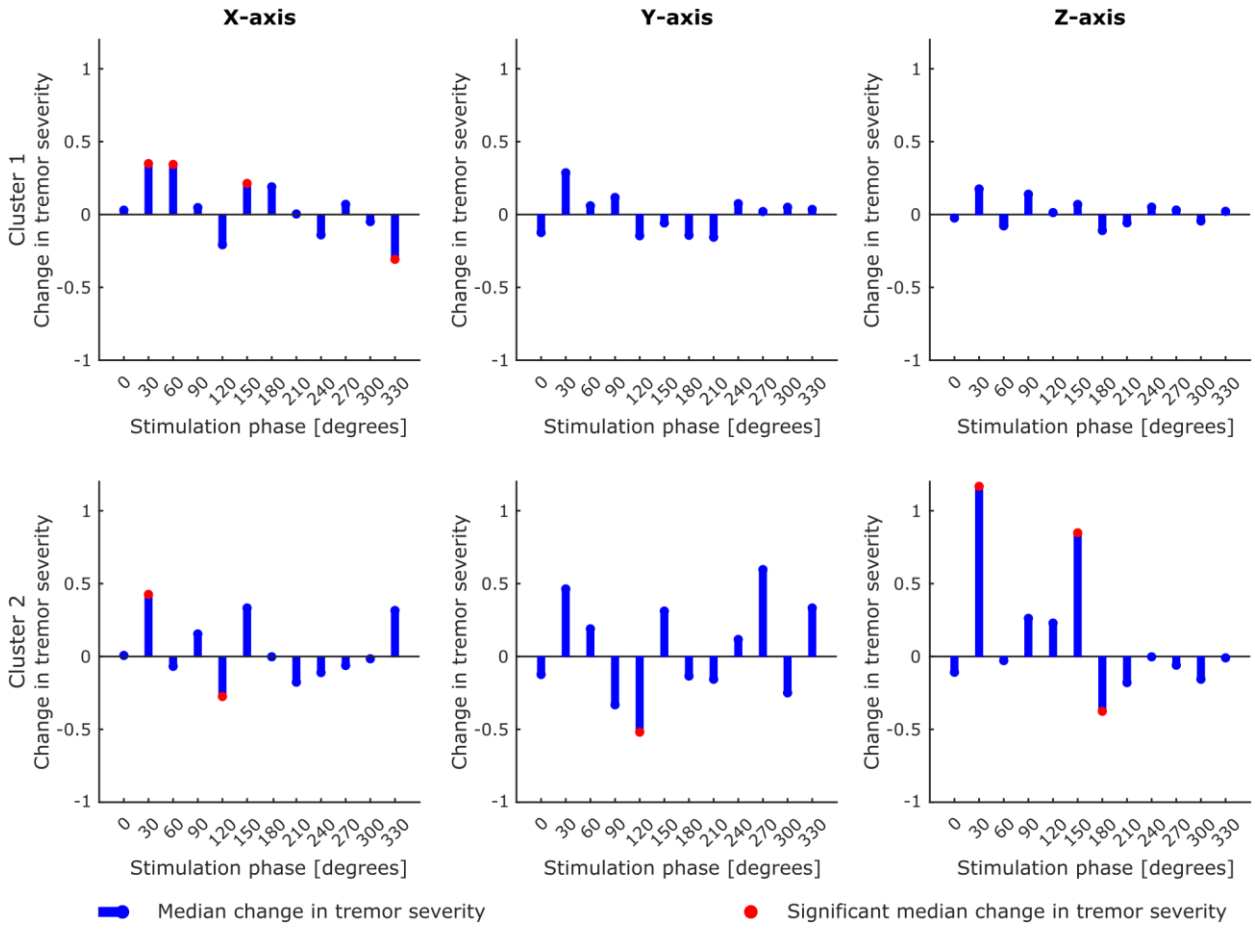


Figure 2.4: Example phase-amplitude profiles for one study participant. *These plots show the median change in tremor severity at each phase for the three accelerometer axes and two clusters. Significant median change in tremor severity was identified with respect to the tremor variability during the without stimulation condition following Bonferroni correction for 12 comparisons.*

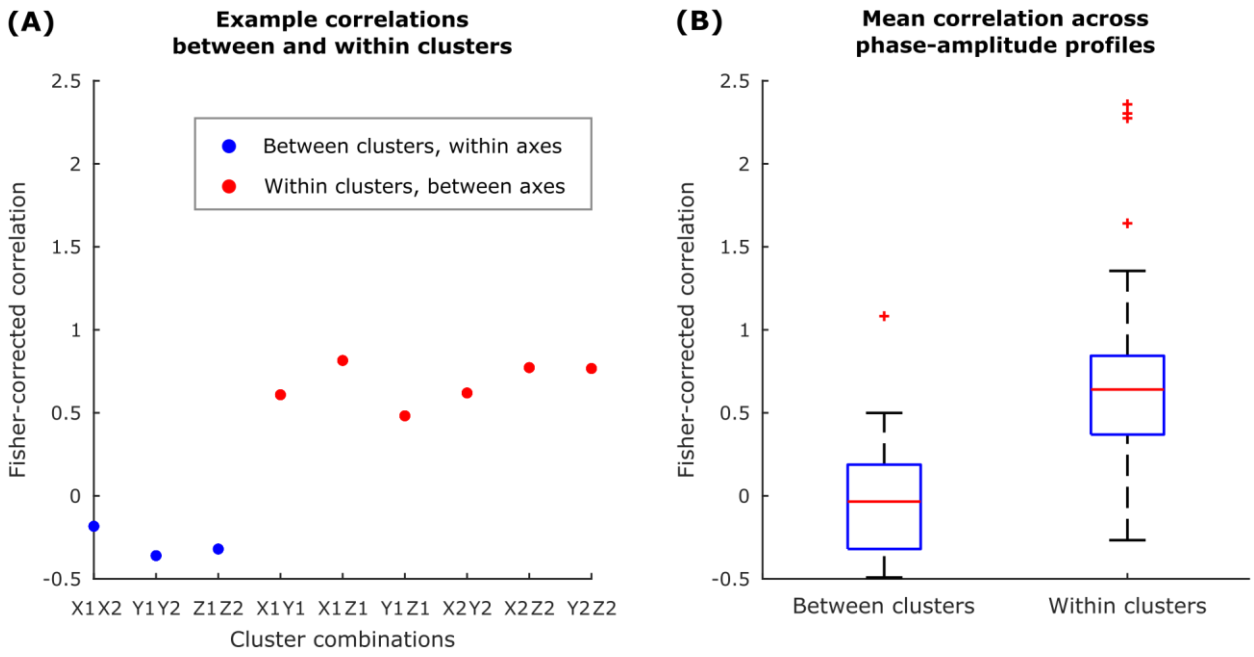


Figure 2.5: Fisher-corrected correlation between and within clusters. *(A) Example of the Fisher-corrected correlations for each cluster combination in one study participant. (B) Mean between and within clusters of the Fisher-corrected correlation across participants.*

	Significant suppression	**Significant amplification**	**Chance level**
Bins	12/828	16/828	3.45/1656
Plots	12/69	12/69	3.45/138
Participants	5/10	6/10	1/20

Table 2.2: Summary of number of instances with significant changes in tremor severity. *Reported values consist of the number of phase bins, plots and study participants displaying significant tremor suppression or amplification, as well as the number of bins and plots expected at the chance level considering that the Bonferroni correction was applied.*

2.3.4. Angle of stimulation

There was no systematically preferred suppressive or amplifying phase across study participants. *Figure 2.6* shows the number of phase bins across study participants and clusters for which there was significant tremor suppression or significant tremor amplification, at each of the 12 equally spaced stimulation phases (Rayleigh test resulted in p = 0.7204 for suppression and p = 0.2347 for amplification).

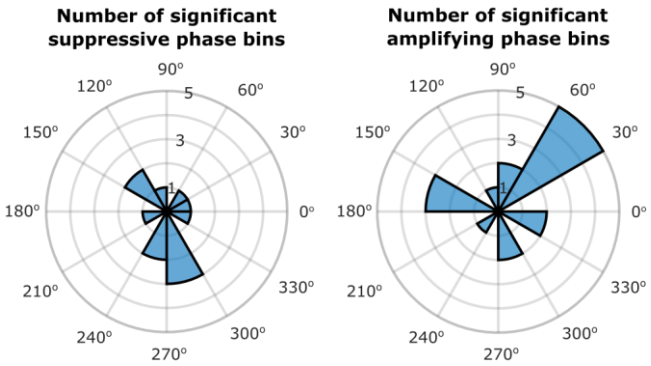


Figure 2.6: Rose plots indicating the number of phase bins for which there was significant tremor suppression or significant tremor amplification at each of the 12 equally spaced stimulation phases. *Rayleigh test for departure from circular uniformity resulted in p=0.7204 for suppression and p=0.2347 for amplification.*

Next, we considered re-aligned stimulation angles. As to be expected, separately aligning stimulation angles to the most suppressive or amplifying stimulation angle observed in each phase-amplitude profile produced non-uniform distributions at the group level (*Figures 2.7A and B*). However, stimulation and its surrogate data (*Figure 2.7C*) aligned to minima differed significantly, as did stimulation and surrogate data

aligned to maxima (F*igure 2.7D*). In the case of suppression, the 150- to 180-degree bins were significantly more likely to show amplitude reduction during stimulation than the surrogates were. Conversely, the 0- to 60-, 90- to 120-, and 240- to 330-degree bins were significantly less likely to be associated with amplitude reduction during stimulation than were the surrogates (*Figure 2.7D; Table 2.3*). The overall pattern was less distinct in the case of amplification, although the probability of amplitude increases and decreases during stimulation were significant in the 60- to 180-, 240- to 270-, and 300- to 330-degree bins, respectively. It should be noted that for both suppression and amplification, these groupings are placed approximately 180 degrees apart.

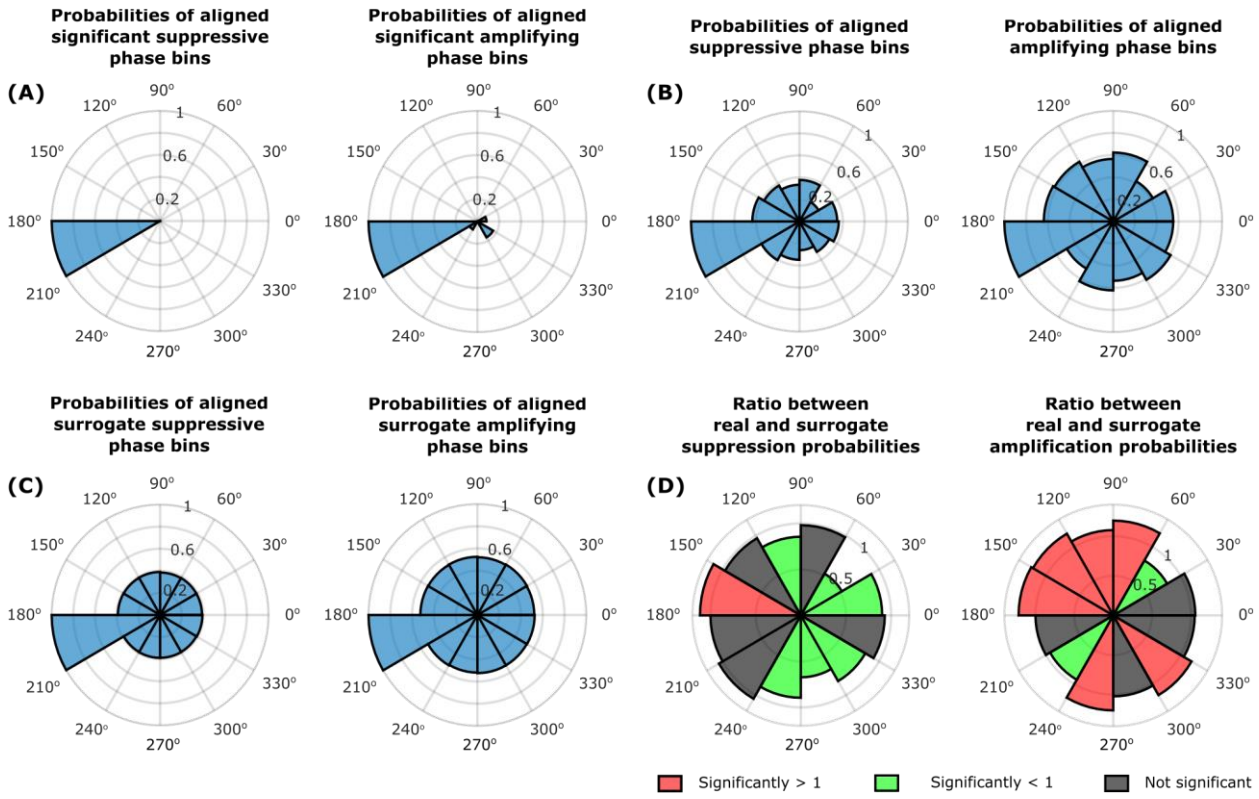


Figure 2.7: Probabilities of changes in tremor severity at each phase bin for real vs. surrogate data*. (A) Rose plots indicating the probability of significant tremor suppression or tremor amplification at each of the 12 equally spaced stimulation phases where the minimum suppression and maximum amplification angles were realigned to 180 degrees. Rayleigh test resulted in p = 2e-8 for suppression and p = 0.0002 for amplification. (B) Rose plots indicating the probability of tremor suppression or tremor amplification at each of the 12 equally spaced stimulation phases, regardless of whether tremor modulation was significant, where the minimum suppression and maximum amplification angles in all phase-amplitude profiles were realigned to 180 degrees. Rayleigh test resulted in p = 6e-6 for suppression and p = 0.0334 for amplification. (C) Rose plots generated from surrogate phase-amplitude profiles indicating the probability of tremor suppression or tremor amplification at each of the 12 equally spaced stimulation phases where the minimum suppression and maximum amplification angles were realigned to 180 degrees regardless of whether tremor modulation were significant. (D) Rose plots displaying the*

ratio between the real (B) and surrogate (C) probabilities of suppression or amplification in all phase-amplitude profiles, such that ratios significantly greater than 1 after FDR correction are shown in red, ratios significantly smaller than 1 are shown in green, and ratios that are not significant after FDR correction are shown in grey. Precise p-values are given in Table 2.3.

Phase	Suppression	Amplification
0	0.0071*	0.0425
30	0.0000*	0.0000*
60	0.5763	0.0000*
90	0.0001*	0.0055*
120	0.3972	0.0000*
150	0.0022*	0.0000*
180	1	1
210	0.1875	0.0273*
240	0.0045*	0.0000*
270	0.0000*	0.4148
300	0.0000*	0.0000*
330	0.0522	0.0836

Table 2.3: Statistical comparison between real and surrogate probabilities of change in tremor. *Reported significance values corresponded to Figure 2.7 where rose plots display the ratio between the real (Figure 2.7B) and surrogate (Figure 2.7C) probabilities of all phase bins. Significance values were obtained from paired-sample t-tests between the probability for*

*suppression or amplification for each study participant, axis, and cluster at each phase of the surrogate data, and the probability for suppression or amplification across all participants, axes and clusters for each phase of the real aligned data. *P-values that remain significant after correction by the FDR procedure.*

2.4. Discussion

We have provided evidence that Parkinsonian rest tremor of the hand often exhibits distinct oscillatory patterns, and that the output of a given tremor oscillator can be modulated in amplitude by peripheral stimulation at specific phases, although these critical phases differ between tremor oscillators.

2.4.1. Multiple tremor oscillators

The existence of independent oscillators driving different peripheral tremor components was inferred from the heterogeneity in the pattern of tremulous wrist movement in space, which could be divided into more than one pattern by principal component and cluster analysis in seven out of 10 subjects. The independent nature of these patterns or clusters was supported by cluster separation, significant differences in frequency distribution, significant differences in associated muscle activations and through differences in the phase-amplitude profiles observed during phase-locked peripheral nerve stimulation. Moreover, the mean correlations across phase-amplitude profiles indicate that the amplitude modulation patterns were more similar across different axes in the same cluster than across the same axis from different clusters. Clusters were dynamic with their likelihood of being dominant altering over time. The latter is in keeping with the inconstancy of coherence between neurons oscillating at

tremor frequency, and the inconstancy of the coherence between these neurons and background activity in the STN (Moran et al., 2008). Although Parkinsonian rest tremor is considered to represent the effect of independent oscillators in different limbs (Alberts et al., 1969; Ben-Pazi et al., 2001; Hurtado et al., 2000; P. E. O'Suilleabhain & Matsumoto, 1998; Raethjen et al., 2000), the current study suggests that central tremor oscillators could potentially adopt a much finer structure so that multiple oscillators may contribute to the tremor in a given hand. Electroencephalography and/or local field potentials should be evaluated in order to establish the link between central tremor oscillators and the changes in the pattern of tremulous wrist movement.

Could the presence of more than one cluster during stimulation be due to contamination of the tremulous wrist movements in space by a direct response to stimulation? This is unlikely as we only accepted clusters that were present both with and without peripheral nerve stimulation. In addition, significant differences in frequency and amplitude were found between clusters in the cluster division obtained from the recordings without stimulation. Furthermore, stimulation was performed at just below the motor threshold, so that direct responses were small and inconstant.

2.4.2. Contextual factors shape tremor dynamics

One key observation is that there was no systematic phase at which peripheral stimulation induced tremor amplification or suppression across study participants. Hence significant effects were only evident after phase-amplitude profiles were realigned to their maxima or minima. This was also the case with stimulation of the ventrolateral thalamus in people with essential tremor (Cagnan et al., 2017). It has previously been shown that median nerve stimulation can induce spiking activity in parts of the thalamus which are also implicated in tremor in PD (Hanajima et al., 2004; Maendly et al., 1981; Milosevic et al., 2018; Ohye & Narabayashi, 1979; Vitek et al.,

1994). Therefore, the precise effect of median nerve stimulation could be influenced by the conduction delays between the spindle afferents and the thalamus. Since stimulation is phase-locked to limb acceleration, the precise relationship between tremor and thalamic tremor cells could also impact stimulation effects (Brodkey et al., 2004; Milosevic et al., 2018). These sources of variation across participants could all contribute to the inconsistencies in stimulation phases that significantly modulated tremor (*Figure 2.6* and *Appendix A.1*). As demonstrated here, effective stimulation parameters such as the stimulation phase should therefore be determined individually to mitigate this variability across subjects. An open question is whether or not systematic phases will emerge at which stimulation induces tremor amplification or suppression should we quantify effects from EMG rather than accelerometer signals. However, this is not trivial as it requires identifying and recording EMG signals that are relatively selectively involved in one cluster or another. Challenges in recording quality EMG include contamination by stimulation artefacts. Additionally, EMG may be less practical than accelerometer signals for wearable therapeutic devices, as it requires the maintenance of wet electrodes, which can cause skin irritations and be less convenient.

We should also highlight two important assumptions made in our analysis. The first is that there are no more than two clusters each in the first or second principal components underlying rest tremor of the hand, although this assumption was supported by the distance between the clusters. Second, we assume that the activity of one cluster in each principal component dominates during each 5-second epoch of analysis. Although additional clusters cannot be excluded, their impact is likely to be small. However, we have little evidence to assume that a given cluster consistently dominates throughout each of the arbitrarily defined 5-second epochs of analysis. The presence of one or more additional active clusters within an epoch may again influence the phase at which any amplification or suppression effect predominates, and this

confound will not necessarily be addressed by considering EMG rather than accelerometer activity.

2.4.3. Phase-dependent modulation of tremor

At the individual level phase-amplitude profiles contained more bins with significant tremor amplitude amplification or suppression than could be accounted for by chance. Realignment of effects to the phase bin that afforded maximum amplitude reduction or increase in phase-amplitude profiles highlighted two groupings of phases, associated with significant decreases in the probability of suppression compared to surrogates and placed approximately 180 degrees apart. A comparable effect was evident with regard to the probability of stimulation induced tremor amplification. These observations raise the possibility that each TOP (or cluster) is underpinned by an oscillator with a frequency twice that of the limb tremor, and that peripheral stimulation is interacting with this harmonic. Such a harmonic could be centrally represented in line with the pattern of tremor modulation reported with phase-locked transcranial alternating current stimulation in people with Parkinsonian rest tremor (Brittain et al., 2013). Direct recordings of brain activity also point to a coupling of peripheral tremor to central oscillatory activity at twice tremor frequency (Gilron et al., 2021; Hirschmann et al., 2013; Timmermann et al., 2003).

The present results suggest that provided the dominant tremor oscillation is tracked in time, then phase-locked peripheral nerve stimulation may be able to attenuate tremor amplitude. For those subjects with one TOP, determining the stimulation phase to suppress tremor and continuously delivering stimulation phase-locked to this instance would be straightforward. However, the remaining participants in our cohort had two or more tremor components, the dominance of which fluctuated over time. Accordingly, successful stimulation would have to dynamically match the

phase to maximally attenuate tremor to the tremor component dominating at that moment in time, a relationship which could perhaps be established through machine learning. But that is not the only issue impeding the development of phase-locked stimulation at the wrist as a non-invasive therapeutic option. The degree of tremor attenuation achieved by phase-locked stimulation when this was maintained at the appropriate phase for 5-second periods is also modest (36% suppression). Sustaining stimulation at the optimal phase for longer may potentially improve the degree of attenuation (Brittain et al., 2013; Cagnan et al., 2017), as might searching for the optimal phase for attenuation with finer phase resolution and determining changes in tremor clusters with finer temporal resolution. Finally, given that coupling of peripheral tremor to central oscillatory activity may be at twice tremor frequency, then trials of stimulation that is phase-locked to this central harmonic are also warranted. This would require the determination of sensitive phases from phase-amplitude profiles derived by stimulating at twice the frequency of TOPs in the periphery.

2.4.4. Limitations of the current study

We have already alluded to the importance of polymyography when investigating any consistency between stimulation phases promoting maximal suppression and amplification of tremor amplitude. Evaluation of changes in central tremor oscillators through electrocorticography and local field potentials will be needed in order to confirm the relationship between peripheral changes in tremor form and central rhythms. Another related limitation of our analyses is that temporal resolution was 5 seconds which may be too coarse to capture rapid shifting between tremor clusters and is likely to only reveal which TOP dominates within each temporal window. This might also explain the complex form of many phase-amplitude profiles and why they have relatively wide confidence limits as the 5-second analysis windows may be capturing more than one tremor component. In addition, our cohort was

relatively small, and we did not investigate the effects of movement or posture on TOPs. It therefore remains to be seen whether these latter conditions change the precise distribution of spinal motor neurons recruited within a cluster, and thereby modify the tremor trajectory in space. Our small cohort also does not allow us to explore any relationship between disease progression or phenotype, and the number and organisation of tremor clusters. Finally, the occurrence of distinct tremor modes, characterised by changes in the dominant axis and significant differences in centre frequencies, may complicate accurate online phase estimation. This is particularly challenging when applying the zero crossings method to a single tremor axis under the assumption of a fixed tremor centre frequency.

2.4.5. Challenges and future directions

Tremor shows great variability within and across individuals. Peripheral stimulation parameters that effectively modulate tremor may therefore vary across people with PD and resting tremor, but critically may also vary in time as demonstrated in this study. In order to maximise peripheral stimulation efficacy, stimulation parameters should be optimised individually. Similarly, to account for potential changes in tremor form, which could influence efficacy of peripheral stimulation, parameters for this non-invasive therapy may need to be occasionally adjusted. Considering the vast number of parameter combinations (e.g., pulse width, amplitude, frequency and pattern), peripheral stimulation parameters may need to be optimised outside of the laboratory setting using a wearable peripheral stimulator that is capable of remote parameter optimisation. Such an adaptive system could also be used to track an individual's tremor form in real time using percentage tremor power in different accelerometer axes and adjust stimulation parameters accordingly to sustain stimulation efficacy. Automated parameter optimisation schemes such as Bayesian

parameter optimisation could be critical in this context in order to achieve parameter optimisation both across individuals and time (Grado et al., 2018).

2.5. Conclusions

We have provided evidence that Parkinsonian hand tremor may be the product of multiple oscillators leading to discrete patterns of acceleration in three-dimensional space. Oscillators tend to be sensitive to peripheral stimulation, and this leads to discrete patterns of stimulation-phase dependent suppression and amplification. These observations are important in helping to explain tremor variability, and need to be taken into account if phase-locked stimulation is to be developed as a potential therapeutic intervention to suppress Parkinsonian rest tremor (Brittain et al., 2013; Cagnan et al., 2017). In particular, the suppressive phase of stimulation may change according to which oscillator dominates at a particular moment in time. Similarly, certain phases, which also change according to distinct oscillators, significantly increase the tremor. The issue of multiple oscillators may be relevant to the development of treatments in other neurological disorders such essential and dystonic tremor, where phase-locked stimulation has been explored as a potential therapeutic technique (Cagnan et al., 2017; Holt et al., 2019; Peles et al., 2020).

3. Design of an adaptable, phase-tracking peripheral device

This chapter describes the state-of-the-art for real-time phase-estimation algorithms, our physical and software choices in the design of a wrist-worn phase-tracking device, as well as our system verification strategy and results. We thus present the two main innovations of our device: system portability and the phase tracker adaptability (tracking changes in the tremor's dominant axis and centre frequency). The software design described in this chapter was presented at an international conference.

Conference poster: *Arruda, B. S., Benjaber, M., Fleming, J., Denison-Smith, A., Toth, R., Sharott, A., McNamara, C., Denison, T., Cagnan, H., July 2022. Developing a wrist-worn system for online phase-tracking of pathological tremor signals and electrical stimulation delivery. In 2022 44th Annual International Conference of the IEEE Engineering in Medicine and Biology Society (EMBC), Glasgow, Scotland, UK.*

3.1. Background and system requirements

The laboratory-based system explored in the previous chapter had two major drawbacks linked to hardware and software.

First, the system described in *Chapter 2* was developed for use in a laboratory setting. It used various externalised elements, such as a filter, amplifier, analogue-to-digital converter, and computer. Those limited the utility of the system for longitudinal studies and for potential therapeutic interventions leveraging peripheral nerve stimulation. To investigate long-term effects of peripheral nerve stimulation, data acquisition for periods of time beyond the sporadic 1-hour-long sessions in a clinical

setting is required. As we envision eventual integration of this system in patients' daily lives, we must create a small, lightweight, and comfortable wearable device. The hardware therefore needed to be updated to address these limitations.

Second, the software needed to be rewritten—since our user needs dictated that the algorithm should be executed using a microprocessor alone without externalised amplifiers, converters, filters and software that can only run on desktop computers. The main innovation was to address the challenge described in the previous chapter: the high variability of tremor, reflected as changes in both the axis of maximum tremor excursion, as well as in the tremor frequency with highest power.

In summary, our work presented in this chapter consisted of developing a portable wrist-worn device that runs a phase-tracker adaptable to variations in tremor. The only element kept externalised was the electrical stimulator: we used a CE-marked device instead of an on-board implementation. Using a CE-marked system helped to streamline the ethics pathway. However, the system was designed such that it could also interface with an in-house built stimulator in future designs.

We verified the wearable system through three methods: algorithmically, using a vibration plate, and by wearing the device and performing tremor-like movements. We end this chapter discussing the verification results as well as future steps regarding testing this system in people with Parkinson's disease (PD).

3.1.1. Design requirements

The software and hardware selected for the portable wrist-worn device's design aimed at addressing our user needs. These system requirements are further described below and summarised in *Table 3.1*.

First, the system must support research investigating the effects of phase-locked peripheral electrical stimulation on Parkinsonian rest tremor. This investigation starts with recording tremor signals, occurring in three dimensions, using a triaxial accelerometer.

Second, phase of these tremor signals must be estimated in real time.

Third, the phase tracker must account for the input signal's variability as exhibited by Parkinsonian rest tremor (Arruda et al., 2021). The axis of largest tremor excursion, also called the dominant axis, can change, as well as the centre frequency of the signal. The study outlined in *Chapter 2* showed significant changes in centre frequency as well as the emergence of distinct tremor oscillatory patterns[1] (Arruda et al., 2021).

Changes in the dominant axis will lead to inaccuracies in the phase estimation, including potential loss of the phase reference. For instance, consider a scenario in which the tremor nearly vanishes along the axis currently being tracked for phase estimation (refer to *Figure 2.3A* in *Chapter 2*). This would result in a substantial decrease in the signal-to-noise ratio (SNR) of the reference signal. Concurrently, if the tremor increases in amplitude along a secondary axis, this axis would then become the dominant one. Such a shift poses a challenge for accurate phase tracking, as the system must adapt to these changes in tremor dynamics.

[1] Distinct tremor oscillation patterns were identified following cluster division, performed considering 5-second epochs of accelerometer-recorded tremor data. Clusters lasted 214.8 ± 136.8 seconds (mean ± SD) with significant median instantaneous centre frequency differences of 0.1 ± 0.2 Hz across clusters for each accelerometer axis. Median instantaneous frequencies ranged by 0.9 ± 0.5 Hz (mean ± SD) and up to 2 Hz across epochs of each axis, cluster, and participant.

Similarly, changes in the centre frequency, if not properly accounted for, can lead to phase estimation inaccuracies[2]. This aligns with previous findings that highlighted the variable period of PD tremor as a significant challenge in accurate phase estimation (Saifee et al., 2016). The phase tracker must be designed to adapt to frequencies in a range encompassing that of Parkinsonian rest tremor, typically observed around 3 to 7 Hz, with some accounts extending this range up to 8 Hz (Agapaki et al., 2018; Deuschl, Raethjen, et al., 2000). To ensure comprehensive coverage and add a 1 Hz safety margin, we have defined our frequency range of interest from 2 to 8 Hz.

Fourth, all elements for data collection, processing, and storage must be self-contained within a portable system, which could be used outside of a laboratory setting in its potential future applications. This portability would allow for longitudinal data recordings capturing long-term effects of stimulation, as well as for potential therapeutic use of the wearable system in the daily lives of people with PD.

Fifth, the system must be small and lightweight: it is a wearable device intended for use on the wrist and must be comfortably worn as a bracelet, without disrupting natural movements of the study participant. While there are technologies that aim to alleviate pathological tremor by imposing a weight on the upper limb, such as weighted feeding utensils (Sabari et al., 2019), the specific impact of those weighted devices on tremor is yet to be extensively quantified. Therefore, to prevent potential confounding effects, our wrist-worn system is designed not to significantly dampen tremors through its weight.

[2] In a MATLAB implementation of the zero crossings phase estimation method applied to a pure sinusoidal at 5 Hz, offsets of 1 and 2 Hz in the assumed centre frequency in relation to the actual centre frequency (5 Hz) led to phase errors of 18 ± 10 and 35 ± 21 degrees (mean ± SD), respectively.

Sixth, the system's storage capabilities must be sufficient to record data for the whole duration of the intended in-clinic tests (which last 48 min), including a safety margin.

Seventh, the fully-charged battery must last for the entire in-clinic tests, whose duration is also specified in protocols, and include a safety margin.

Eighth, the sensor must detect oscillations with amplitudes at the minimum levels deemed adequate for phase estimation in *Chapter 2* (refer to *Section 2.2.1—Cohort*)[3]. This corresponds to a mean tremor envelope of approximately 0.4 m/s^2, or 0.04 g (Arruda et al., 2021).

Finally, the system's phase estimation error must consistently stay below the target phase resolution. With an anticipated phase resolution of 60 degrees, the system requires a maximum mean phase error below 30 degrees to ensure distinct stimulation delivery across the six target phases (0 to 300 degrees). This error margin also takes into account the phase resolution constraints imposed by storage and sampling rate limitations, necessary for the duration of our intended protocol. Further details on protocol and software choices influencing resolution will be discussed in *Section 3.3—Software design*.

[3] Participants whose tremor levels were below those reported in Table 2.1 were excluded from the data analysis in Chapter 2, as their tremor amplitude was deemed too low for reliable phase estimation.

Supported therapy research	The device supported research investigating the effects of phase-locked peripheral electrical stimulation on Parkinsonian tremor.
Phase estimation algorithm	Phase tracker that operates in real-time on accelerometer-recorded signals.
Adaptability to tremor variations	Algorithm's adaptive element accounted for changes in the tremor dominant axis and centre frequencies ranging from 2 to 8 Hz.
Portability	All elements for data collection, processing, and storage implemented as a portable system.
Comfortable physical design	Small and lightweight system, comfortably worn as a bracelet.
Data storage	Sufficient memory for the duration of the intended in-clinic tests (48 minutes), with a safety margin.
Battery life	Sufficient battery for the duration of the intended in-clinic tests, with a safety margin.
Signal level	Ability to detect tremors corresponding to the minimum levels deemed suitable for phase estimation, in line with previous studies (mean envelope ~0.04 g).
Phase error	Phase estimation by the algorithm with a maximum mean phase error of less than 30 degrees.

Table 3.1: User needs informing the design of the wrist-worn system.

This wearable device is intended for peripheral electrical stimulation, interfacing with a human study participant. Therefore, we needed to account for potential risks and their mitigations when designing the system. Risk mitigations, aimed at ensuring study participant safety and device integrity, are summarised in *Table 3.2*. These measures were implemented to both ensure the comfort of study

participants during testing and maintain the physical integrity of the device. Additionally, we aimed to mitigate risks associated with the wearable system's use in individuals with implantable devices, as well as to prevent any issues that might arise from misuse.

Stimulation limits	Stimulation amplitude was increased manually, gradually, in 0.1 mA incremental steps, continuously asking for verbal feedback from the study participant regarding whether the levels were comfortable. Stimulation levels were capped at 10 mA to ensure participant comfort during certain stimulation settings.
Prevention of current surges from the USB port	The design ensured that the device did not need to be connected to any external chargers or computers while in use by a participant. The battery and memory lasted beyond the duration of a recording session, thus charging or data transfer would not occur while the device was attached to the participant.
Safety of participants with implantable devices	The screening criteria eliminated from the study any participants with an implantable device to ensure their safety.
Prevention of injuries resulting from device misuse	Testing was conducted in controlled conditions under close inspection of the experimenter. Stimulation was only turned on while the device was securely placed on the participant's wrist. A serious risk would be short-circuiting the device across the participant's heart if they held the electrode poles with both hands.

Table 3.2: Risk mitigations for the wrist-worn system investigational use on people with Parkinson's disease.

3.1.2. Phase estimation methods

Real-time phase estimation is crucial to the functionality of our wrist-worn system. Parkinsonian rest tremor, inherently non-sinusoidal and variable in period, is often treated as a sinewave with a single dominant frequency for simplicity in phase estimation (Chan et al., 2022; Saifee et al., 2016; Vaillancourt & Newell, 2000). This approximation allows for the application of traditional phase estimation techniques, however, these methods struggle to accurately represent the phase dynamics of tremor signals exhibiting complex non-sinusoidal features. Consequently, the assumption of sinusoidal behaviour necessitates extensive filtering to address noise and the harmonics commonly found in tremor signals. An additional challenge posed by Parkinsonian tremor signals is their variability in amplitude, as reflected by changes in dominant axis, as well as in centre frequency, requiring an adaptive component to this filtering. This subsection explores characteristics of three phase tracking methods, leading to the selection of a technique particularly well-suited to meet the unique requirements of our system.

Zero Crossings

The phase-tracking system discussed in *Chapter 2* employed a simple method based on the zero crossings (Arruda et al., 2021; Reis et al., 2021). In simple terms, it consists of identifying the points at which the band-pass filtered signal crosses zero and whether these zero-crossings indicate a change in the signal in a positive or negative direction. If we take a sinusoidal waveform, four points can be easily identified: the signal's peaks and troughs (which are the zero crossings of the differentiated signal) as well as its mid-rising and mid-falling (*Figure 3.1*). Thus, this is a method of simple implementation and light computation.

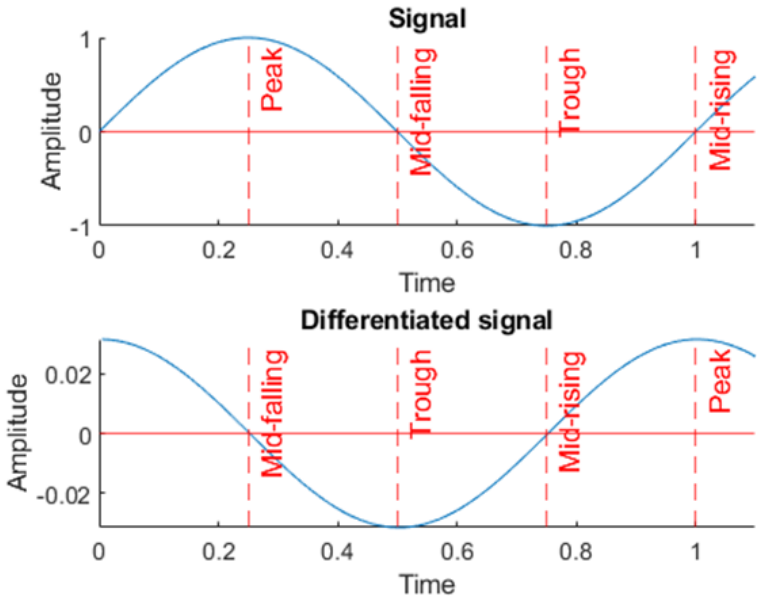


Figure 3.1: Zero crossings of a signal and its differentiation*. The signal's peak, mid-falling, trough, and mid-rising can be identified from its zero crossings and those of the differentiated signal.*

For more complex oscillations, the method depends on identifying the most prominent frequency and approximating the signal as a sinewave at that frequency. The method then assumes that the waveform is sinusoidal and crosses zero at regular intervals, and estimates phases by considering the expected elapsed time between the zero crossing and each target phase.

It is important to note that the technique does not contain any method for estimating the signal's centre frequency. Instead, this frequency must be defined a priori, for example, by performing a baseline recording, computing its power spectral density, and identifying the frequency with the highest power. If the centre frequency

fluctuates, which can happen in Parkinsonian tremor, inaccuracies are introduced in the phase estimates.

Additionally, the zero-crossing method requires the signal to be band-pass filtered around the expected centre frequency. Band-pass filtering makes the method more reliable because it reduces noise, which can introduce false zero crossings and lead to inaccurate phase estimation. The filter reduces interference from frequencies other than that of interest as well as from harmonics of the centre frequency.

However, the band-pass filter introduces phase delays, which can cause a misalignment between the processed signal and the real-time tremor events. While stationary time delays can be characterised and compensated for, accurately aligning the signal in real-time scenarios remains challenging. Additionally, the filtering process may lead to signal alterations, particularly considering that a band-pass filter constrains the signal around a fixed centre frequency, which may not accurately represent the naturally fluctuating dominant frequency of Parkinsonian tremor.

Hilbert transform

Another widely used phase estimation method is the Hilbert transform, which provides the ground-truth, instantaneous phase of an oscillation (Cohen, 2014). In the context of phase tracking an analytic signal, the Hilbert transform corresponds to its imaginary component. The instantaneous phase, $\phi(t)$, of a real-valued signal $x(t)$ is calculated from its Hilbert transform, $H(x(t))$, as: $\phi(t) = tan^{-1}\left(\frac{H(x(t))}{x(t)}\right)$. This technique provides accurate estimates for non-sinusoidal signals, as well as for oscillations with amplitude and frequency fluctuations.

This procedure is highly sensitive to noise, which can significantly affect its accuracy in unfiltered data. In the presence of substantial noise, the Hilbert transform

estimates the phase over the noise as well, severely compromising the phase estimation accuracy. Therefore, the Hilbert transform must be preceded by a band-pass filter around the signal's frequency of interest, applied forward and backward to prevent phase shifts (Cohen, 2014). *Figure 3.2* shows a signal (noisy, forward band-pass filtered, and forward and backward band-pass filtered) along with its Hilbert transform for each scenario.

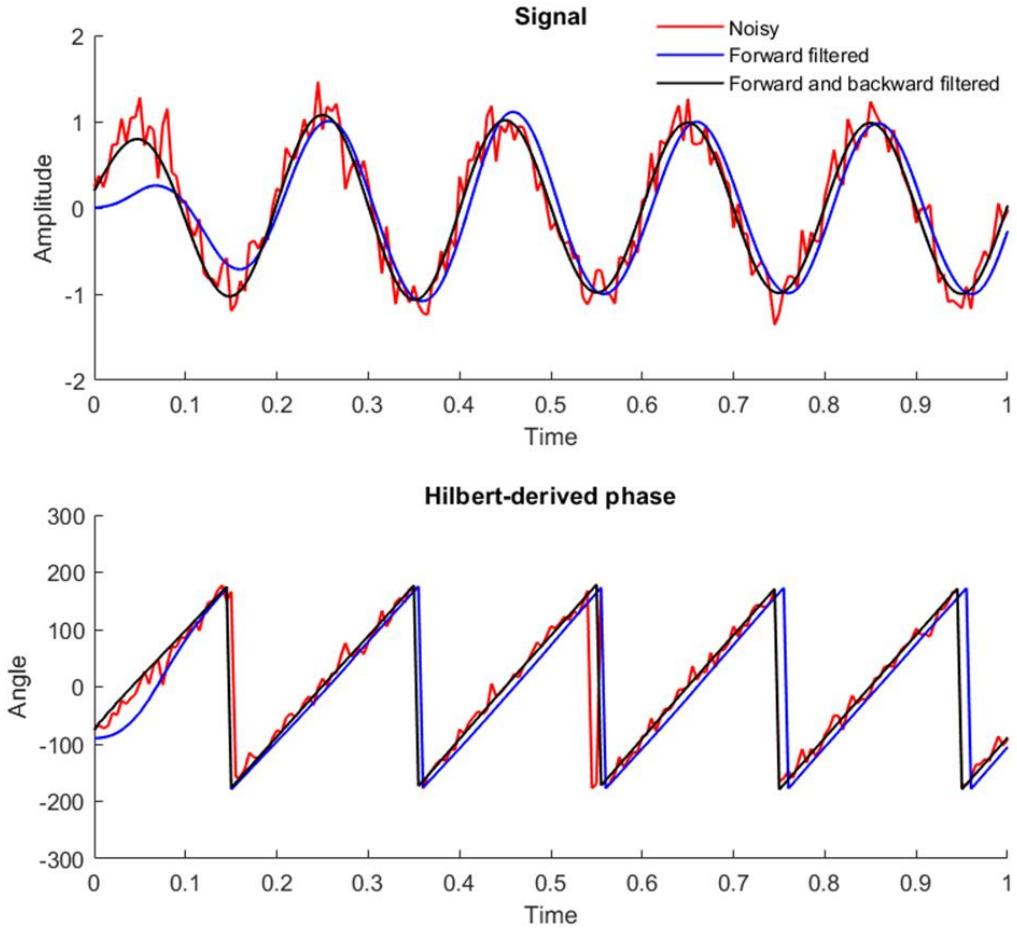


Figure 3.2: Example signals and their respective Hilbert-derived phase estimates*. Signals are displayed in its noisy (raw) form, forward band-pass filtered, and forward and backward*

band-pass filtered, along with their respective instantaneous phases as derived from the Hilbert transform.

Although the Hilbert transform is extensively used in offline data analysis, implementing it in real-time phase estimation is challenging because this approach is inherently non-causal, meaning that the system outputs depend on both past and future values of the signal.

Still, several researchers developed online phase-tracking methods involving the Hilbert transform (Blackwood et al., 2018; Chen et al., 2013; Schreglmann et al., 2021; Zrenner et al., 2018, 2020). One such technique involves correcting signal edges using a causal band-pass filter applied to the analytic signal's discrete Fourier transform (Schreglmann et al., 2021). This filter selectively reduces distortion and maintains continuity between signal ends. In contrast, other approaches are computationally heavy, typically requiring higher order filters, and involve forward predicting the data using autoregressive models and estimating the instantaneous phase by applying the Hilbert transform to the prediction (Wodeyar et al., 2021; Zrenner et al., 2018, 2020).

State-space models

There are other methods to estimate phase online, called state-space models. These models describe how a system evolves over time, accounting for its underlying dynamics. State-space models have two main elements: (i) an observation equation, representing the measured values of the system—encompassing, for example, noise—and (ii) a state equation, attempting to capture internal values of the system—for

example, its instantaneous phase to be estimated. They model rhythms as a noise-driven harmonic oscillator, explicitly separating signal from noise (Matsuda & Komaki, 2017; Soulat et al., 2022; Wodeyar et al., 2021).

In practice, the state equation represents the real and imaginary components of the complex, analytic signals with each state variable corresponding to an oscillator at a fixed frequency. The state equation takes in the analytic signal and rotates it at that frequency, whereas the observation equation sums the real component of that signal, resulting in the prediction. From the rotating phasor corresponding to the real and imaginary components of the signal, we directly calculate the estimated phase and magnitude of an oscillation (Wodeyar et al., 2021).

State-space models typically apply a Kalman filter, which makes them particularly effective at accounting for noise in the system. A Kalman filter is a recursive algorithm used to optimise the phase estimate by comparing a value predicted by the model with the observed value, including noisy observations. There are two assumptions required for use of a Kalman filter, which, strictly, are held by state-space models: (i) the observation and state equations are linear; and (ii) the observation noise as well as the state covariance are Gaussian (Kalman, 1960; Wodeyar et al., 2021).

These models are computationally lighter than phase estimation approaches related to an online Hilbert transform incorporating autoregressive forecasting. Additionally, unlike the zero crossings method and the Hilbert transform, state-space models do not require isolating a narrowband of the signal through a band-pass filter a priori. Instead, the state-space model on itself isolates a band of interest, which is determined based on a user-defined scaling factor and target centre frequency. This target frequency is set in alignment with the expected centre frequency of the input signal. Also, because state-space models treat noise and signal separately, they avoid

folding noise into the estimate, reducing its impact (Wodeyar et al., 2021). Still, state-space models typically consider a fixed centre frequency, whereas the dominant frequency of the input signal may fluctuate, introducing errors in the estimate.

Here, we chose our phase estimation approach: a simplified state-space model, which functions as a modified Kalman filter but does not include the component corresponding to the estimate of the Kalman gain (McNamara et al., 2022). Instead, the gain factor is empirically derived, ensuring lighter computation more suitable for wearable device implementations. Additionally, the original model was validated empirically, rather than through formal mathematical demonstration of traditional Kalman filter assumptions, such as linear observation and state equations, and Gaussian observation noise and state covariance.

The key factors influencing our choice were the adaptability of this method, as it tolerates unstable, noisy oscillations without requiring intensive filtering beforehand, and its computational efficiency, facilitating implementation in a wearable device. We extended the algorithm by incorporating adaptive elements to account for the variability of Parkinsonian tremor, as discussed in *Section 3.3—Software design*.

In making this decision, we weighed the trade-offs between computational complexity, adaptability, and accuracy, ultimately prioritising the ability to handle noisy oscillations and the feasibility of implementation in a wearable device. A full Kalman approach was not used due to its heavier computational burden and the requirement for formal mathematical assumptions that may not hold in the context of Parkinsonian tremor.

Next, we will explore the physical design of this miniaturised system for phase-locked peripheral nerve stimulation, followed by the system's software design.

3.2. Physical design

3.2.1. Hardware

Hardware components were chosen aiming at minimising device size while allowing for sufficient memory, battery life, and processing power to estimate phase and run intended experimental protocols. Key components used to build the wrist-worn system are listed below and outlined in *Figure 3.3*.

(i) A Teensy 4.0 development board. The board was selected for its compact size (approximately 18x36x5 mm) and high performance, featuring an ARM Cortex-M7 processor running at 600 MHz. The elapsed time for each loop of the software was consistently below 100 µs, well within the minimum requirement imposed by the sampling rate of 208.03 Hz, which implied an elapsed time of 4807 µs.

(ii) An Adafruit LSM6DSRTR triaxial accelerometer. This sensor measures linear acceleration in the ranges, specified by the user, of ±2, 4, 8, or 16 g (where 1 g equals 9.80665 m/s^2). The range was set to ±16 g to prevent the detection of minor vibrations that could introduce noise into the data. This setting was also found to be adequate for detecting signals at the minimum predicted tremor levels.

(iii) A W25Q128JVSIQ SPI flash memory chip with 16 MB capacity, sufficient for the duration of one 48-minute-long recording session.

(iv) Two push-buttons, implemented to start or stop distinct stages of the experimental protocol upon a button press.

(v) A Red-Green-Blue (RGB) light emitting diode (LED), which provided visual feedback to the experimenter regarding whether the distinct protocol stages were successfully initiated or stopped.

(vi) A 3.7 V, 500 mAh Lithium Polymer battery, with a compact size and providing charge sufficiently beyond the requirement (48 minutes) for the duration of one testing session.

(vii) A custom-printed circuit board (PCB) integrating all components.

The PCB, designed for minimal size, was circular shaped (*Figure 3.4*). This system was designed by an engineer working with the team (Moaad Benjaber).

The hardware was designed to send transistor-transistor logic (TTL) pulses to either a CE-marked externalised stimulator box (Digitimer Constant Current Stimulator DS7A), or an in-house built electrical stimulator with a 100 V power supply[4], to deliver stimulation of up to 10 mA through stainless steel bar dry electrodes. Due to time constraints for implementing and safely testing an in-house built stimulator in this thesis, a CE-marked stimulator was used as the only non-portable element.

[4] The 100 V power supply voltage requirement was defined based on the skin-electrode impedance, which was measured from six people at the desired stimulation levels (just below the current amplitude that evoked visible muscle activation). For dry, stainless steel electrodes with conductive paste, the voltage compliance was 82 ± 34 V (mean ± SD), and for dry, stainless steel electrodes without conductive paste, it was 96 ± 31 V (mean ± SD).

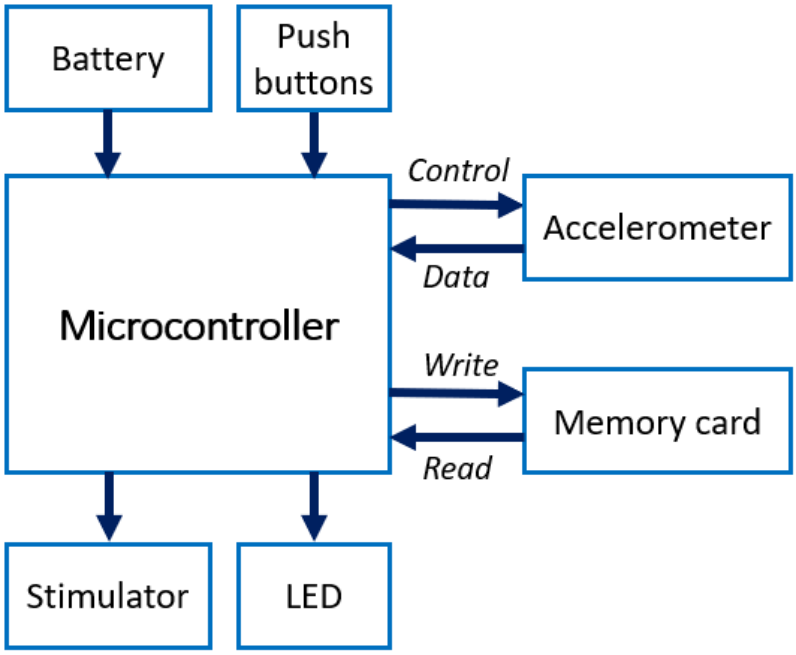


Figure 3.3: Block diagram showing hardware components of the wrist-worn system. *The microprocessor board interfaces with a triaxial accelerometer, a memory chip, an RGB LED, two push buttons, a battery, and a stimulator.*

The battery could be charged through a magnetic connector on the PCB while connected to it, or externally while disconnected from the system. When fully charged, the battery lasted for 4 hours, which was well beyond the safety margin required for the approximately 1-hour-long in-clinic test.

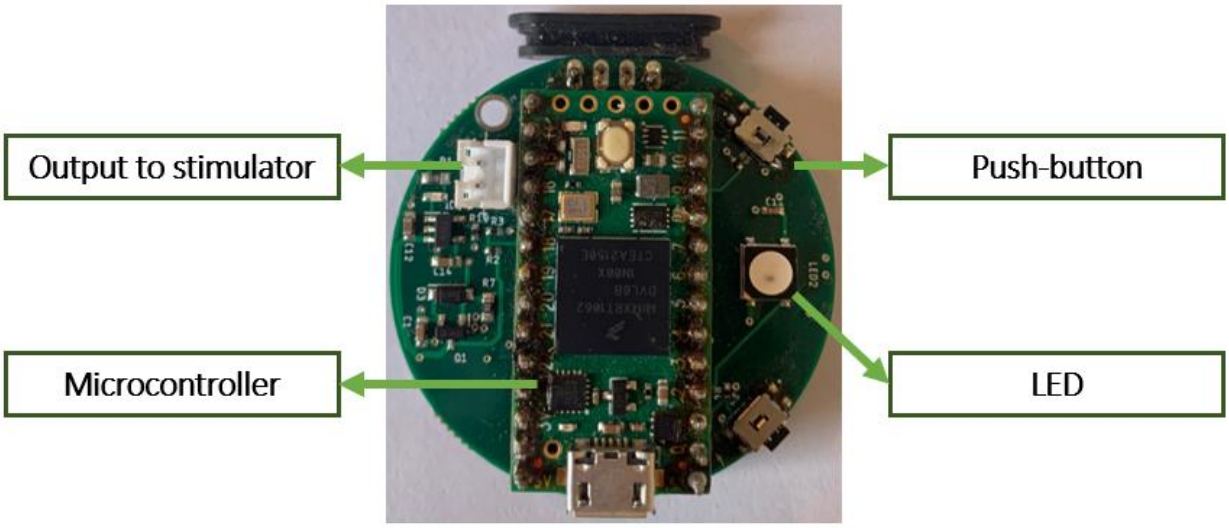


Figure 3.4: The circular-shaped PCB.

3.2.2. Enclosure

An enclosure was designed and 3D-printed to house all system components, with the exception of the externalised stimulator, and built to tightly fit around the circular-shaped board. The enclosure parts were printed in acrylic butadiene styrene (ABS) plastic using a fused deposition modelling 3D-printer (Stratasys F170). ABS plastic, known for its safety and non-toxicity for direct skin contact, is commonly used in 3D prototyping. It is also valued for its durability and cost-effectiveness (Harris et al., 2015).

The enclosure contained four components (*Figure 3.5*): (i) a circular base, with one small tower to which the board could be secured; (ii) an open cover, which tightly clipped on to the first component and allowed for easy visualisation of the LED, as well as for cables to exit the system and connect to the externalised stimulator; (iii) and two push buttons in-between the other two elements.

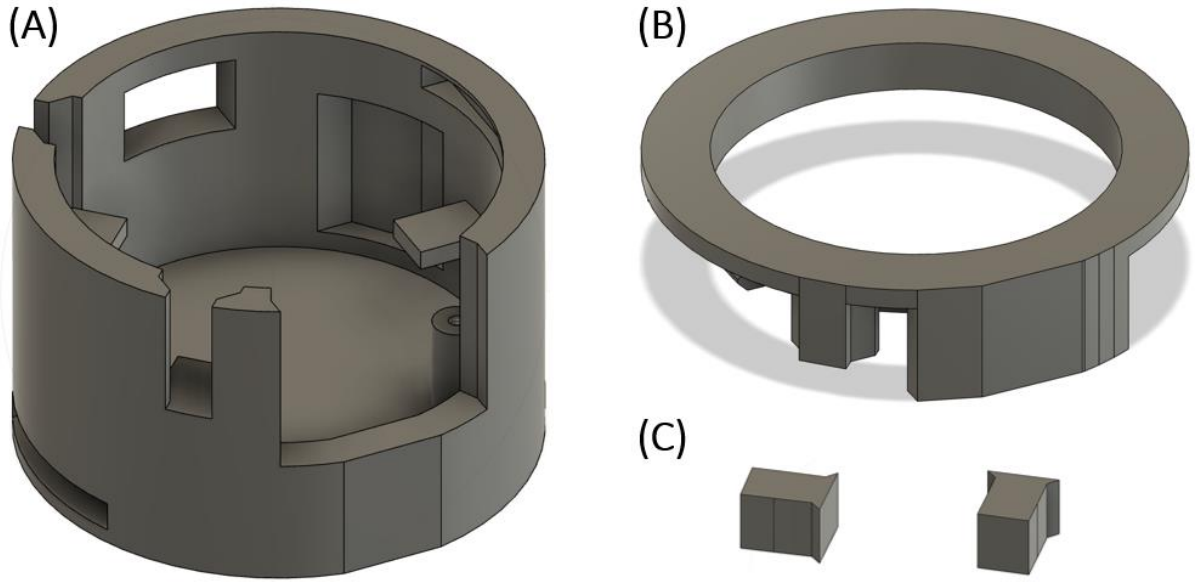


Figure 3.5: The wrist-worn system's 3D enclosure design. *(A) The base; (B) the open cover; and (C) the two push buttons.*

The enclosure base and cover were attached by a snap-fit mechanism. There were three supports parallel to the base, aligned with the tower, and the board was placed on them. The tower led to a gap in between the circuit board and the bottom of the enclosure, and the battery was placed in this gap, securely attached to the base with strong double-sided tape. This design ensured that none of the components would move around the enclosure during the experiment, which was important to prevent artefacts in the accelerometer data.

The push buttons directly contacted the switches in the board. Two holes on the side of the enclosure allowed for connection with a micro-USB cable and a magnetic charger. There was a gap in the base for placement of the wristband. The bar electrodes were also placed around the wristband. The side of the enclosure was carved at the

point that aligned with the battery connector, as it slightly exceeded the size of the board, to avoid damaging the connector by pushing it against the wall. The overall enclosure design was aimed at minimising its size.

3.3. Software design

3.3.1. Overview

The central component of the software consisted of the phase estimation algorithm, based on an existing phase tracker originally written for an integer implementation (McNamara et al., 2022). We redeveloped this algorithm in single-precision floating-point, first in an offline (non-causal), MATLAB-based version, and then in an online, C++-based version, using the Arduino IDE (version 2.0.3).

Our main contribution to the existing phase tracker was to add a self-tuning strategy which allowed the system to adapt to changes in the tremor axis of maximum excursion (dominant axis) and centre frequency.

Additionally, our system features included signal pre-processing in real-time (preceding its use by the phase-tracker); a method to calculate changes in tremor severity online (using an estimation of the tremor envelope); data saving to the memory card; as well as a user interface.

Data was sampled and stored at a rate of 208.03 Hz. This rate, the highest allowed by the memory constraints of our system, was selected from the options provided by the 'Adafruit_LSM6DOX' Arduino library used for the sensor. The choice of this rate was guided by the need to store data for up to 48 minutes of recordings, while also aligning with the accelerometer sampling rate options defined in the library. It is important to note that this sampling rate is significantly above the minimum value

stipulated by the Nyquist theorem. With the maximum centre frequency of interest being 8 Hz, to prevent aliasing and accurately sample a signal, the Nyquist theorem dictates a minimum sampling rate of twice this frequency, or 16 Hz. Additionally, considering the system's design to target six possible phases (ranging from 0 to 300 degrees at 60-degree intervals), the signal should ideally be sampled at least six times the Nyquist rate, amounting to 96 Hz. Therefore, our chosen sampling rate of 208.03 Hz satisfactorily exceeds these minimum requirements.

3.3.2. Phase estimation algorithm

The online phase tracker utilised a modified Kalman filter implemented in single-precision floating-point. The original algorithm (McNamara et al., 2022) employed integer operations to estimate neural oscillation phases, allowing its use in less powerful microprocessors. However, this approach limited performance due to the need for data type conversions, resulting in accumulated errors. To address this, we adapted the algorithm to a floating-point implementation.

Following the state-space model framework, the algorithm represented the analytic signal (x_{est}), with its real and imaginary components, as a vector rotating in the two-dimensional space at the reference frequency (f_c) and defined by sine and cosine waves centred at that frequency (*Figure 3.6*).

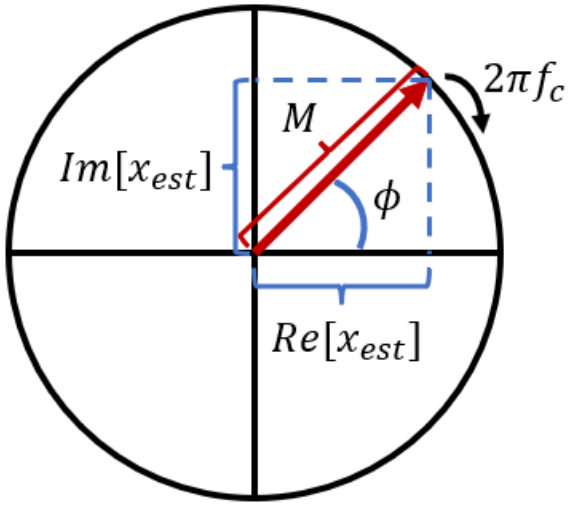


Figure 3.6: The rotating analytic signal in a two-dimensional space. *The signal's real component is represented along the horizontal axis and the imaginary component along the vertical axis. From those components, the phase (ϕ) and magnitude (M) can be calculated.*

The real component of the analytic, estimated signal is recursively subtracted from the input signal (x_{in})—or the observed value—defining, for each time step (t), an error term (e). This error, a measure of how much we can trust the model, is used to adjust the signal estimate, as in *Equation 3.1*:

$$e(t) = x_{in}(t) - Re[x_{est}(t)] \quad \text{(Equation 3.1)}$$

The estimated signal can then be decomposed into a rotating phasor defined by two components, 90 degrees out of phase, called a and b. The real and imaginary components are thus calculated at each time step t, as in *Equations 3.2* and *3.3*.

$$Re[x_{est}(t)] = a(t) \cdot sin(2\pi f_c t) + b(t) \cdot cos(2\pi f_c t) \quad \text{(Equation 3.2)}$$

$$Im[x_{est}(t)] = b(t) \cdot sin(2\pi f_c t) - a(t) \cdot cos(2\pi f_c t) \quad \text{(Equation 3.3)}$$

For each time step t, the real and imaginary components, as previously described, are calculated based on the error term derived from the preceding time step $(t-1)$. This process is represented in *Equations 3.4* and *3.5*.

$$a(t) = a(t-1) + G \cdot e(t-1) \cdot sin\,(2\pi f_C \cdot t) \quad \text{(Equation 3.4)}$$

$$b(t) = b(t-1) + G \cdot e(t-1) \cdot cos\,(2\pi f_C \cdot t) \quad \text{(Equation 3.5)}$$

Those components, a and b, capture the rotation of the phasor and characterise the state equations, encompassing the system's underlying dynamics—their phase and magnitude. The phase can then be recalculated as the two-argument arctangent of Re and Im, as shown in *Equation 3.6*:

$$\phi = atan2(Im[x_{est}\,(t)], Re[x_{est}\,(t)]) \quad \text{(Equation 3.6)}$$

The signal's magnitude can also be obtained from the real and imaginary components as in *Equation 3.7*.

$$M = \sqrt{Im[x_{est}\,(t)]^2 + Re[x_{est}\,(t)]^2} \quad \text{(Equation 3.7)}$$

In this model, G is a fixed value which can be thought of as an analogue to the Kalman filter gain. This real-valued term is between 0 and 1, and it multiplies the error used to recursively adjust the model. A low G reduces the error's impact in adjusting the model whereas high G increases the error's ability to adjust the estimate. Thus, in a hypothetical scenario of high trust in the model—for example, if x_{in} being tracked is a nearly sinusoidal wave with minimal noise—G should be close to zero. Similar to the gain of a Kalman filter, the value of G must be chosen to minimise the phase estimation error. This error can be determined by comparing the phase estimated by the model to that derived from the gold-standard Hilbert transform. A variety of gain values was

tested for Parkinsonian rest tremor as inverse powers of 2, and the phase estimates obtained with them were compared with the Hilbert-derived phases. Through this trial-and-error process, 0.25 was selected as the optimal choice, as it demonstrated the closest performance to the Hilbert transform.

In practice, the model operates as an adaptive band-pass filter whose width is defined by G and should be chosen according to the noise levels of the system. As a result, x_{in} does not need to be band-pass filtered a priori. However, for the model, the input signal should be centred around zero. If the signal has an offset, for example due to unfiltered DC components, this will interfere with the model and the phase estimate. Therefore, the signal must be high-pass filtered at a low corner frequency for offset removal prior to being input to the phase tracker.

Figure 3.7 summarises the algorithm, including the equations utilised.

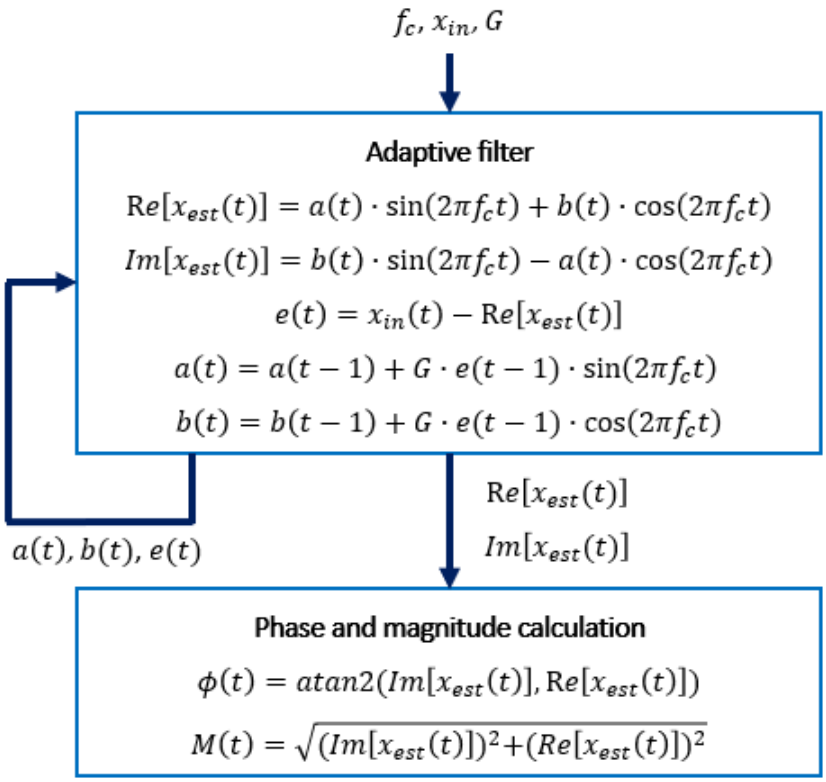


Figure 3.7: Phase tracking algorithm core operations. *The input signal is compared to an estimate generated from the sine and cosine waves centred at the frequency of interest. The error, corresponding to the difference between these signals, adjusts the signal's estimate. The phase and magnitude are obtained from the estimate's real and imaginary components.*

3.3.3. Adaptive strategy accounting for tremor's variability

For our wrist-worn device application, x_{in} consists of accelerometer-recorded Parkinsonian rest tremor oscillations. Those signals correspond to the triaxial acceleration occurring as the user moves their arm in space. Tremor happens in three dimensions, and the dominant axis can fluctuate over time, thus the axis used as x_{in} needs to be adjusted accordingly. Additionally, the tremor centre frequency may also

change and f_c must adapt to that, in order to ensure that the model operates at the frequency closest to that of the signal.

We accounted for the variability of tremor by implementing a self-tuning, adaptive strategy. This new component consists of running in parallel various streams of the phase tracker, each of them corresponding to one combination of tremor axis, used as x_{in}, and f_c, within the target tremor signals' band of interest.

As our implementation focused on Parkinsonian rest tremor, typically occurring from 2 to 8 Hz, we considered f_c values within that range and with 1 Hz resolution, thus resulting in seven possible input frequencies. Those were run for each of the three axes (x, y, z), all high-pass filtered for offset removal, amounting to a total of 21 phase estimation streams continuously processed in parallel (*Figure 3.8*). Due to processing limitations, the frequency resolution was maintained at 1 Hz, and only seven centre frequency values were considered. The chosen frequency resolution was sufficient to meet our preset phase error requirements and running more parallel streams would have caused the system to overflow.

We chose to use parallel streams instead of restarting the algorithm periodically for different parameters to avoid reintroducing time delays and a phase estimation start-up error. In C++, the 21 phase estimation streams were run in parallel as 'queue' objects defined within a class.

One optimal phase tracking stream was chosen periodically at certain timings, accounting for the specifics of the testing protocol. In the intended tests with study participants, phase-locked stimulation would be delivered in blocks, each of them at a single phase and lasting 10 seconds, preceded by a 10-second break without stimulation. Stream selection therefore occurred prior to the start of each 10-second

stimulation block and the chosen axis was kept throughout the block, to avoid switching the phase reference mid-block.

Before each stimulation block begins, the dominant axis is selected as the one with the largest moving average, μ_{axis}, of the absolute value of the signal's amplitude over the previous 10-second window, as summarised in Figure *3.8A*. The moving average provides a low-pass filtered metric of the axis amplitude. *Figure 3.9*, in turn, exemplifies the dominant axis selection based on the moving average for three test sinewaves, out of phase. The blue signal started with the largest amplitude, then it was overtaken by the red signal. Initially, the phase tracker continued considering the blue signal, but once the red signal's moving average became the largest, the phase tracker adapted accordingly.

Similarly, f_c is determined by first computing, for each of the seven frequency streams, the absolute value of e, the error signal corresponding to the difference between x_{in} and x_{est}. The 10-second moving average (μ_{error}) is taken again, but now from the absolute value of this error. As the error reflects how well the estimated analytic signal represents the measured signal, the phase estimation stream with the smallest moving average corresponds to the one closest to the centre frequency of x_{in}. For the axis already identified as the dominant one, f_c was then selected as the one corresponding to the stream with the smallest μ_{error} (*Figure 3.8B*). Phase tracking is then locked to this stream and subsequently used for stimulation.

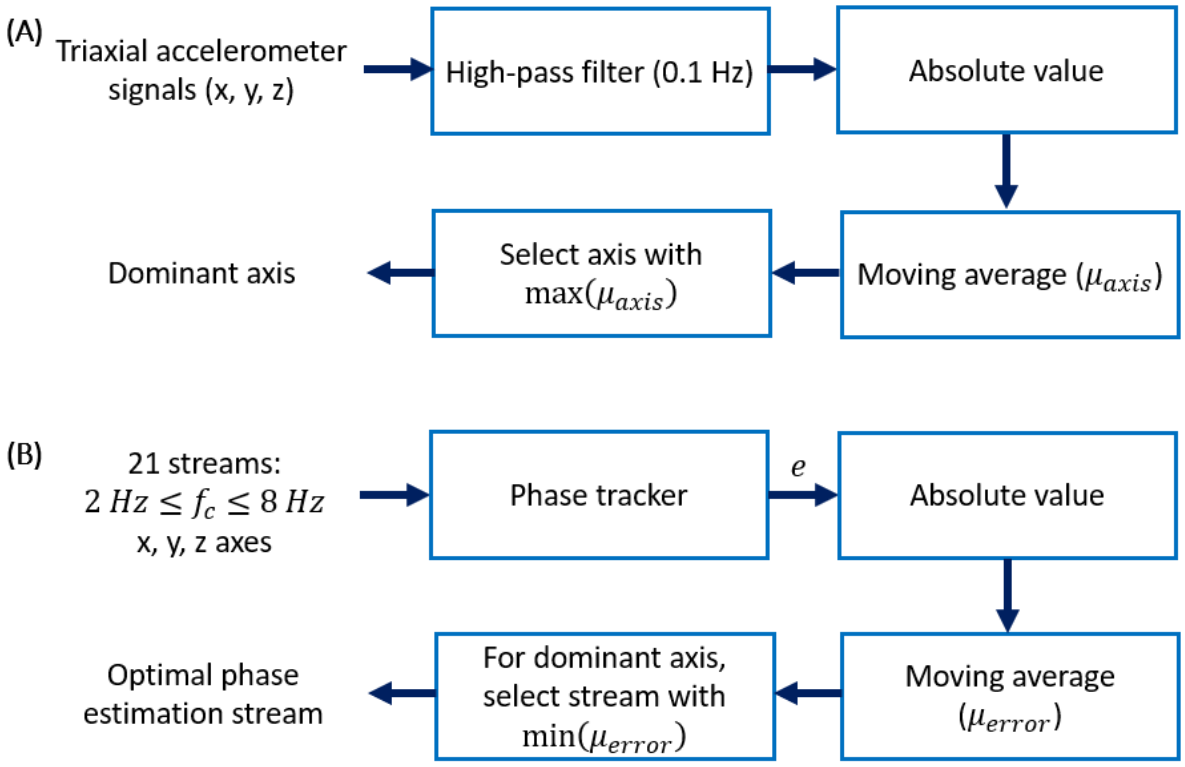


Figure 3.8: The self-tuning strategy to select the dominant axis and centre frequency best corresponding to those of the tremor. *(A) Dominant axis selection strategy based on the absolute value of the input signal's moving average. (B) Centre frequency selection based on the moving average of the absolute value of the phase tracker's error signal. Note that an offset removal filter must first be applied to the input signal.*

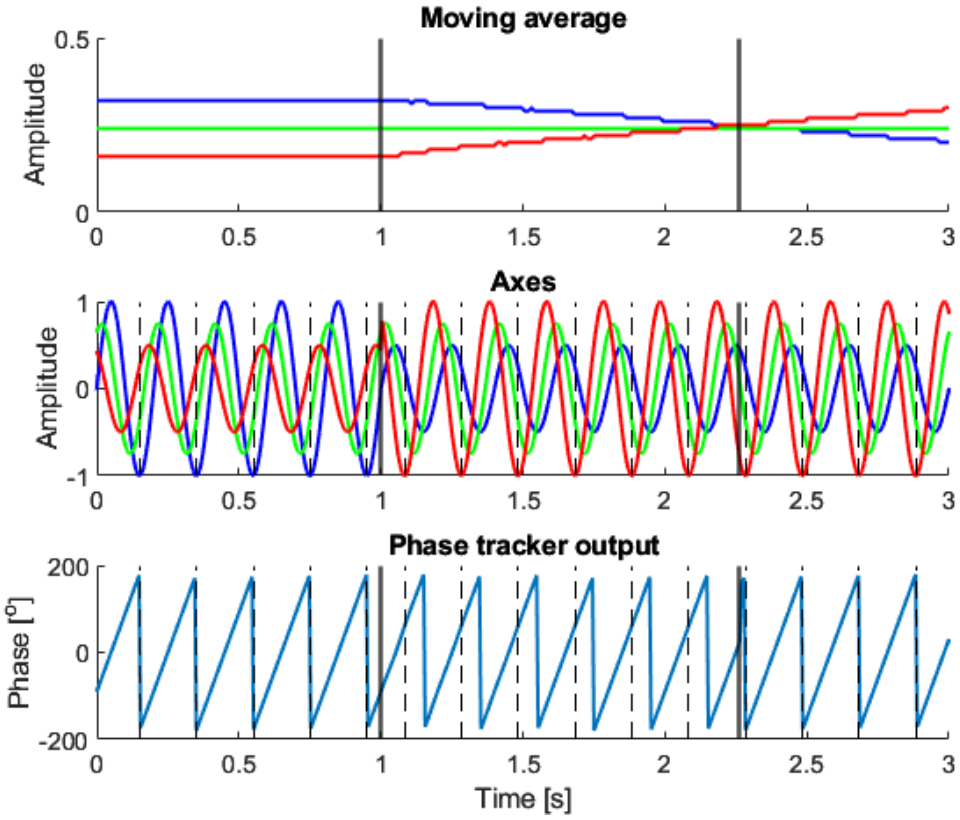


Figure 3.9: Dominant axis selection in example signals. *The dominant axis is selected according to the moving average of the absolute value of the signal amplitude. Example signals were pure sinewaves at 5 Hz with distinct amplitudes and phase shifts.*

3.3.4. Pre-processing

Before being inputted to the phase estimation algorithm, raw data from the triaxial accelerometer was high-pass filtered for offset removal (*Figure 3.10*). Filtering was required because accelerometer recordings typically present a DC shift, caused by gravitational acceleration as well as changes in temperature or in the device structure due to mechanical wear (Luinge & Veltink, 2004).

This offset must be removed prior to phase estimation, as the algorithm assumes waveforms centred around zero. To that end, we used a high-pass SOS direct-form I second order Butterworth filter, with cut-off frequency at 0.1 Hz. Filter coefficients were generated using the MATLAB 'filterDesigner' tool.

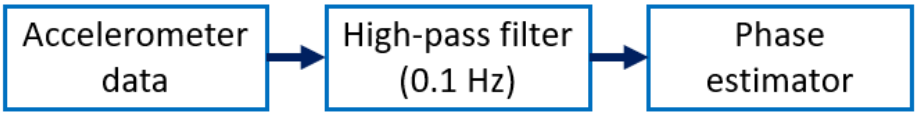


Figure 3.10: Block diagram of the data pre-processing stream. *The triaxial accelerometer axis was high-pass filtered at 0.1 Hz, and then inputted to the phase tracker.*

3.3.5. Calculation of change in tremor severity

The testing protocol involves providing stimulation at eight distinct stimulation states and later identifying the state that most suppresses the tremor. These states consisted of six phasic stimulation conditions at distinct target phases, a non-phasic stimulation condition, and sham (no stimulation). We chose to restrict the number of target phases to six to keep the testing duration to a small window and minimise the time during which study participants must stay in-clinic for the study.

To identify the most suppressive state, the system must compute a metric that we defined as the change in tremor severity, calculated individually at each 10-second stimulation block to reflect the impact of each stimulation state on tremor. After the presentation of all stimulation blocks, the system computed the median change in tremor across all blocks in each of the eight states. We considered the state with the

smallest median as the most suppressive one. Further details on this procedure are presented below.

Change in tremor severity was calculated from an online approximation of the tremor envelope, which was obtained from the three axes of the accelerometer. The approximated envelope was calculated using the following sequence of operations: (i) band-pass filtering from 1 to 9 Hz to safely encompass our frequency range of interest (2 to 8 Hz); (ii) rectification, performed by calculating the absolute value using a C++ function specific for floating-point numbers in order to avoid conversion errors; and (iii) low-pass filtering at a cut-off frequency of 4 Hz[5]. Both filters were SOS direct-form I second order Butterworth, with single-precision floating-point coefficients generated using the MATLAB 'filterDesigner' tool. The operations are summarised in *Figure 3.11*. *Appendix A.2* provides further details regarding the characterisation of this online filter.

From this on-board envelope approximation, at each 10-second stimulation block, we took the mean (μ_i) in the 1 second prior to the onset of the block, as well as the mean in the last 1 second of stimulation (μ_f). Finally, we computed the change in tremor severity as: $\frac{\mu_f - \mu_i}{\mu_i}$. In this calculation, we restricted the resolution of μ_i and μ_f to three decimal places. To prevent division by zero, when μ_i was equal to zero, change in tremor severity was assigned 'NaN'.

The change in tremor severity, calculated at each block, was saved along with its corresponding stimulation state. After completion of all stimulation blocks, the system computed the median change in tremor severity across each state, and then considered the state with the lowest median as the most suppressive one.

[5] The filter corner frequency of 4 Hz was determined through iterative testing with trial tremor signals. Among various frequencies tested within the tremor range, this value resulted in an envelope that closely resembled that obtained from the Hilbert transform method in comparisons conducted in MATLAB.

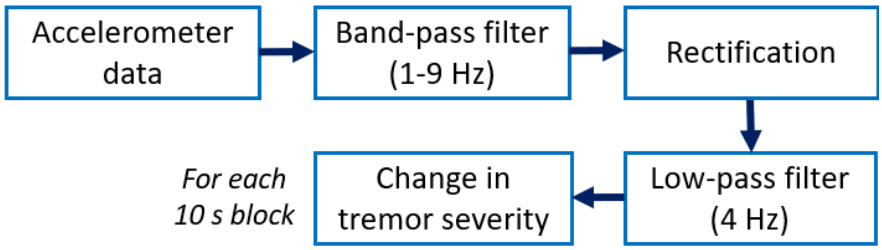


Figure 3.11: Block diagram representing the operations to calculate the tremor envelope and subsequent change in tremor severity for each stimulation state presentation.

3.3.6. Triggering stimulation

Stimulation was initiated by sending a TTL pulse to the stimulator through a digital output pin on the development board. In the phasic stimulation state, this occurred when the phase estimate closely matched the target phase. To prevent instances where the phase resolution imposed by our sampling rate might result in missing the target phase, triggering was allowed if the tracked phase fell within an error budget centred around the target phase. Additionally, stimulation could only be triggered every other sample (provided at half the sampling rate, i.e., 104.015 Hz). Therefore, to further avoid missed stimulation during tremor cycles, triggering was permitted if either the phase at a given sample or its previous one matched the target phase, accounting for the error budget. Once stimulation was triggered, five pulses were delivered at half the sampling rate, and subsequent stimulation could not be triggered for a time interval equal to half the oscillation period (defined as $1/f_c$), aiming to prevent multiple triggering points within a single wave cycle. *Figure 3.12* illustrates the need to account for the error budget when triggering stimulation. It presents an example oscillation at 5 Hz, its tracked phase, and the target phase of 180 degrees. The samples may miss the target phase if the error budget is not accounted for.

The theoretical phase resolution can be approximated by computing $f_c/f_s \cdot 360$ degrees. We experimentally determined the error budget value for each target centre frequency considered by the wrist-worn system. This was performed by utilising an oscilloscope (PicoScope 2000 Series) to provide an analogue input (pure sinewaves at 2 to 8 Hz, encompassing the range of target tremor oscillations) to the wrist-worn system. We sampled the input at the accelerometer's rate, applied the phase estimation algorithm, and identified the lowest acceptable error margin for consistent stimulation at each wave cycle. *Table 3.3* provides this error budget for each target centre frequency.

The possibility of reducing the error budget by increasing the sampling rate, and consequently enhancing the phase resolution, was considered. However, this approach would compromise the available memory and shorten the duration of the recordings. We decided against this adjustment, as the current sampling rate is already at the maximum level that supports the intended protocol duration. Additionally, the existing error budget aligns with the phase error tolerance defined in the user requirements.

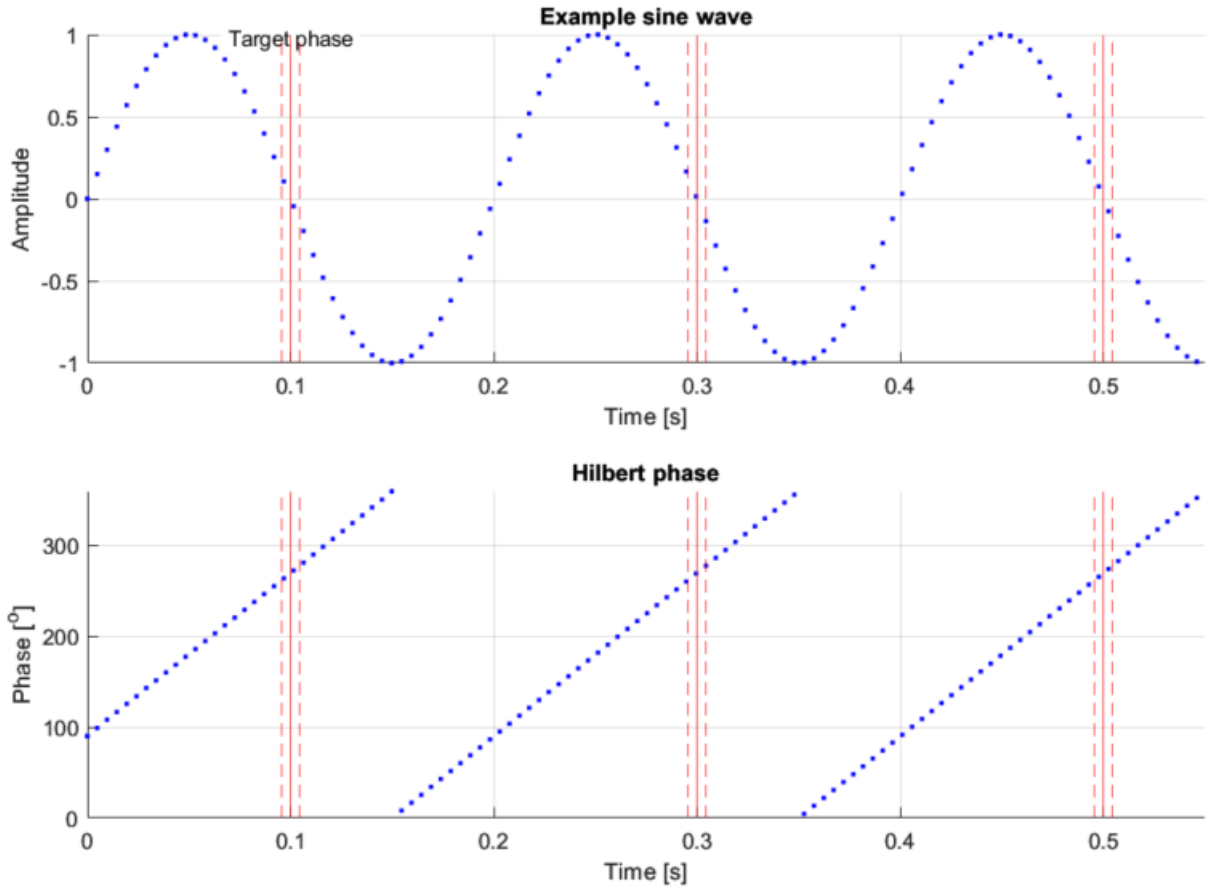


Figure 3.12: Example sinewave and its estimated phase sampled at the wrist-worn device's accelerometer sampling rate. *The example target phase of 180 degrees is highlighted in a solid red line, and the error budget in a hashed red line, to demonstrate that an error margin should be allowed when triggering stimulation, otherwise there might be wave cycles in which stimulation triggering is missed.*

Tremor centre frequency [Hz]	Error budget [deg]
2	5
3	6
4	8
5	10
6	12
7	13
8	14

Table 3.3: Acceptable phase error margin within which stimulation was triggered for each target centre frequency considered.

3.3.7. Data saving

Data was saved during the experiment and retrieved using the 'SerialFlash' Arduino library. At each iteration, we recorded to a large file in the memory card, as single-precision floating-point (float) values, (i) all three accelerometer axes, high-pass filtered at 0.1 Hz, and (ii) the phase estimated in real time at the dominant axis.

As ASCII character values (char), we saved: (i) the sample number (to ensure no samples were missed in the recordings or data retrieval), (ii) the centre frequency identified by the self-tuning element of the system, (iii) the dominant axis identified by the system, (iv) the stimulation output (recorded as 1 if a trigger was sent to the stimulator at that data point, and as 0 otherwise), (v) and the stimulation state (recorded as the number, 1, 2, 3, 4, 5, 6, 7, or 8, corresponding to each state).

The data in the memory card could be read through a command line interface (CLI) after the experiments and saved to a computer as a '.txt' file. With our chosen sampling rate of 208.03 Hz, the system could store data for 51 minutes, surpassing our minimum requirement of 48 minutes.

3.3.8. User interface

The elements of the user interface involved the RGB LED, two push-buttons, and a CLI. The experimenter interacted with the system to start, resume, or stop the protocol, or to access the CLI, by pressing the device's push buttons. Pressing the switches caused the LED to flash in different colours to inform the experimenter that the buttons were successfully activated. Detailed instructions on navigating the user interface are provided in the *Appendix A.3*.

3.4. Verification procedure

3.4.1. Offline, MATLAB-based algorithm characterisation

Initially, we developed an offline version of the phase estimation algorithm in MATLAB to assess its performance and to verify its accuracy against the on-board version implemented in C++ on an Arduino platform. We evaluated the offline algorithm using MATLAB-generated sinewaves with centre frequencies ranging from 2 to 8 Hz, which corresponded to the target tremor centre frequencies in the online algorithm. These signals were sampled at 208.03 Hz, matching the sampling rate of the accelerometer in our wrist-worn system, and their individual duration corresponded to 5,000 seconds. We tested the waveforms under three distinct conditions: (i) in their pure form; (ii) with added noise, followed by high-pass filtering using a second-order Butterworth filter set at 0.1 Hz, similar to the on-board filtering; and (iii) with added

noise, followed by band-pass filtering using a second-order Butterworth filter spanning 1 to 9 Hz.

To ensure the robustness of our algorithm and its applicability to real-world scenarios, we intentionally subjected it to coloured noise, including brown and pink noise, which deviate from Gaussian distributions. This approach allowed us to assess the phase tracker's performance under conditions reflecting the typical noise encountered in accelerometer recordings. Coloured noise provided a suitable testing environment, as it is known to be more representative of accelerometer noise than white noise (Pavlov & Petrov, 2020). We replicated common drifts observed in accelerometer recordings and mimicked noise produced by electronic components of inertial motion sensors by adding brown noise, which simulates a random walk process, and pink noise (Blum & Dambeck, 2020; Pavlov & Petrov, 2020). We generated brown noise by integrating white noise, which in itself was produced as a vector of random numbers. Conversely, pink noise was created by filtering white noise to make each frequency component's amplitude inversely proportional to its frequency, thus producing 1/f noise.

To validate the phase tracker's performance, we estimated phase in MATLAB using the Hilbert transform, which is recognised as the gold-standard for phase reference (Cohen, 2014). Given the Hilbert transform's high sensitivity to noise, the input signal must be filtered around the frequency range of interest to ensure accurate phase estimation. Consequently, before applying the Hilbert transform, the test waveforms with added noise were subjected to band-pass filtering using a second-order Butterworth filter ranging from 1 to 9 Hz. For the pure sinewaves, which contained no noise, no filtering was necessary.

Phase error was determined as the absolute value of the difference between the phase estimates obtained from the Hilbert transform and the offline phase tracking algorithm. To account for phase wrapping occurrences, we applied a correction factor: if the error exceeded 180 degrees, we subtracted 360 from the error and then calculated its absolute value. For instance, if the phase estimates were 5 degrees online and 355 degrees offline, the phase error would be calculated as 10 degrees.

To further verify our methodology, we assessed the error metric employed to identify the optimal phase estimation stream. This stream corresponds to the centre frequency that most closely matches the input signal's centre frequency, as detailed in *Section 3.3.3—Adaptive strategy accounting for tremor's variability*. Our verification involved demonstrating that the error signal, defined as the absolute value of the difference between the input and estimated signals, increased proportionally with the disparity between the signal's centre frequency and that of the algorithm. For this analysis, the centre frequency (f_c) in the phase tracker was set at a constant 5 Hz. We then processed high-pass filtered noisy oscillations, generated from sinewaves centred between 2 to 8 Hz (with 0.1 Hz resolution), through the phase tracker. This resulted in frequency offsets ranging from 0 to 3 Hz relative to the fixed f_c. We computed the mean and standard deviation of the error signal over a duration of 5,000 seconds.

3.4.2. Vibration plate tests

To assess the on-board accelerometer's performance in accurately recording oscillations, a comparison was made with a commercially available reference device (Axivity AX3). The reference system's sampling rate was set to 200 Hz, as this was the available option closest to that of the on-board accelerometer. The performance characterisation utilised a system generating stable, controlled oscillations over

extended periods—a low-cost vibration plate typically used for exercise purposes (LifePro Waver Mini Vibration Plate).

The verification process involved comparing the recordings from both accelerometers to ensure similarity in both time and frequency domains. This was performed by taping both the in-house built board and the reference accelerometer together, and subsequently to the edge of the vibration plate.

The vibration plate's oscillations were in the frequency range of 9 to 12 Hz, differing from the target rest tremor range of 2 to 8 Hz. Although the vibration frequencies were constrained by the characteristics of the available equipment, they still approached the typical range of Parkinsonian tremor. For instance, kinetic tremor can extend to 7 to 12 Hz (Deuschl, Raethjen, et al., 2000). Due to the higher vibration frequencies of the testing equipment, we modified the phase tracking algorithm, adjusting its target range from 6 to 12 Hz. However, it is important to note that this higher frequency range was specific to the tests with the vibration plate, and during all other experiments presented in this thesis, the algorithm's target frequencies would revert to the intended 2 to 8 Hz.

The experimenter modulated frequencies by manually adjusting the vibration amplitude, linking increased amplitude with higher frequency. Throughout the test, the vibration frequency underwent two increments, each after approximately 10 minutes, resulting in three distinct centre frequencies. This process permitted verifying that the algorithm correctly identified the appropriate centre frequency and adapted to any changes accordingly.

Data obtained were analysed in MATLAB by synchronising the signals obtained from both accelerometers. Recordings were trimmed to the first and last oscillation

peaks obtained from each device. Their matching time duration was checked by generating time axes at their respective sampling rates and computing the difference between the final time points of the reference and on-board devices.

Correlations were calculated between corresponding axes of the on-board and reference accelerometers over synchronised data segments lasting 9 minutes each. To ensure steady-state recordings were considered, the initial and final 30 seconds of each 10-minute data segment were omitted. Additionally, the on-board signals were down-sampled to match the reference accelerometer's rate of 200 Hz.

To further characterise the systems, we computed the SNR for both the on-board and reference devices. The signal of interest was extracted by applying a forward-and-backward second-order Butterworth band-pass filter (8 to 13 Hz) to each accelerometer axis. The chosen filter ranges were designed to encompass the vibration plate's frequency range of approximately 9 to 12 Hz. Subsequently, noise was computed by subtracting the filtered signal from the unfiltered one. Power was calculated for both signal and noise, representing the sum of the squares of each recording. The SNR was then determined as the absolute value of the ratio between signal power and noise power, and this value was converted to the decibel scale.

The instantaneous frequencies of the on-board recordings were derived through the Hilbert transform applied to their band-pass filtered signals. This involved computing the unwrapped Hilbert phase, followed by applying the approximate derivative to obtain the differential. The mean and standard deviation of the instantaneous frequencies were calculated for each of the three 9-minute-long data segments, aligning with the timings considered in the correlation calculation.

To ensure the consistency and reliability of the on-board accelerometer's phase tracker computation, we conducted a comparison with offline results obtained through a MATLAB-based algorithm. The offline analysis included assessing the estimated phase, selected dominant axis, and selected centre frequency. The dominant axis selection was replicated offline by applying a moving average filter, with a window length matching the online algorithm's (520 samples), to the absolute value of the triaxial accelerometer signals. The axis identified as dominant was the one with the highest moving average, mirroring the on-board algorithm. Given the experimental setup, where the in-house built device was fixed parallel to the vibration plate, it was anticipated that the z-axis would be the singular dominant axis throughout the test. It is noteworthy that the dominant axis was selected at particular time points, corresponding to the start of a 10-second stimulation state presentation. This was mirrored in the offline axis selection verification.

The offline assessment of centre frequency selection involved running seven streams of the algorithm in parallel for each of the three accelerometer axes, each tuned to centre frequencies from 6 to 12 Hz (contemplating those of the vibration plate). The moving average of the error signal, obtained by calculating the absolute value of the difference between the input signal and the signal estimate, was determined offline using the same procedure applied to the accelerometer data. From the seven phase estimation streams corresponding to the dominant axis selected on-board, the one associated with the centre frequency that yielded the lowest error signal was chosen. This allowed for a comparison of centre frequency selection between the online and offline versions of the algorithm.

Finally, we compared the phase calculated on-board with that estimated offline. We defined the phase error as the absolute difference between these online and offline phase estimates, specifically at the stream corresponding to the axis and frequency

selected on-board. Additionally, to address phase wrapping issues, we applied to the error the correction factor outlined in *Section 3.4.1—Offline, MATLAB-based algorithm characterisation.*

Since the wrist-worn system allowed for a budget between the precise estimate and the stimulation phase to avoid missing stimulation points in any given cycle, the precise on-board estimate was also compared with the intended target stimulation phase. As the vibration plate provided expected centre frequencies of 9, 10, and 11 Hz, the error budget was set at 16, 18, and 20 degrees, respectively, computed as described in *Section 3.3.6—Triggering stimulation*.

3.4.3. Experimenter wearing the device

To evaluate the algorithm's performance in conditions resembling in-clinic tests, an experimenter wore the fully assembled device on the wrist, as intended for study participants. After initiating the system and recording the baseline, the experimenter performed a series of five movements lasting approximately 2 minutes each, to simulate stable arm shaking, akin to Parkinsonian tremor. The three axes' orientation, illustrated in *Figure 3.13*, guided the movements: (a) up-and-down, perpendicular to the hand (x-dominant); (b) sideways, parallel to the hand (y-dominant); (c) arm over a chair's armrest, mimicking the in-clinic position and also producing a y-dominant movement; (d) forward and backward (x-dominant); and (e) rotational. While movements (a), (b), and (d) might be less likely in a realistic experimental setting with a study participant, they served to verify the algorithm's adaptation to dominant axis changes, given their clearly defined oscillations along a single axis.

Similar to the analysis conducted with the vibration plate, as outlined in *Section 3.4.2—Vibration plate tests*, we compared the on-board dominant axis, frequency

selection, and phase estimation with those of the offline, MATLAB version of the algorithm.

The final characterisation involved performing 1 minute of movement with five distinct amplitudes to determine the minimum signal levels necessary for effective tremor detection. The process began with the sensor in a static position (no movement), followed by the experimenter generating the lowest amplitude tremor achievable. For each movement, we computed the phase error between the online and offline versions of the algorithm, as well as the SNR on the dominant axis. Additionally, we measured the mean and standard deviation of the tremor envelope on the dominant axis.

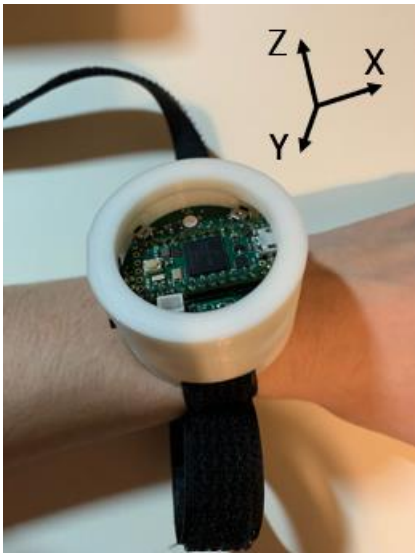


Figure 3.13: The experimenter wearing the fully assembled system on their wrist and the three axes orientation considered during the test and analysis.

3.5. Verification results

3.5.1. Offline, MATLAB-based algorithm characterisation

The algorithm demonstrated performance nearly identical to the Hilbert transform when applied to pure sinewaves, exhibiting a phase error close to zero. *Table 3.4* presents the mean and standard deviation of the error in relation to the phase derived from the Hilbert transform for all the oscillations tested. For signals that were either band- or high-pass filtered, the phase error ranged approximately between 1 to 3 degrees. Notably, the mean phase error remained within 0.6 degrees across these filtered signals, underscoring the algorithm's effectiveness without the necessity of a band-pass filter.

Centre frequency [Hz]	Error, pure sinewave (mean ± SD) [deg]	Error, band-pass filtered (mean ± SD) [deg]	Error, high-pass filtered (mean ± SD) [deg]
2	0.0 ± 0.3	1.4 ± 1.1	2.0 ± 1.7
3	0.0 ± 0.3	1.5 ± 1.1	1.8 ± 1.4
4	0.0 ± 0.2	1.5 ± 1.2	1.7 ± 1.3
5	0.0 ± 0.2	1.6 ± 1.3	1.8 ± 1.4
6	0.0 ± 0.2	1.8 ± 1.4	1.9 ± 1.5
7	0.0 ± 0.2	2.1 ± 1.6	2.2 ± 1.7
8	0.0 ± 0.2	2.7 ± 2.0	2.7 ± 2.1

Table 3.4: Error defined by the phases calculated using the Hilbert transform and the MATLAB-based phase estimation algorithm. *The phase error was calculated as the absolute*

value of the difference between the phases estimated with both methods for a pure sinewave, a band-pass filtered noisy signal, and the same noisy signal high-pass filtered.

Figure 3.14 displays the first second of phase estimates obtained using the Hilbert transform on band-pass filtered oscillations, alongside those from the phase tracker applied to both band- and high-pass filtered signals, illustrating a nearly perfect alignment. Additionally, this figure captures the initial start-up error and its subsequent stabilisation.

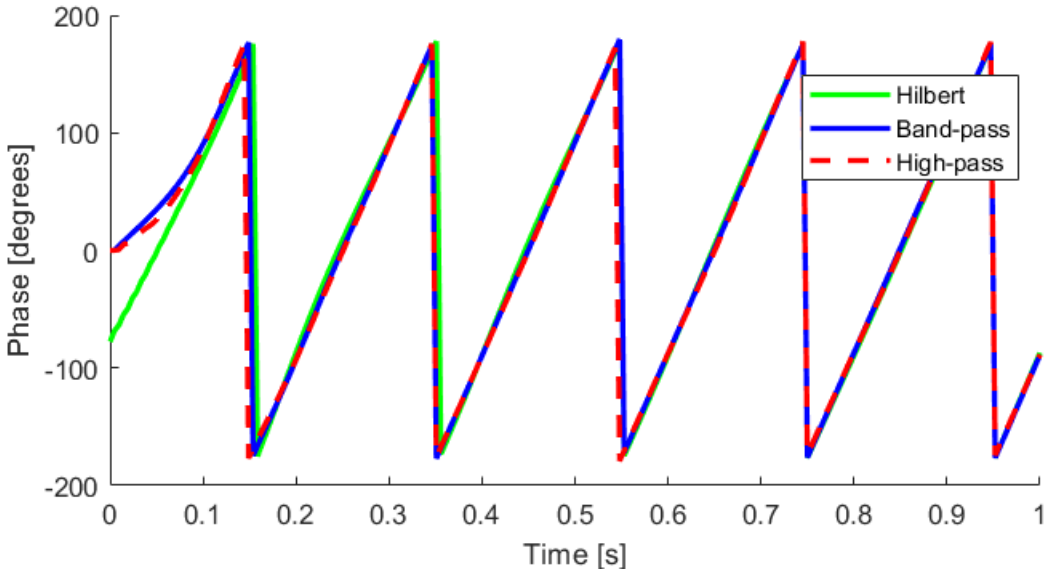


Figure 3.14: Example algorithm performance for band- and high-pass filtered oscillations centred at 5 Hz against the phases derived from the Hilbert transform. *In the initial milliseconds, a start-up error is introduced, until the estimate matches the Hilbert reference angle.*

Figure 3.15 further illustrates the start-up error associated with the algorithm, across pure, band-, and high-pass filtered oscillations. Each time the algorithm initiates, it introduces a phase error of approximately 90 degrees. However, when the algorithm's centre frequency (f_c) aligns with that of the signal, this start-up error quickly stabilises to below 10 degrees within the first second.

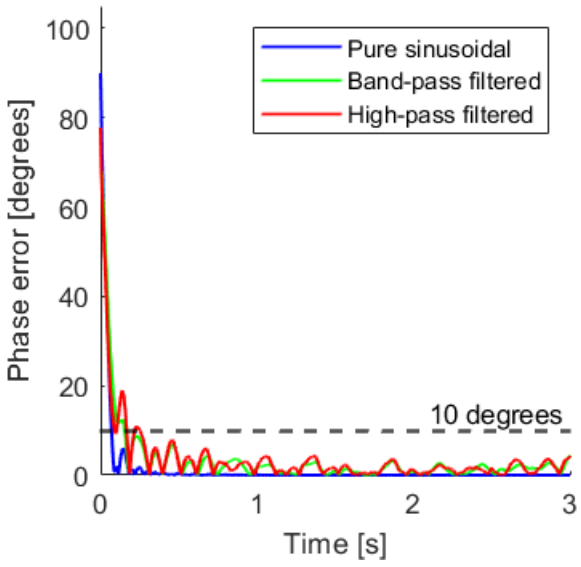


Figure 3.15: Example start-up phase error observed in a pure 5 Hz sinusoidal wave, as well as in band- and high-pass filtered signals. *In these examples, the algorithm's target frequency was aligned with the signal's dominant frequency. In all cases, the phase error stabilises below 10 degrees within the first second. Notably, the error reaches zero in the case of the pure sinewave.*

The error signal, defined as the difference between the input and estimated signals, grew proportional to the frequency offset between the algorithm's centre

frequency (f_c) and that of the signal. This relationship is depicted in *Figure 3.16*, where the error increases with a larger frequency offset. The results confirmed that for offsets as small as 0.1 Hz, which was the resolution used in this test, this error metric effectively reflects the phase estimation stream with f_c closely matching the most prominent frequency.

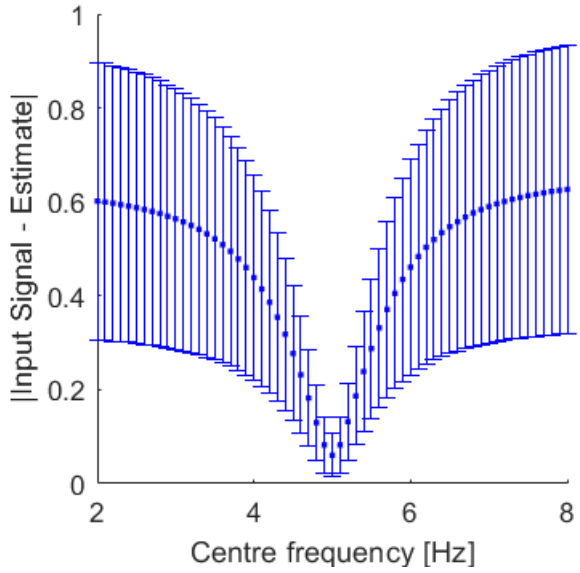


Figure 3.16: Mean and standard deviation of the absolute value of the difference between input and estimated signals. *Example signals were high-pass filtered oscillations centred at 2 to 8 Hz, with 0.1 Hz resolution, and the algorithm was operated with a centre frequency of 5 Hz. The error signal clearly increased proportionally to the centre frequency offset.*

3.5.2. Vibration plate tests

On-board and reference accelerometers comparisons

The triaxial accelerometer signals recorded on-board matched those obtained with the reference device. After synchronisation, the difference between the time axes of the reference and on-board accelerometers was smaller than 0.0005 seconds. Correlation values for each of the three synchronised data segments considered are reported in *Table 3.5*. It is worth noting that their absolute values were above 0.9 in all cases. Axes y and z were inversely correlated across the two accelerometers due to distinct sensor orientations. *Figure 3.17* pictures an example correlation vs. lag plot, corresponding to recording segment 2.

In an ideal scenario, the absolute value of the correlation would be equal to 1 in all cases, indicating a perfect match between the on-board accelerometer recordings and those of the reference device. However, due to the experimental setup and intrinsic differences in the sensors, achieving a perfect correlation was not expected. Firstly, the devices were taped together, and any small gap between them could introduce variations in the recordings. Secondly, differences in the sensors' structures could affect the signal quality. *Table 3.6* presents the SNR for each sensor and axis, considering the triaxial accelerometer recordings band-pass filtered from 8 to 14 Hz as the signal of interest. Although SNR values were similar for each axis across sensors, the differences observed reflect the inherent variations and structural disparities between the sensors. Additionally, the SNR was higher for the z (dominant) axis, aligning with expectations as the movement was more prominent along this axis.

Segment	X	Y	Z
1	0.93	-0.94	-0.97
2	0.91	-0.93	-0.95
3	0.96	-0.96	-0.98

Table 3.5: Correlation between each of the three axes recorded with the on-board accelerometer and the reference device. *Values were computed for three 9-minute steady-state segments at distinct centre frequencies.*

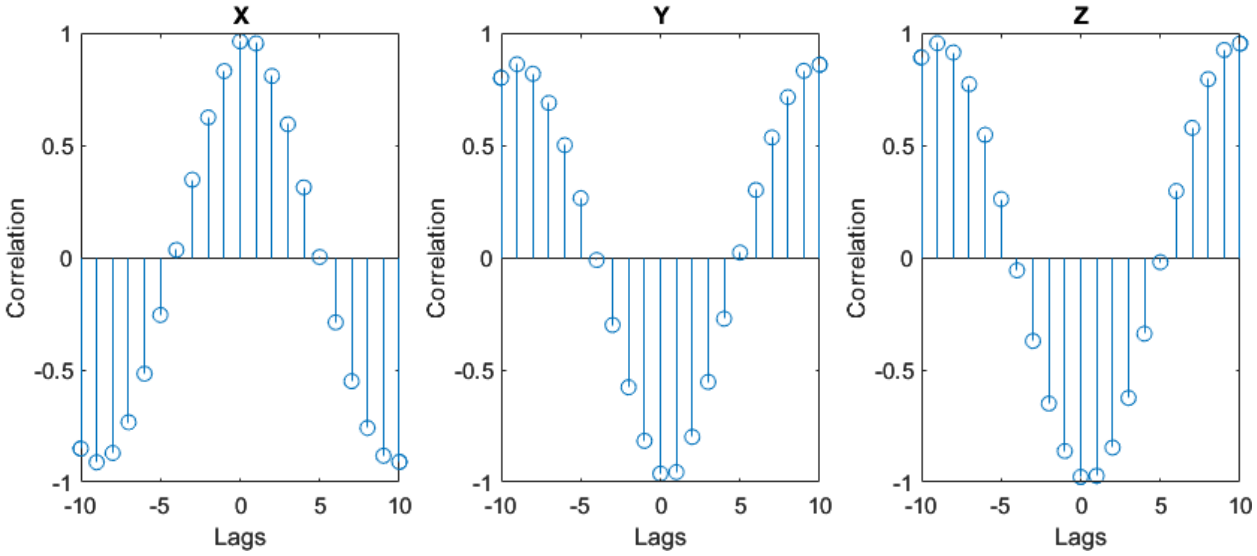


Figure 3.17: Example correlation vs. lag plots for all three axes of both sensors. *The correlations were computed using data corresponding to the second 9-minute data segment analysed.*

Sensor	X	Y	Z
On-board	9.2	10.5	14.6
Reference	11.8	9.4	16.3

Table 3.6: SNR for each axis of both the on-board and reference sensors. *Values, provided in dB, remained within 3 dB across both sensors.*

On-board and offline, MATLAB-based phase-tracker performance comparisons

Next, we present the on-board and offline algorithm performance comparisons. The dominant axis selected on-board and offline was z throughout the testing, as expected considering the accelerometer placement on the vibration plate. *Figure 3.18A* illustrates the moving average used for the dominant axis calculation, with the drop points corresponding to the moments when the vibration plate was switched off in between vibration settings. We can observe the already expected increase in amplitude across the three segments considered. *Figure 3.18B*, in turn, shows the dominant axis selected on-board and offline.

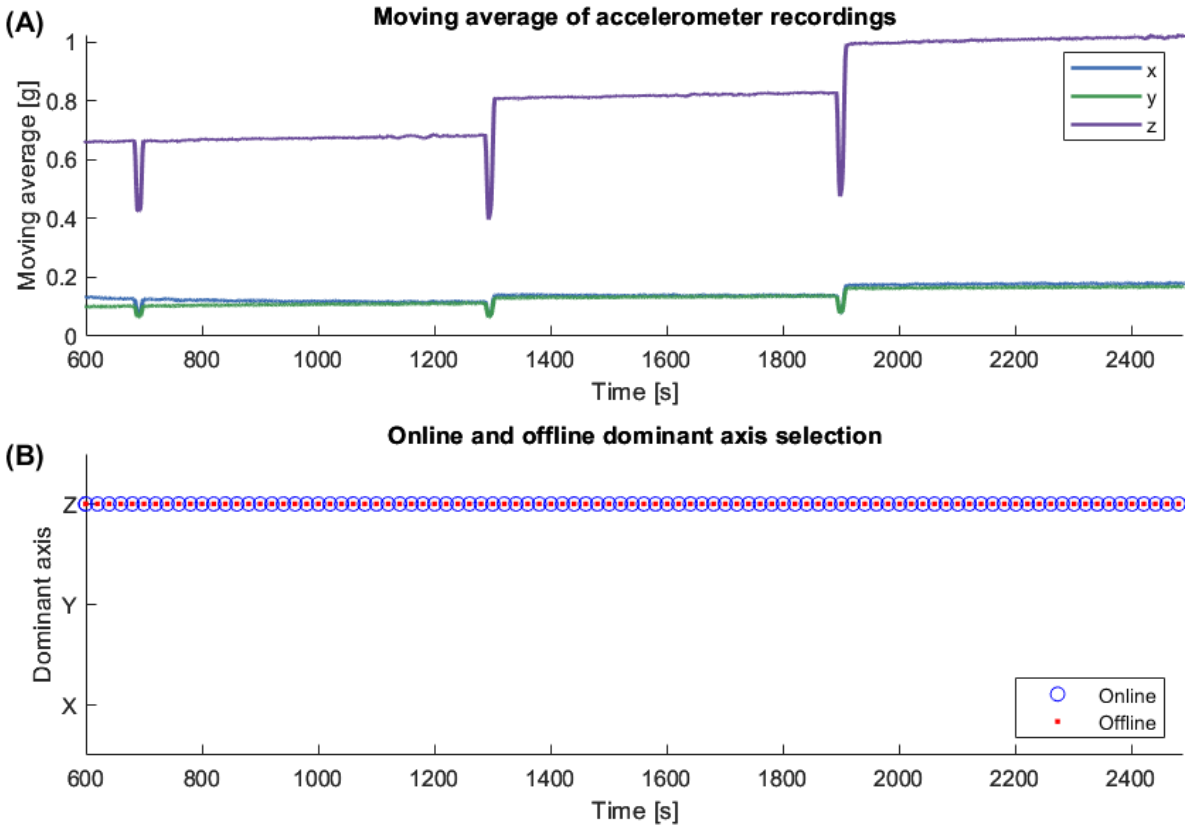


Figure 3.18: On-board and offline moving average-based selection of the dominant axis for tests with a vibration plate*. (A) The offline moving average calculation of the absolute value of the three accelerometer axes, with z featuring as the dominant one throughout the recording using the vibration plate. (B) On-board and offline dominant axis selection at the points when the dominant axis was updated.*

The centre frequencies selected, both online and offline, matched in the majority (94%) of the 10-second windows considered. However, mismatches occurred when the instantaneous vibration centre frequency was approximately 10.6 Hz, resulting in selected centre frequencies of either 10 or 11 Hz. *Table 3.7* provides the instantaneous

frequency at each segment. As depicted in *Figure 3.19A*, the error signal's moving average, utilised for frequency selection, was remarkably close between the two-phase estimation streams (for 10 and 11 Hz), reflecting the precise frequency falling between these two streams, closer to 11 Hz by only 0.1 Hz. The discrepancy between online and offline centre frequency selection, shown in *Figure 3.19B*, may be attributed to intrinsic differences between C++ and MATLAB computations, including rounding differences.

Segment	**Centre frequency (mean ± SD) [Hz]**	**Phase error (mean ± SD) [deg]**
1	9.0 ± 0.0	0.1 ± 0.1
2	9.7 ± 0.0	0.2 ± 0.2
3	10.6 ± 0.0	0.4 ± 0.2

Table 3.7: Mean and standard deviation of the instantaneous frequency and phase error at each recording segment considered for tests with a vibration plate. *Error is defined as the absolute value of the difference between the on-board estimated phase and the one obtained from the offline MATLAB version of the algorithm.*

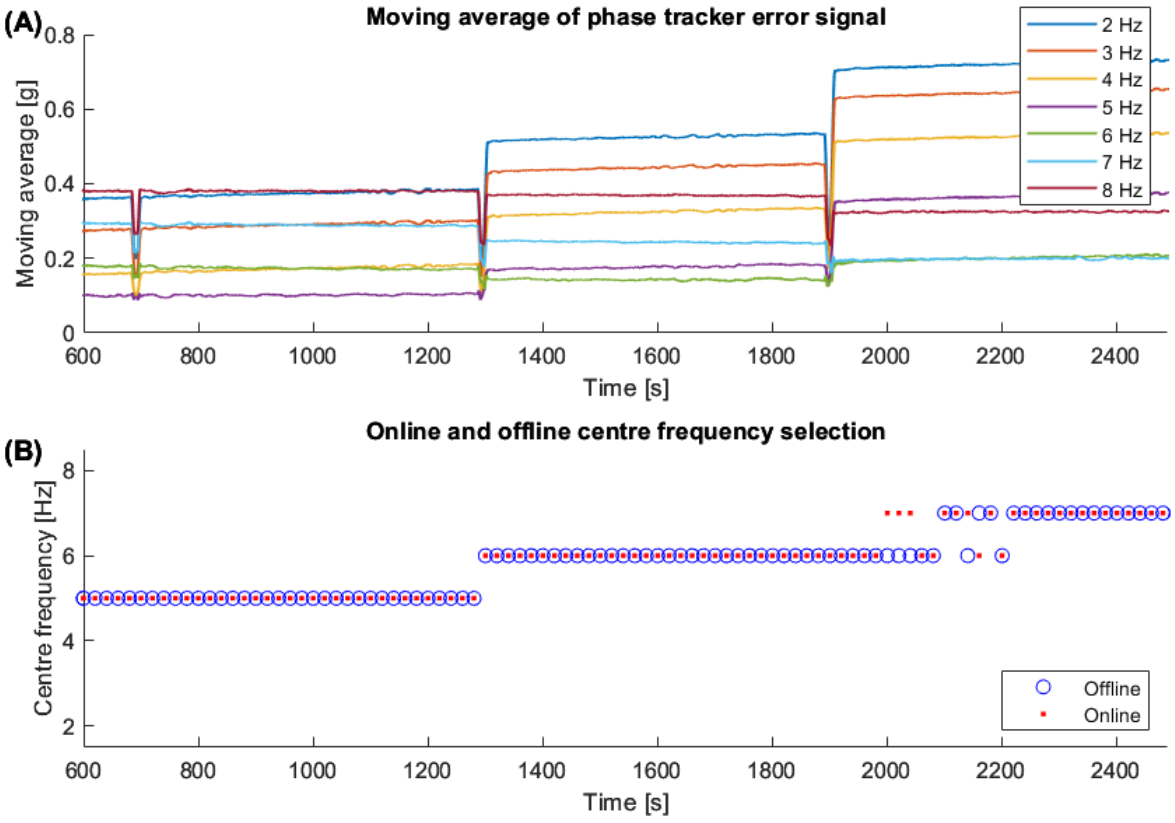


Figure 3.19: On-board and offline error signal-based selection of the centre frequency for tests with a vibration plate. *(A) The offline moving average calculation of the phase tracker error signal for z, selected as the dominant axis. (B) On-board and offline dominant axis selection at the points when the dominant axis was updated.*

The online phase estimation closely matched the offline computation in the MATLAB-based version of the algorithm, affirming the reliability of the on-board phase tracker. *Table 3.7* presents the mean and standard deviation of the phase error, indicating the difference between the online and offline phase estimates during the three 9-minute segments considered. The mean phase error consistently remained below 0.5. *Figure 3.20* illustrates the time course of the phase error throughout the

recording, remaining close to zero, except for brief periods corresponding to when the vibration plate automatically switched off after 10 minutes of recordings. This aligns with the algorithm's requirement for a signal to estimate phase reliably; when the signal amplitude approaches zero, the algorithm cannot reliably estimate phase as there is no reference.

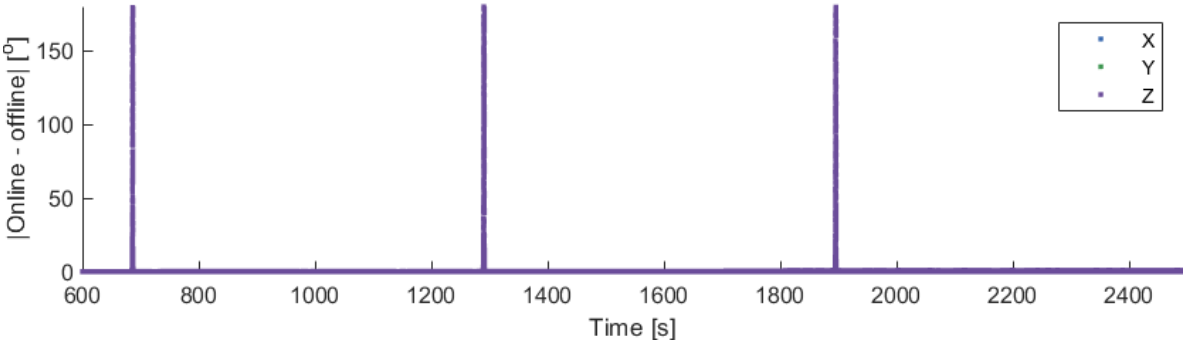


Figure 3.20: Phase error time course during the random search condition for tests with a vibration plate. *Error is defined as the absolute value of the difference between the on-board estimated phase and the one obtained from the offline MATLAB version of the algorithm. The tracked dominant axis for phase estimation was z throughout the recording. The phase error remained consistently near zero, except for the epochs when the reference accelerometer signals dropped to zero.*

Due to the sampling rate restrictions, which required stimulation triggering to be permitted when the tracked phase matched the target one, accounting for an error budget, we also computed the error defined between the precise online phase estimate and the target phase. *Figure 3.21* illustrates the target and exact stimulation phases, presented in their order of occurrence, during the entire recording. This shows that

stimulation covered the range of desired target phases. Although the exact stimulation phase could misalign with the target one because of the error budget and sampling rate restrictions (outlined in *Section 3.3.6—Triggering stimulation*), stimulation remained around the target phase, and the error at stimulation was 8.9 ± 6.1 degrees (mean ± SD)—consistently below the 30-degree error tolerance preset by the user requirements.

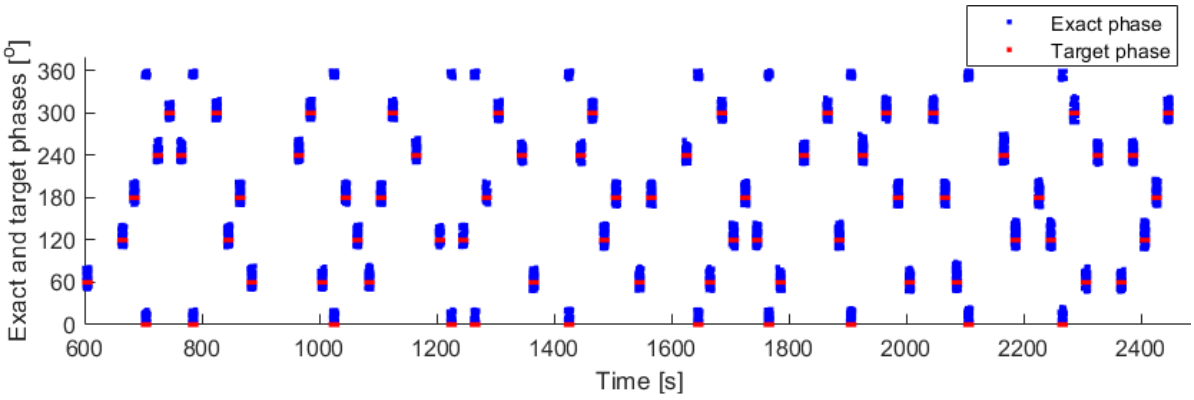


Figure 3.21: Exact (in blue) and target (in red) stimulation phases during the random search condition, covering six target phases presented in random order, for tests with a vibration plate. *The phases do not perfectly align due to sampling rate restrictions, but the stimulation phases remained close to the target phase and below the predetermined 30-degree mean error limit.*

3.5.3. Experimenter wearing the device

The on-board dominant axis consistently matched the one selected offline from a moving average of the axes for all data segments considered. *Figure 3.22A* illustrates

the moving average calculation, highlighting moments when one axis clearly overtakes another. In *Figure 3.22B*, the online and offline axis selections are presented, clearly demonstrating the dominance of one axis in movements (a), (b), and (d): z, y, and x, respectively, as expected.

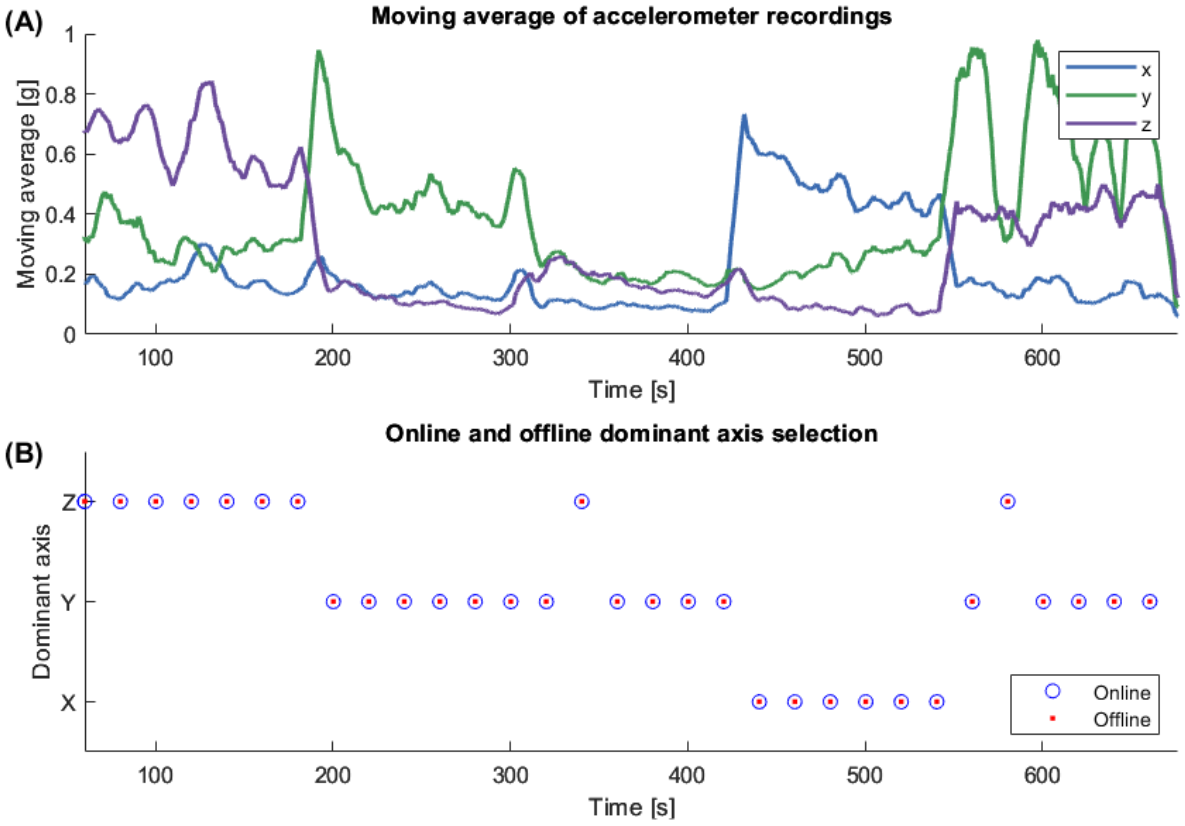


Figure 3.22: On-board and offline moving average-based selection of the dominant axis for tests with an experimenter wearing the device. *(A) The offline moving average calculation of the absolute value of the three accelerometer axes throughout the recording with an experimenter wearing the device and performing different movements. (B) On-board and offline dominant axis selection at the points when the dominant axis was updated.*

The frequency selection onboard matched the offline results in 68% of the segments analysed. In 29% of these segments, there was a minor discrepancy where the frequency selected online differed from the offline selection by 1 Hz, and in 3% of segments, the difference was 2 Hz. Among the segments with matching frequencies, the disparity between the lowest (selected) error signal moving average and the second-lowest value was 0.020 ± 0.015 g (mean ± SD). Conversely, in the segments with mismatched frequencies, the difference between the error signal moving average of the streams selected online and offline was approximately an order of magnitude smaller, at 0.005 ± 0.004 g (mean ± SD).

This observation suggests that there were instances where the moving average of the error signal, corresponding to streams with different centre frequencies, exhibited very close values (refer to *Figure 3.23A*). The mismatches may be attributed to inherent discrepancies between the C++ and MATLAB computations, likely due to rounding disparities. Additionally, the centre frequency in the tremor mimicked by the experimenter was not constant, typically fluctuating around 3 to 5 Hz, as displayed in the instantaneous frequency moving average and standard deviations in *Table 3.8*. When the exact centre frequency lies in between two integer options, it may be assigned to either as their corresponding error signal moving averages are closely valued. This is expected to occur in real-world tremor. *Figure 3.23B* illustrates the comparison of online and offline frequency selections. It is important to note that the frequency selection, similar to the dominant axis, is updated every 20 seconds, preceding each 10-second stimulation state.

The phases estimated on-board closely aligned with those estimated offline in MATLAB for all movements examined, as detailed in *Table 3.8*. This table presents the mean and standard deviation of the error, defined by the absolute value of the difference between the online and offline phase estimates for each movement. *Figure*

3.24 illustrates the phase error's time course throughout the test, demonstrating that it remained consistently low, with occasional brief spikes during transitions between movements with the changes in dominant axes tracked for phase estimation.

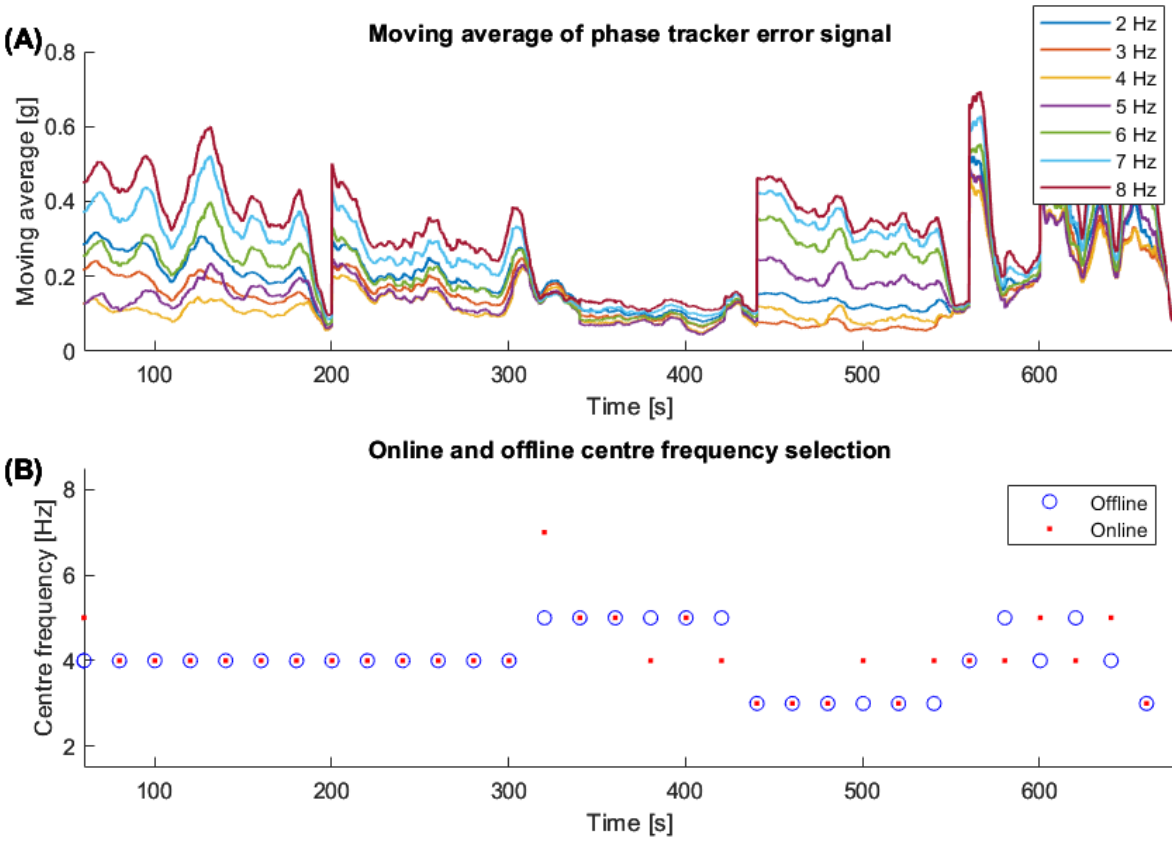


Figure 3.23: On-board and offline error signal-based selection of the centre frequency for tests with an experimenter wearing the device. *(A) The offline moving average calculation of the phase tracker error signal corresponding to the dominant axis selected on-board. (B) On-board and offline dominant axis selection at the points when the dominant axis was updated. This occurred every 20 seconds, before the onset of a 10-second state.*

Movement	Centre frequency (mean ± SD) [Hz]	Phase error (mean ± SD) [deg]
(a) Z-dominant	4.2 ± 0.7	0.1 ± 0.0
(b) Y-dominant	4.5 ± 2.9	0.1 ± 0.1
(c) In-clinic test position	4.6 ± 1.6	0.2 ± 0.4
(d) X-dominant	3.4 ± 1.7	0.1 ± 0.2
(e) Rotational	4.3 ± 2.8	0.1 ± 1.2
Overall	4.4 ± 2.0	0.1 ± 0.6

Table 3.8: Mean and standard deviation of the instantaneous frequency and phase error at each recording segment considered for tests with an experimenter wearing the device. *Error is defined as the absolute value of the difference between the on-board estimated phase and the one obtained from the offline MATLAB version of the algorithm.*

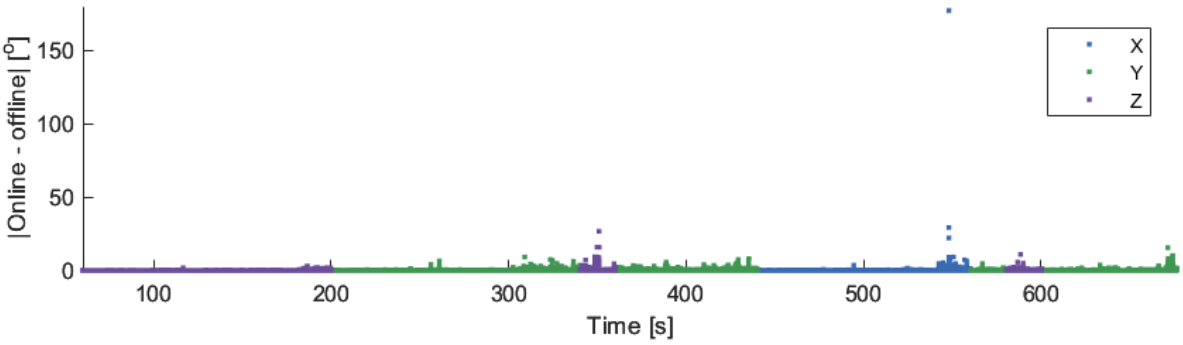


Figure 3.24: Phase error time course during the random search condition for tests with an experimenter wearing the device. *Error is defined as the absolute value of the difference between the on-board estimated phase and the one obtained from the offline MATLAB version of the algorithm. Changes in the dominant axis tracked by the on-board system are indicated by*

representing x-axis dominant trials in blue, y-dominant trials in green, and z-dominant trials in purple.

The error during stimulation, calculated by comparing the precise phase tracked on-board with the target phase, was notably low at 4.8 ± 4.2 degrees (mean ± SD), significantly below the 60-degree resolution of the target phases. *Figure 3.25* shows both the target and the actual stimulation phases, underscoring that stimulation was consistently triggered near the target phases, even when considering an error budget for stimulation triggering (see *Section 3.3.6—Triggering stimulation*).

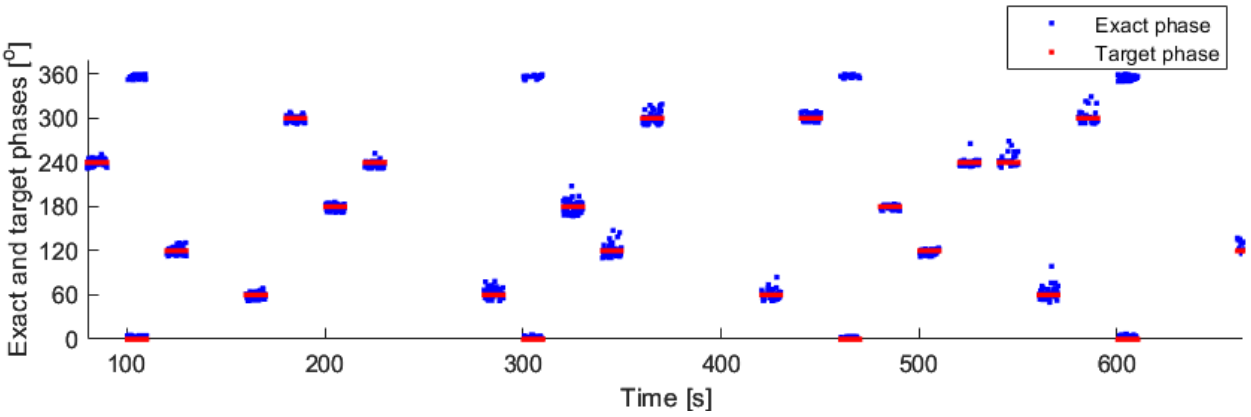


Figure 3.25: Exact (in blue) and target (in red) stimulation phases during the random search condition, covering six target phases presented in random order, for tests with an experimenter wearing the device. *The phases do not perfectly align due to sampling rate restrictions.*

In the final characterisation, which entailed movements at five distinct amplitudes, the lowest tremor amplitude generated aligned with the requirements specified in *Table 3.1* (see *Section 3.1.1—Design requirements*). Notably, when the signal amplitude was zero, the phase error between the online and offline algorithms was approximately 90 degrees. This indicates that the algorithm produces random outputs in the absence of a phase reference, as phase cannot be estimated without a tremor signal. Remarkably, even at the lowest signal levels and in conditions with low SNR—at or below zero—the algorithm successfully estimated phase with a mean error below the stipulated minimum of 30 degrees. This underscores its inherent filtering capabilities, particularly around the target centre frequency. It is also noteworthy that the phase error decreased as the signal amplitude increased, suggesting an improved algorithm performance in lower noise scenarios—as expected.

Movement	**Dominant axis envelope (mean ± SD) [g]**	**Dominant axis SNR (mean ± SD) [dB]**	**Phase error (mean ± SD) [dB]**
Rest	0.00 ± 0.00	0.0	90.2 ± 51.5
Amplitude 1	0.04 ± 0.03	0.0	3.1 ± 13.6
Amplitude 2	0.20 ± 0.6	-0.4	0.5 ± 0.9
Amplitude 3	0.78 ± 0.17	10.8	0.1 ± 0.1
Amplitude 4	2.34 ± 0.55	16.7	0.0 ± 0.0

Table 3.9: Accelerometer signal characteristics and phase error at distinct tremor amplitudes*. Values reported correspond to the characterisation of the accelerometer signals at the dominant axis (SNR and mean and standard deviation of the envelope) and the phase error*

between the on-board and offline algorithm versions, derived from five 1-minute-long movements at distinct amplitudes.

3.6. Discussion

The wrist-worn system and phase-tracking algorithm introduced in this chapter have demonstrated effectiveness in providing real-time phase estimation of tremor-like accelerometer-recorded oscillations in a wearable format. Our phase estimation approach is adaptable, and accommodates fluctuations in both the dominant axis and centre frequency of the triaxial accelerometer signals. In this section, we discuss the results obtained with our phase tracker and in-house built device. Additionally, we explore the current system's limitations, as well as potential avenues for future research.

3.6.1. Summary system characteristics against design requirements

The system's characteristics successfully met the established minimum design requirements in key areas including phase error, accelerometer signal levels, sampling frequency, memory, and battery life of the device. Notably, the phase error at the target stimulation phase remained below the error tolerance, reiterating that the sampling rate choice was sufficient to capture the required phase resolution. These criteria, along with the values obtained with the phase-tracking algorithm and wrist-worn device, are summarised in *Table 3.10*.

Metric	Requirement	System characterisation
Maximum mean phase error	Below 30 degrees	Precise error: 3.1 ± 13.6 degrees at minimum amplitude levels; close to zero in positive SNR cases. Error at stimulation with emulated tremor signals: 4.8 ± 4.2 degrees (mean ± SD).
Minimum signal level	Mean dominant axis envelope of at least 0.04 g	Mean dominant axis envelope of 0.04 g
Sampling frequency	At least 96 Hz	208.03 Hz
Storage capabilities	At least 48 minutes (in-clinic tests protocol duration)	51 minutes
Battery life	At least 48 minutes (in-clinic tests protocol duration)	Up to 4 hours

Table 3.10: A comparison of the minimum quantitative requirements against the performance achieved by the phase tracking algorithm and wrist-worn device.

3.6.2. Phase tracker verification

The performance of the phase estimation algorithm was thoroughly validated across various scenarios, including tests with an offline tracker in MATLAB using synthetic signals, as well as its on-board version using both stable oscillations from a vibration plate and real-world tremor simulations by an experimenter wearing the system. In MATLAB, when compared to the gold-standard Hilbert transform, the algorithm consistently maintained a mean phase error well below 15-degrees. Notably, the phase errors from high- and band-pass filtered signals varied by less than 1 degree,

underscoring the robustness of our approach and its efficacy without relying on band-pass filtering. This aspect is particularly advantageous since intensive filtering around the frequency of interest can cause phase delays and signal distortions (Wodeyar et al., 2021).

Comparative analysis between the on-board system and the offline algorithm demonstrated a high degree of consistency, with phase errors frequently approaching zero. This observation attested to the online algorithm's reliability in real-world applications. One characteristic of the system, however, was its tendency to output random values in the absence of a signal, underscoring its reliance on an input data with non-zero amplitude—as expected. Disparities between the online and offline versions, including minor discrepancies, may be attributed to inherent differences in the C++ and MATLAB computations, such as rounding errors. Overall, these tests have successfully established a reproducible MATLAB implementation of the algorithm, increasing the confidence in the online algorithm's results.

A notable characteristic of the algorithm was the introduction of a start-up phase error of approximately 90 degrees each time it was activated, as illustrated in *Figure 3.15*. While this error stabilised rapidly, typically within less than 1 second, its regular reintroduction could be problematic—particularly in the context of calculating the error signal's moving average, which is crucial for determining the optimal frequency selection. This initial start-up error substantiated our decision to run multiple phase tracking streams in parallel, instead of periodically reinitialising them.

3.6.3. Adaptive strategy

A key innovation in the phase estimation approach introduced in this chapter is the system's built-in adaptability. This feature allows for periodic adjustments to

changes in the dominant axes and centre frequencies of accelerometer-recorded tremor. The on-board strategy for selecting the dominant axis has proven to be both effective and consistent, aligning with every tested scenario of the offline validation. This capability addresses a significant limitation identified in the phase tracking system discussed in *Chapter 2*, namely its inability to adapt to changes in the dominant axis (Arruda et al., 2021). Our new system successfully overcomes this challenge.

In the majority of cases, the centre frequency selection was consistent across both online and offline implementations. However, attention should be directed towards the segments where mismatches occurred. These mismatches were typically observed in segments where the error signals' moving averages of two phase estimation streams were close, approximately an order of magnitude smaller than the smallest difference in matching streams. Such scenarios likely arise when the actual dominant frequency of a segment lies between two frequency streams, leading to small error signal differences between both. In these instances, inherent computational disparities between the MATLAB and C++ versions of the algorithm, such as rounding errors, could result in different centre frequencies being selected. While increasing the number of centre frequency streams (for example, enhancing the resolution from 1 Hz to 0.5 Hz) might seem like a solution, such discrepancies could persist whenever the true signal frequency is situated between two streams. Ultimately, we decided against increasing the number of streams to prevent computational delays and avoid overloading the system. Although there were mismatches between the online and offline frequency selections, these discrepancies were typically minor, usually amounting to only 1 Hz. This observation supports the validity of our frequency selection strategy as an effective means to accommodate variability in tremor dominant frequencies.

There are alternative methods to our self-tuning strategy. One such approach involves periodically conducting a power spectral density estimation to select the frequency of interest. However, this method might demand more computational resources than the basic mathematical operations used in our current algorithm, and could introduce variable time delays. Another possibility is to periodically run the self-tuning blocks (as shown in *Figure 3.8*) while tracking only one stream most of the time. We chose not to pursue this option because it would require the algorithm to run for several seconds to collect enough data for accurate stream selection and to allow the error signal's moving average to stabilise, thereby introducing a time delay. Nevertheless, in other applications involving systems similar to ours, these alternative approaches could be considered as potential optimisation strategies.

3.6.4. Limitations of the current system

The phase estimation algorithm effectively tracks phase within the established design requirements in the presence of a signal. However, it is important to note, as shown in *Table 3.9*, that the phase error tends to increase with decreasing SNR. This is due to inherent characteristics of the algorithm that may impact its performance. The algorithm is based on a simplified Kalman filter model; however, it lacks a gain optimisation component. In this approach, the gain (G) is empirically determined and remains constant, unlike a traditional Kalman gain that dynamically adjusts in response to fluctuations in process noise and measurement noise. Furthermore, the current implementation of the algorithm assumes that the input signal is sinusoidal. This assumption potentially limits its effectiveness in accurately tracking phases of non-sinusoidal signals, which could be encountered in real-world applications, including Parkinsonian tremor signals.

Additionally, allowing for a certain error margin between the target and actual stimulation phases introduced discrepancies in our system. This error budget, described in detail in *Section 3.3.6—Triggering stimulation*, was implemented to ensure consistent delivery of stimulation. While this budget inevitably increases the phase error, it is a necessary compromise to guarantee regular stimulation. Even with this error budget in place, the discrepancy between the target and tracked phases remained below the designated error limit in our design requirements during both the vibration plate tests and the trials with an experimenter wearing the device. We chose to adhere to a more conservative error budget, prioritising the assurance that stimulation would not be missed in any wave cycle.

While this system represents significant progress in the development of a device for at-home use beyond clinical settings, further refinement is necessary to adapt it to such applications. Although the current battery provides a considerable safety margin for intended 1-hour tests (lasting approximately 4 hours), for chronic ambulatory use during the waking hours, a battery life of approximately 16 hours would be required. Achieving this extended battery life may involve integrating a more powerful battery and implementing system optimisation strategies, such as a sleep mode that reduces the system's functions when tremor activity has ceased.

Memory constraints currently limit the duration of recordings with our device. While the existing memory capacity suffices for the 48-minute protocol designed for testing in a laboratory setting, expanded storage would be essential for real-world, out-of-lab applications. Adapting this system for ambulatory use necessitates significant changes to its memory architecture. Possible solutions could include integrating a wireless transmission component to periodically offload data to an external user interface. Additional memory optimisation may involve reducing the number of variables stored—various values were saved during our initial testing to ensure the

device functioned as intended, but following the system's validation, they may no longer be required.

Finally, in its current form, the wrist-worn system interfaces with an external, CE-marked stimulator. For use outside clinical settings, the development of a portable, integrated stimulator is essential. Safety considerations are crucial in designing a device for unsupervised use. Particularly, safety mechanisms must be incorporated to prevent stimulation unless the device is correctly positioned on the wrist. This precaution is required to ensure that users do not inadvertently touch the electrode ends with both hands during stimulation. Such contact could lead to serious injury by causing the electrical current to short-circuit through the heart.

3.6.5. Future directions

A crucial step forward in our research is the validation of the wrist-worn system in individuals who present Parkinsonian rest tremor. This will enable us to ascertain whether the performance of the phase tracking algorithm, as demonstrated in the verification tests of this chapter, remains consistent with real-life pathological tremor. Ultimately, we aim to investigate the effects of phasic stimulation, triggered by this system, on tremor experienced by the study participants. Should phase-locked peripheral electrical stimulation demonstrate significant therapeutic benefits, we envision future research expanding into adapting the system for ambulatory, at-home usage, beyond in-clinic settings.

3.7. Conclusion

In this chapter, we introduced a self-contained, wrist-worn device equipped with an adaptable phase estimation algorithm successfully implemented for tremor-

like oscillations recorded by an accelerometer. This portable system uniquely adapts to variations in tremor characteristics, such as centre frequencies and the axis of maximum excursion, thereby overcoming limitations identified in the study presented in *Chapter 2*. Our custom-built device paves the way for further investigations into the potential benefits of phase-locked peripheral nerve stimulation as a treatment for upper-limb pathological tremor.

4. Validation of an in-house built wrist-worn system for phase-locked peripheral nerve stimulation in people with Parkinson's disease

This chapter outlines the validation of our adaptable, phase-tracking wrist-worn system. We assessed the system's phase-tracking performance and adaptability in a cohort of three people with Parkinsonian rest tremor. Additionally, we examined the impact of peripheral electrical stimulation, both phase-locked to the tremor and non-phasic, administered to the median nerve in these participants. The chapter concludes by delving into the implications of the results for research exploring adaptive, phase-locked peripheral stimulation as a potential approach to mitigating pathological tremor.

4.1. Introduction

The adaptive wrist-worn phase-tracking system, detailed in *Chapter 3*, underwent comprehensive verification through computer simulations and benchtop tests. This chapter outlines the procedure employed to validate the device in a cohort of individuals with Parkinson's disease (PD) rest tremor. Subsequently, we delve into the analysis of the collected data, examining the observed effects of stimulation. The chapter concludes with reflections on the lessons learned from the device validation and outlines potential avenues for future research.

Phase-specific electrical stimulation at the median nerve has demonstrated significant modulation of Parkinsonian and essential tremor (ET), particularly when considering instantaneous changes in tremor. In individuals with PD, phasic stimulation resulted in significant median tremor suppression (36%) and amplification

(117%) (Arruda et al., 2021). Conversely, in those with ET, phasic stimulation led to modest but statistically significant tremor modulation (Reis et al., 2021). Notably, studies on ET have indicated that stimulation parameter optimisation, including stimulation phase, can effectively reduce tremor power by up to 65% (Kim et al., 2022). Moreover, constant, non-phasic high-frequency peripheral nerve electrical stimulation has shown promise in suppressing ET, with significantly larger improvement in subject-rated tasks during treatment in relation to sham: a 49% vs. a 27% reduction, respectively (Isaacson et al., 2020; Pahwa et al., 2019).

However, a comparative study examining the effects of phasic and constant (non-phasic, open-loop) peripheral nerve stimulation in individuals with PD is lacking. A main limitation in implementing such investigations in people with PD is the extensive variability of Parkinsonian rest tremor, with the dominant tremor axis switching several times across minutes-long recordings, and significant changes in tremor centre frequency occurring (Arruda et al., 2021)[6]. Similarly, only instantaneous effects of phasic stimulation, within 5-second windows, have been explored in people with PD, and the impact of prolonged phasic stimulation, lasting several minutes, is yet to be investigated (Arruda et al., 2021).

In this chapter, we performed a preliminary validation with individuals having PD for a system designed to account for the variability in Parkinsonian tremor, while estimating the phases of these oscillations in real time. The system's adaptable element allowed for switching the tracked tremor dominant axis and centre frequency. Previously, the system was validated in bench-top tests and mimicked tremor.

[6] Distinct tremor oscillation patterns were identified following cluster division, performed considering 5-second epochs of accelerometer-recorded tremor data. Clusters lasted 214.8 ± 136.8 seconds (mean ± SD) with median instantaneous centre frequency differences of 0.1 ± 0.2 Hz across clusters for each accelerometer axis. Median instantaneous frequencies ranged by 0.9 ± 0.5 Hz (mean ± SD) and up to 2 Hz across epochs of each axis, cluster, and participant.

In this study, we aim to test whether: (i) the phase tracker accurately estimates phase in accelerometer-recorded pathological tremor signals; (ii) the system adapts to changes in the tremor axis of maximum excursion and its centre frequency; (iii) when a subject-specific optimal stimulation state is selected (phasic or constant non-phasic stimulation), stimulation significantly modulates tremor. Additionally, we showcase the robustness of the wrist-worn system through in-clinic tests with study participants.

4.2. Materials and methods

This section describes the study participants, recording, and data analysis procedures.

4.2.1. Cohort

The device was validated in a cohort of three male study participants exhibiting Parkinsonian rest tremor predominantly in their right hand. All three regularly took medication for their PD motor symptoms but omitted their last medication dose before the study. This study received approval from the Health and Social Care Research Ethics Committee A (HSC REC A) of the Health Research Authority, National Health Service (NHS, UK), in accordance with the Declaration of Helsinki (reference number: 19/NI/0009). All participants provided informed consent before participating in the tests. As part of the recruitment process, participants were screened to exclude individuals with a personal or family history of epilepsy or those with implantable devices. Stimulation sensation was evaluated through a five-point Likert scale questionnaire having the following options: “The stimulation was easily tolerated: A) Strongly disagree; B) Disagree; C) Neither agree nor disagree; D) Agree; E) Strongly agree”. Participant information is summarised in Table 4.1.

Participant	1	2	3
Age [years]	63	59	62
Gender	Male	Male	Male
Arm tested	Right	Right	Right
Parkinson's disease medication state	On, omitted last dose	On, omitted last dose	On, omitted last dose
Random search stimulation amplitude [mA]	5.0	10.0	5.0
Continuous stimulation amplitude [mA]	4.5	10.0	5.0
Tremor amplitude (mean ± SD) [g]	0.43 ± 0.12	0.23 ± 0.13	0.59 ± 0.26

Table 4.1: Individual study participants' characteristics. *Tremor amplitude was obtained from the envelope of the most frequent dominant axis in the recordings obtained without stimulation before the first (random search) stage of the testing protocol.*

4.2.2. Data acquisition equipment

The wrist-worn system executed various stages of the experimental protocol, recording participants' tremor using an on-board triaxial accelerometer (sampling rate of 208.03 Hz). It estimated the tremor phase in real-time using the algorithm outlined in *Section 3.3—Software design*, triggered stimulation through an externalised CE-marked device (Digitimer Constant Current Stimulator DS7A), and saved data to a

memory card. The externalised stimulator delivered pulses via a stainless-steel bar electrode attached to the device's wrist strap.

4.2.3. Testing protocol

Each study participant was instructed to sit on a chair, placing their arm over the chair's armrest to allow unrestricted arm movement as their tremor emerged. Participants were directed to refrain from voluntary movements in their tremor-dominant hand and to avoid actively suppressing their tremor.

First, the device was placed on the wrist with the most prominent tremor, positioning the bar electrode over the median nerve on the wrist's ventrum. Electrode paste was applied to reduce skin-electrode impedance. The electrode's position over the median nerve was verified through electrical stimulation, ensuring a visible contraction of the thumb and confirming the participant's perception of the tingling sensation induced by stimulation. Stimulation during subsequent stages was capped at the highest level below the motor threshold that participants found comfortable.

The experimental protocol comprised two stages, each preceded by a baseline recording. The first stage, following a 10-minute baseline, was the random search, lasting approximately 27 minutes. Ten blocks, each with eight stimulation states, were presented. Before initiating each block, the presentation order of the states was randomly shuffled without repetition to prevent confounding order effects in the results.

The eight stimulation states were: (1) phasic stimulation at 0 degrees, (2) phasic stimulation at 60 degrees, (3) phasic stimulation at 120 degrees, (4) phasic stimulation at 180 degrees, (5) phasic stimulation at 240 degrees, (6) phasic stimulation at 300

degrees, (7) constant open-loop stimulation, and (8) sham condition (no stimulation). Each state was presented for 10 seconds, followed by 10 seconds of no stimulation.

In the phasic stimulation settings, five pulses were delivered at each target phase at a frequency of 104.015 Hz, which is half of the accelerometer's sampling rate. This frequency was also used for non-phasic, open-loop stimulation. The selection of 104.015 Hz was primarily for implementation convenience, as it represents a simple fraction (half) of the sampling rate. Additionally, this frequency approximates 100 Hz, identified in previous research as the most effective frequency (among 50, 100, or 200 Hz) for peripheral stimulation in ET treatment, thereby aligning with frequencies shown to be suppressive in other clinical settings (Kim et al., 2022).

The second stage, presented after a 1-minute baseline, involved continuous stimulation for 10 minutes at the single stimulation state selected according to an on-board envelope approximation as the most suppressive. If the sham condition was chosen as the most suppressive, the second most suppressive state was then used for continuous stimulation. The entire protocol lasted approximately 48 minutes. *Figure 4.1* provides a visual summary of the recording stages in the protocol.

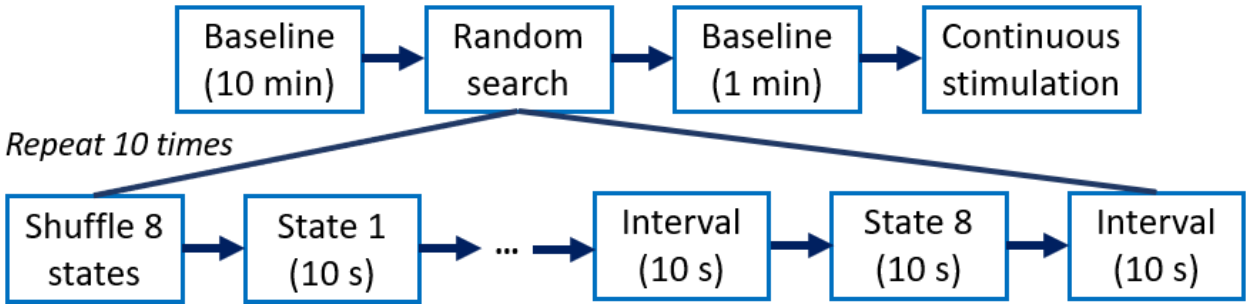


Figure 4.1: Experimental protocol recording stages. *A 10-minute baseline precedes the random search, then followed by a 1-minute baseline and continuous stimulation. Random search consists of 10 blocks, each containing eight randomly shuffled stimulation conditions presented for 10 seconds followed by a 10-second interval.*

4.2.3. Data processing and analysis

The MATLAB (MathWorks, R2022b) data analysis involved (i) validating the phase estimator's performance through comparison with its offline version (outlined in *Section 3.4.1—Offline, MATLAB-based algorithm characterisation*), (ii) examining the impact of stimulation during random search, (iii) generating confidence intervals to assess the significance of tremor changes during the random search, and (iv) exploring the effects of continuous stimulation at the selected optimal state.

The tremor envelope played a role in all analysis stages outlined above. The offline envelope was obtained by applying the Hilbert transform to all accelerometer-recorded data points. Before applying the Hilbert transform to the accelerometer data, we performed band-pass filtering using a second-order, forward and backward, Butterworth filter. This filter operated within the frequency range of 1 to 9 Hz, aiming to cover the range of tremor frequencies of interest, specifically from 2 to 8 Hz.

Subsequently, the envelope was obtained by computing the Hilbert transform and taking its absolute value.

4.2.4. Phase estimation algorithm's performance

Raw triaxial accelerometer data collected during the random search and continuous stimulation protocol stages served as input for an offline MATLAB-based phase-tracker. Similar to the online phase-tracker, 21 algorithm streams ran concurrently for each participant. These streams corresponded to the three accelerometer axes and seven centre frequency values (ranging from 2 to 8 Hz with 1 Hz increments). For offline comparison, the phase estimator stream corresponding to the dominant tremor axis and the selected centre frequency from the online version were chosen.

Phase error was computed for each data point by determining the absolute difference between the online (on-board) and offline (MATLAB-based) versions of the algorithm. To address instances of phase wrapping, a correction factor was applied: for errors surpassing 180 degrees, 360 was subtracted from the error and the absolute value of this difference was computed. The mean and standard deviation of this phase error were then calculated for both random search and continuous stimulation conditions.

The precise online phase estimate was anticipated to remain well within the error tolerance predefined in *Chapter 3* (see *Section 3.1.1—Design requirements*). However, a perfect alignment with the target stimulation phase was not expected, as the phase resolution imposed by the sampling rate (208.03 Hz) must be accounted for. An error budget, as detailed in *Chapter 3*, was then considered, allowing stimulation if the target phase fell within the budget to avoid missing stimulation points. This is

further explained in *Section 3.3.6—Triggering stimulation*. A phase error was defined as the absolute difference between the target phase and the precise online phase estimate. Similar to the online vs. offline phase estimate comparison, a correction factor was applied to address wrapping around cases by subtracting 360 from the phase error's absolute value when it exceeded 180 degrees. Finally, the mean and standard deviation of the error were computed for both random search and continuous stimulation conditions.

A final comparative analysis was conducted between the phase estimated by the on-board system in the random search condition and the phase derived from the Hilbert transform applied to signals band-pass filtered from 1 to 9 Hz. The phase error was defined between the absolute value of these two estimates and corrected as above to address phase wrapping cases.

4.2.5. Adaptation to changes in the tremor dominant axis and centre frequency

To confirm the reproducibility of the on-board dominant axis and centre frequency selection, we conducted a comparison with results obtained from a MATLAB-based algorithm. For the offline replication of dominant axis selection, we applied a moving average filter (with a window length of 520 samples, or 10 seconds) to the absolute value of the triaxial accelerometer signals. These signals were down-sampled by a factor of 4, mirroring the on-board process. The dominant axis was identified as the one with the highest moving average, just before the onset of a 10-second state presentation, aligning with the on-board algorithm's approach.

For centre frequency selection, seven streams of the algorithm were run in parallel for each accelerometer axis offline, each tuned to centre frequencies from 2 to

8 Hz, as was done on-board. We calculated the moving average of the error signal, derived from the absolute difference between the input signal and its estimate. Out of these streams, the one with the lowest error signal was chosen for the dominant axis selected on-board, facilitating a comparison of centre frequency selection between online and offline versions.

To further characterise frequency selection, we also computed the instantaneous frequencies from the on-board recordings using the Hilbert transform applied to band-pass filtered signals (1 to 9 Hz). This involved computing the unwrapped Hilbert phase and its approximate derivative. For each 10-second segment considered in the frequency selection, we computed both the median (as a non-standardised metric) and the standard deviation.

4.2.6. Random search stimulation state-amplitude response profiles

The envelope of the triaxial tremor data collected during the random search condition served as a basis to assess the impact of the eight distinct stimulation states on each participant's tremor. This analysis involved individually examining the 10-second segments during which different stimulation states were presented, along with the last second of the 10-second interval without stimulation that preceded them.

The change in tremor severity at each stimulation state presentation (or trial) was computed by calculating the mean tremor severity in the 1 second prior to the trial's initiation (μ_i) and the mean in the last 1 second of stimulation (μ_f). The change in tremor severity per 10-second trial was then determined as: $\frac{\mu_f - \mu_i}{\mu_i}$. This calculation allowed for the assessment of the instantaneous effects of stimulation within each 10-second trial, normalised to a scale where -1 denoted complete tremor suppression, zero indicated no change in the tremor, and positive values indicated amplification.

Subsequently, trials were organised per participant based on the dominant axis being tracked by the wrist-worn system. For instance, all y-dominant trials were grouped together, with all x- and z-dominant trials removed from that analysis.

Phasic stimulation trials characterised by high phase error (previously computed as the absolute value of the difference between online and offline phase estimates) were excluded from the analysis. High phase error was defined as 10-second trials where the mean error, added to its standard deviation, exceeded 30 degrees, which corresponded to half of the phase resolution. Those were excluded because the effects of phasic stimulation could not be reliably assessed when phase could not be estimated accurately.

Following that, the change in tremor severity values were organised based on the eight corresponding states, and the median change was calculated for each state. Profiles illustrating the median change in tremor severity per state were subsequently constructed. The significance of the change in tremor severity in these plots was assessed as outlined below.

Bonferroni-corrected confidence limits

The Bonferroni-corrected confidence intervals were calculated individually for each tremor axis and participant using the envelope of the corresponding accelerometer recordings obtained during baseline recordings (without stimulation). To generate these confidence limits, 50,000 10-second segments were randomly drawn from each tremor axis envelope without stimulation, allowing for potential overlap in time. Subsequently, the change in tremor severity was computed for each segment as $\frac{\mu_f - \mu_i}{\mu_i}$, where μ_i represented the mean envelope in the 1 second preceding the 10-second segment, and μ_f was the mean in the last second of the 10-second segment.

Thereafter, the average number of trials per state (denoted as n) was calculated for each participant. From the previously created distribution with 50,000 points, n points were drawn 1,000,000 times, resulting in a second distribution. The Bonferroni correction for multiple (eight states) comparisons was applied to this distribution with 1,000,000 points, generating upper and lower confidence intervals for the stimulation state-amplitude response profiles.

4.2.7. Continuous stimulation effects

To evaluate the impact of continuous stimulation at the state identified as optimal, the mean and standard deviations of the dominant tremor axis's envelope were calculated for three distinct conditions: the 1-minute baseline (without stimulation), the 10-minute continuous stimulation, and the final 1-minute segment of continuous stimulation. To determine whether there were statistically significant differences in the central tendencies between the 1-minute baseline and the final 1-minute recording with stimulation, we focused again on the envelope of the most frequently identified dominant axis for each participant. In this analysis, we employed the non-parametric Wilcoxon rank-sum test to compare the tremor envelopes of the baseline recording and final minute of stimulation.

Additionally, we calculated the median, representing the 50^{th} percentile, of the envelope for each axis during the non-stimulation recording condition. We then determined the percentage of envelope segments that remained below this baseline median throughout the entire 10 minutes of stimulation, as well as during the final 1 minute of stimulation. To assess the significance of the differences in durations between these stimulation segments and the baseline recordings, we employed the Wilcoxon rank-sum test.

4.3. Results

4.3.1. Phase estimation algorithm performance

The performance of the phase estimation algorithm was consistent with the results obtained from the verification of the wrist-worn system (refer to *Section 3.5—Verification results*). The mean overall phase error, computed using the exact values for all data points where phase was estimated both online and offline, remained below 0.5 degrees for two study participants (labelled P1 and P3). P2, however, exhibited a slightly higher mean and standard deviation of the error, with the mean surpassing 2 degrees during the random search recording condition. The mean phase error, defined between the precise online phase estimate and the target stimulation phase, remained within the error budget accounting for sampling rate restrictions as defined in *Chapter 3*. *Table 4.2* presents the mean and standard deviation of these errors, both overall and at the target stimulation phase. All values, as presented in *Table 4.2*, consistently stayed well below the phase error tolerance of 30 degrees. These results reinforced the reliability of the phase estimation algorithm in capturing accurate phase information in the context of this experimental protocol.

The random search stimulation condition encompassed all six target phases presented in a random order, as anticipated. *Figure 4.2* illustrates the target and exact stimulation phases, in their presentation order, during the random search for all study participants. The precise stimulation phase may not align perfectly with the target phase due to the error budget and sampling rate restrictions, as summarised in *Table 4.2*. However, it consistently remained in close proximity, as depicted in *Figure 4.2*.

To explore the disparities in the mean overall errors between P1 and P3 compared to P2, when higher phase errors (as shown in *Table 4.2*) were observed, the

time courses of these errors were plotted for each study participant. *Figure 4.3* illustrates the error time courses for all three study participants during the random search condition.

Participant	Overall error, random search (mean ± SD) [deg]	Overall error, continuous stimulation (mean ± SD) [deg]	Error at stimulation, random search (mean ± SD) [deg]	Error at stimulation, continuous stimulation (mean ± SD) [deg]
P1	0.2 ± 0.5	0.4 ± 2.8	4 ± 3	-
P2	2.4 ± 12.3	0.9 ± 4.8	6 ± 5	4 ± 3
P3	0.2 ± 0.3	0.2 ± 0.4	6 ± 8	8 ± 11

Table 4.2: Phase errors for each study participant during random search and continuous stimulation conditions. *The first two columns depict the error (absolute value of the difference) between the online (on-board) and offline (MATLAB) phase estimates, considering all data points during both random search and continuous stimulation conditions. The last two columns present the error defined between the precise online phase estimate and the target stimulation phase. The error is not provided for P1 under the continuous stimulation condition because the selected stimulation setting was open-loop for that participant.*

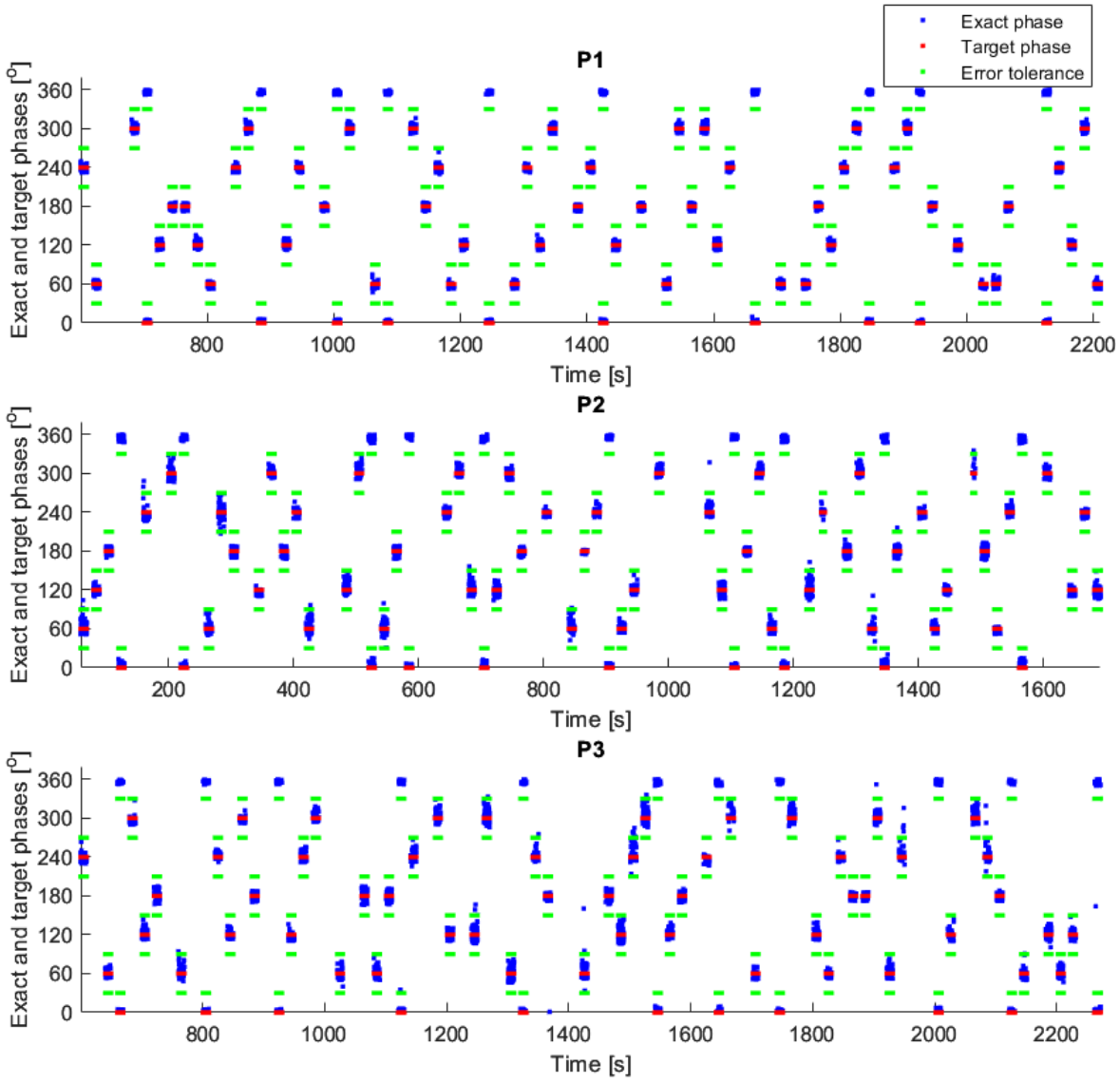


Figure 4.2: Exact (in blue) and target (in red) stimulation phases during the random search condition for all study participants, covering six target phases presented in random order. *The phases do not perfectly align due to sampling rate restrictions, but the stimulation phases remained close to the target phase and below the predetermined 30-degree mean error limit (in green).*

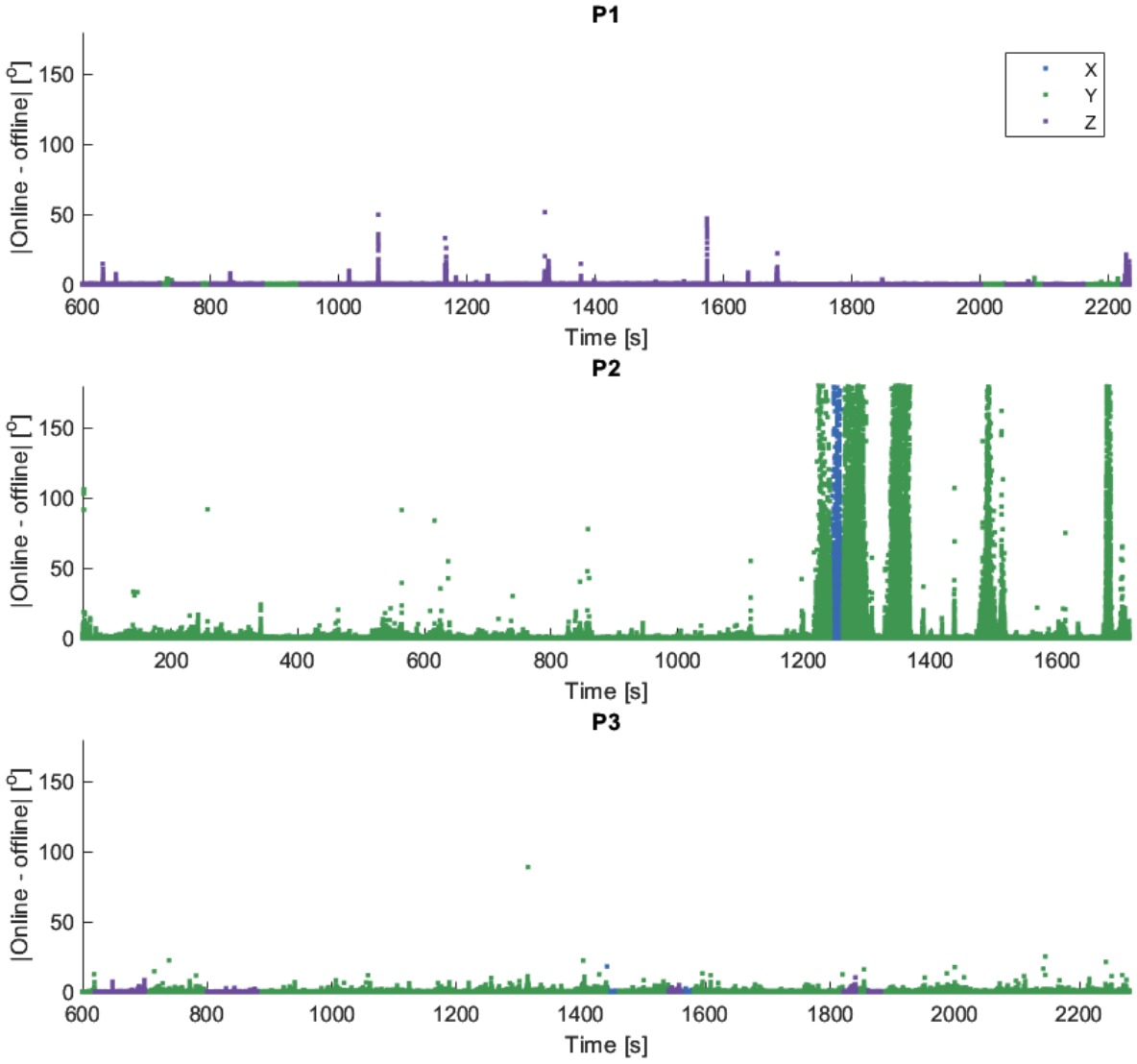


Figure 4.3: Phase error time courses for each study participant during the random search condition. *Error is defined as the absolute value of the difference between the on-board estimated phase and the one obtained from the offline MATLAB version of the algorithm. Changes in the dominant axis tracked by the system are indicated by representing x-axis dominant trials in blue, y-dominant trials in green, and z-dominant trials in purple. High phase error, evident in P2, occurred in segments during which the tremor stopped.*

Particularly in the case of P2, there were noticeable segments with high phase error. Specifically, when the tremor signal is too low or disappears (indicating the absence of tremor), the algorithm lacks a phase reference, leading to random outputs, as discussed in *Chapter 3*. This occurs because there cannot be any phase estimate without a tremor signal. In segments with low error, the envelope for the tracked axis measured 0.29 ± 0.14 m/s^2 (mean ± SD). Conversely, the envelope for segments with high error approached zero: 0.03 ± 0.07 m/s^2 (mean ± SD). *Figure 4.4* illustrates examples of random search 10-second segments, distinguishing between high and low phase error. High phase error segments are identified as those with the mean error plus standard deviation surpassing 30 degrees.

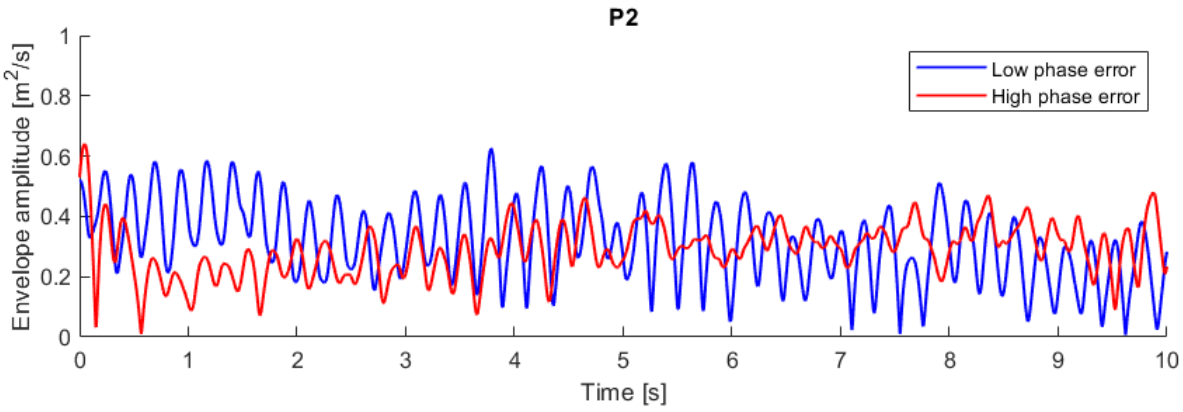


Figure 4.4: Example 10-second segments obtained during the random search condition. *The segment with the mean phase error (absolute value of the difference between online and offline estimates) closest to the median of those classified as 'low' error is displayed in blue. In contrast, the segment corresponding to the mean phase error closest to the median of the segments classified as 'high' error is displayed in red.*

In the final characterisation with the Hilbert transform, for P1, the overall phase error was found to be 5.2 ± 8.2 degrees (mean ± SD), aligning with previous characterisations of the algorithm (as discussed in *Section 3.5.1—Offline, MATLAB-based algorithm characterisation*). However, in participants P2 and P3, the errors were, respectively, 26.0 ± 31.5 and 21.0 ± 26.3 degrees (mean ± SD). While the observed mean error for participants P2 and P3 remained within the predefined 30-degree margin, it was notably higher. This increase may be partly attributed to instances where the online error spiked due to drops in accelerometer signals and consequent loss of phase reference, as particularly evident for P2 in *Figure 4.3*. Additionally, as shown in *Table 4.1*, P2's mean tremor amplitude was below the minimum levels we previously characterised for accurate signal detection and phase estimation (refer to *Section 3.1.1—Design requirements*. The increased variability observed in the tremor signals of P2 and P3 could also contribute to this error. We will delve deeper into this signal variability in the subsequent subsection.

4.3.2. Adaptation to changes in the tremor dominant axis and centre frequency

The dominant axis selection performed consistently with the results obtained in the verification tests presented in *Chapter 3*. As shown in *Figure 4.5*, in most data segments, the axis chosen by the on-board system matched the one selected by the offline version of the algorithm, thus confirming the reproducibility of the on-board axis selection. There was a single exception in one segment for P3, where the discrepancy in the moving average calculation between the axes selected online and offline was less than 0.001 g. This single mismatch instance can likely be attributed to rounding disparities between the on-board C++ implementation and the offline MATLAB-based version.

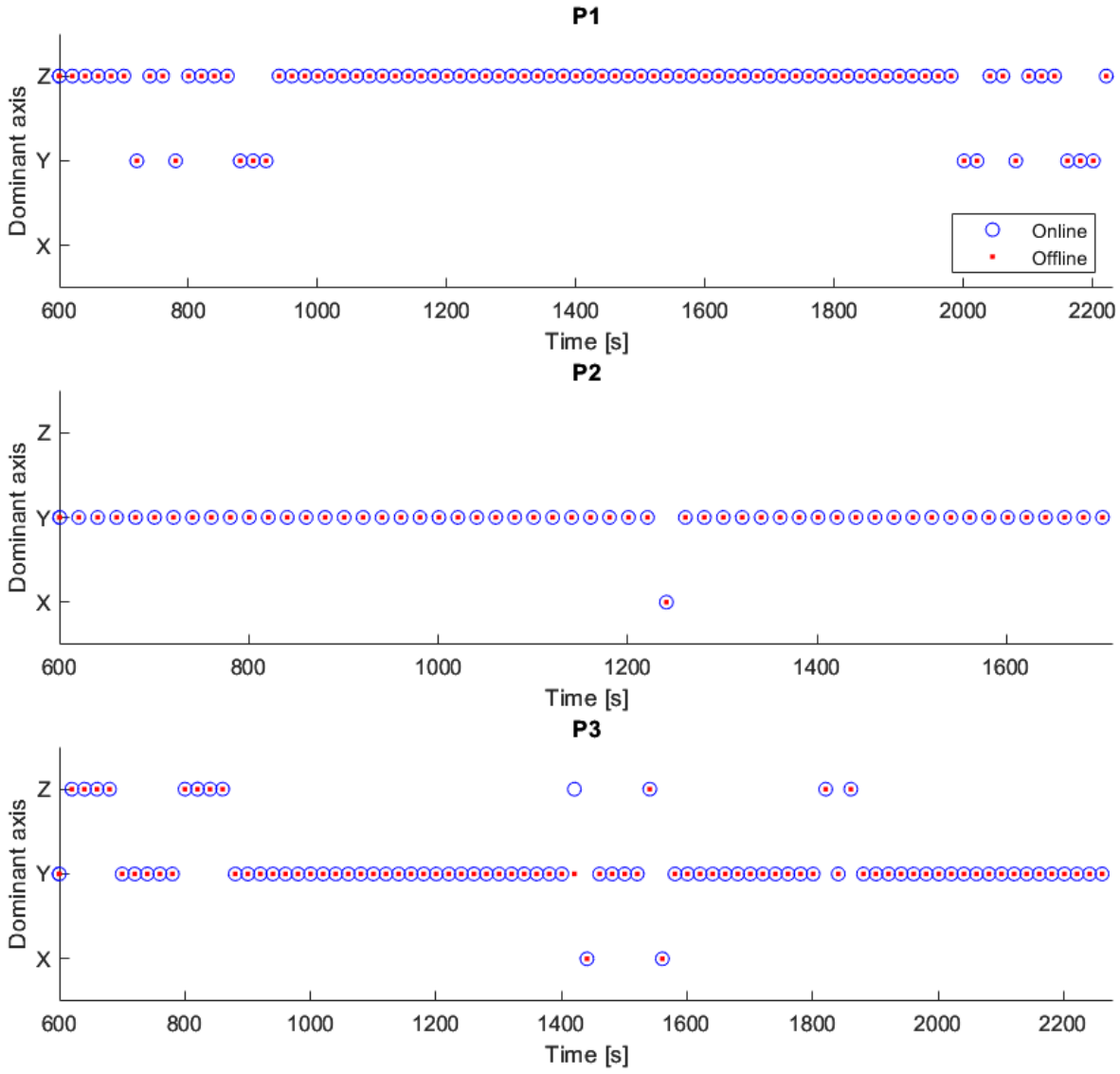


Figure 4.5: Dominant axis selection as performed by the wrist-worn system (online) and in MATLAB (offline) during the random search condition for all study participants. *The dominant axis was updated every 20 seconds based on the moving average of the accelerometer signals. The online selection is indicated in blue and the offline one is marked in red. On-board and offline selection matched for all but one segment.*

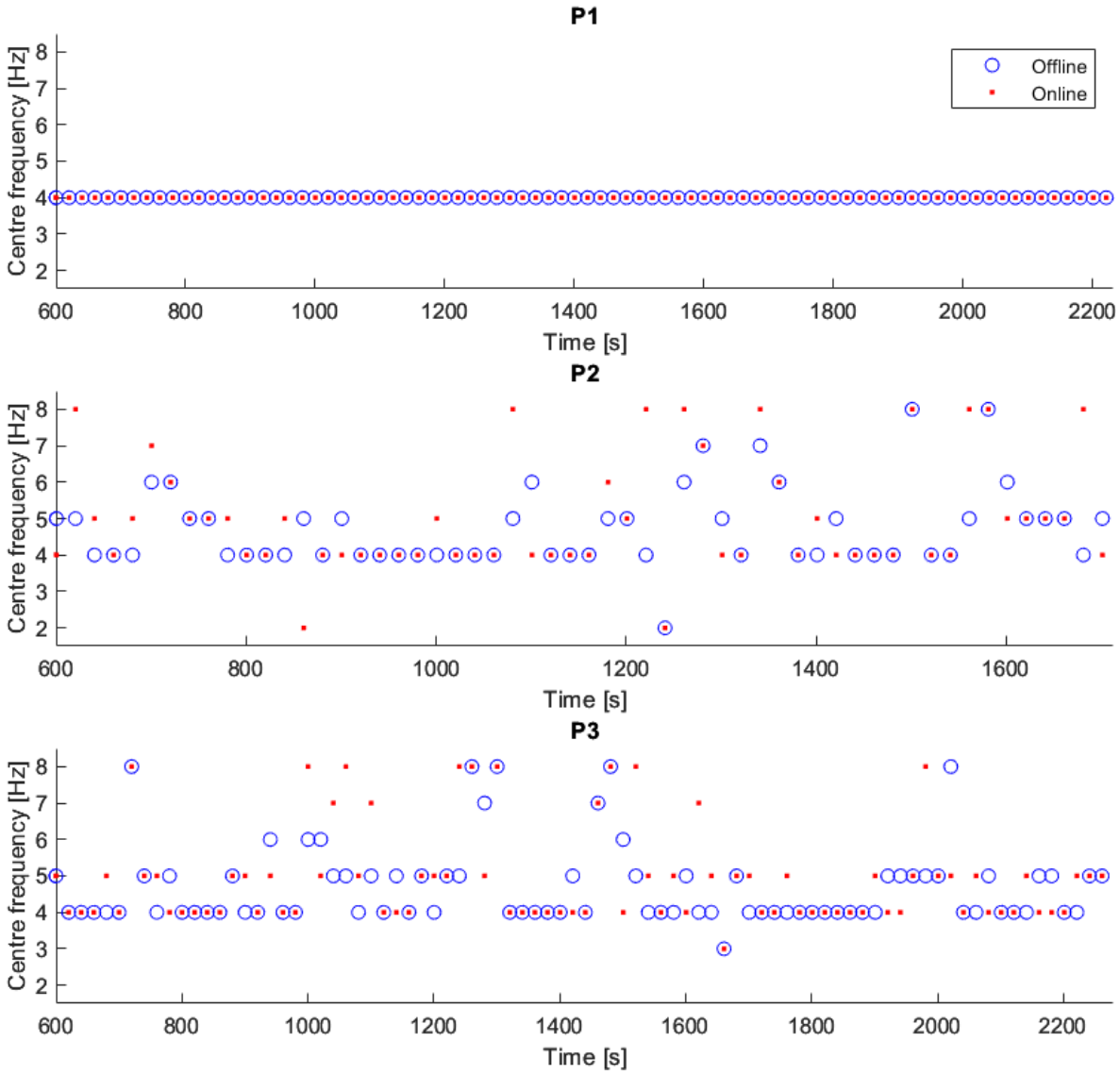


Figure 4.6: Centre frequency selection as performed by the wrist-worn system (online) and in MATLAB (offline) during the random search condition. *The dominant axis was updated every 20 seconds based on the moving average of the accelerometer signals. The online selection is indicated in blue and the offline one is marked in red.*

Further analysis revealed significant differences in tremor behaviour among participants, especially in terms of the consistency of tremor centre frequencies. P1 displayed a remarkably consistent tremor, with the centre frequency constantly selected at 4 Hz. In contrast, P2 and P3 exhibited more variability in their tremor centre frequencies. When comparing the online centre frequency with the median instantaneous frequency (computed offline with a 0.1 Hz resolution), the online frequency in P1 matched within 1 Hz in all cases. This was the case in 71% of segments for P2 and 81% for P3, indicating less consistency in their tremor patterns.

4.3.3. Random search stimulation state-amplitude response profiles

To evaluate the effects of stimulation in various states, we first evaluated the changes in tremor severity for each of the three axes tracked as dominant (see *Figure 4.7*). Only the most frequently tracked dominant axis had enough trials to construct stimulation phase-amplitude profiles using the median change in tremor severity per state. This was because the secondary dominant axis in all participants had at least one state without any trials. *Table 4.3* provides an overview of the total number of trials where each axis was tracked as dominant across all participants.

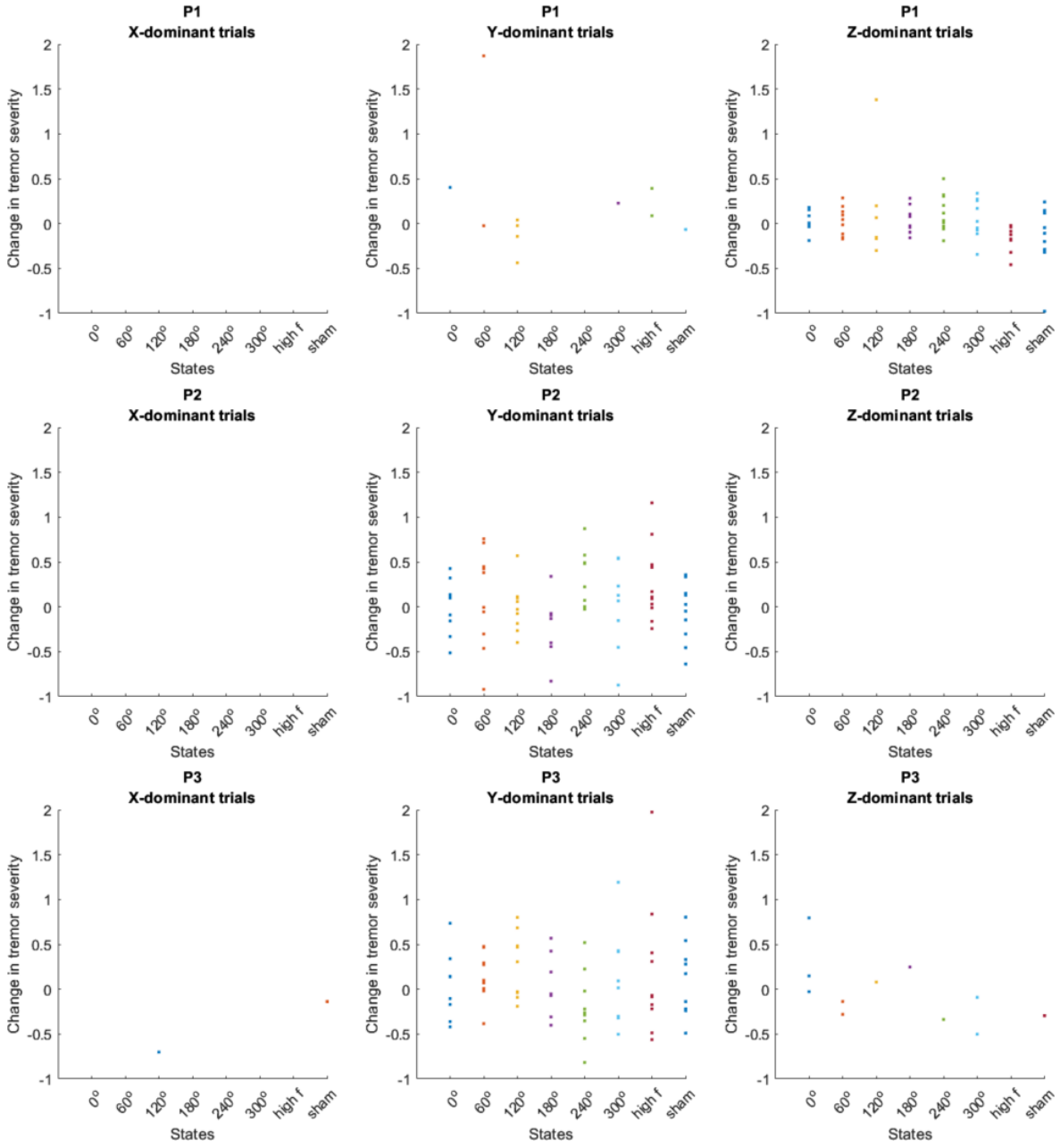


Figure 4.7: Scatter plots illustrating the change in tremor severity at each trial*. Each row corresponds to one of the three study participants, and each column represents the dominant tremor axis tracked by the system during those trials. It is noteworthy that, for the axes that were not the most frequently tracked, there are states without any trials.*

Participant	X-dominant	Y-dominant	Z-dominant
1	0	11	71
2	0	76	0
3	2	71	11

Table 4.3: Number of stimulation trials presented with each axis tracked as dominant for each study participant.

Figure 4.8 illustrates the phase-amplitude profiles for each stimulation state, presenting the median change in tremor severity for all stimulation states, tremor axes, and study participants. The data includes trials where the most frequently occurring dominant axis was tracked. The average number of trials per state, n, used for generating Bonferroni-corrected confidence limits was eight for P1 and P3 and nine for P2.

Without accounting for the confidence limits, median tremor amplification was more common than suppression. Considering that in each plot one bin corresponds to the median change in tremor for one of eight states, 37.5% of the total number of bins exhibited tremor suppression, while 62.5% showed tremor amplification.

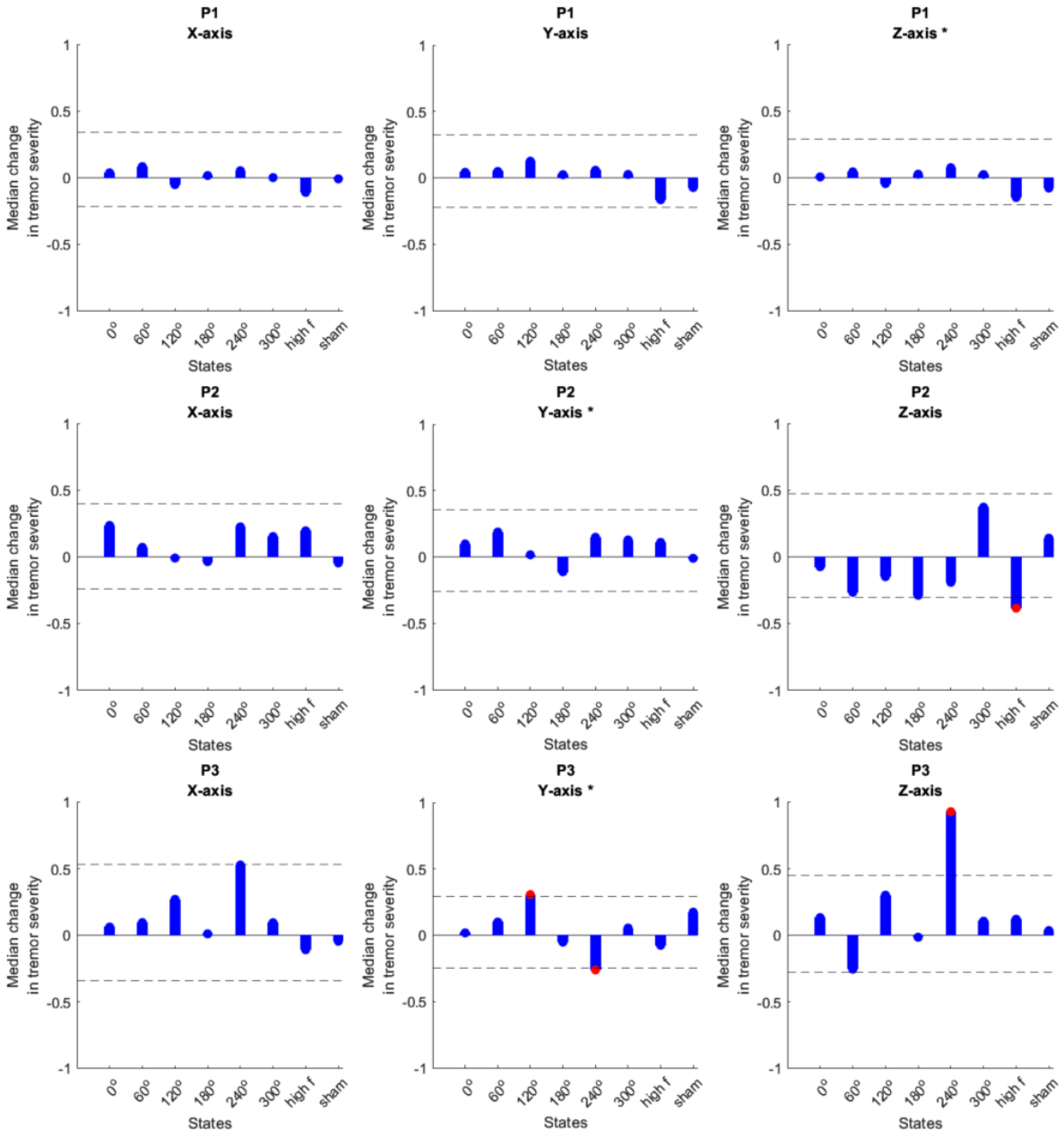


Figure 4.8: Stimulation state-amplitude profiles showing the median change in tremor severity per state. *The confidence limits generated with the Bonferroni correction for eight states comparisons are displayed as a dotted line, and the states for which the change in tremor severity was significant are indicated in red. Most frequently dominant axes, indicated in the plot titles with '*', were z, y, and y, for P1, P2, and P3, respectively.*

Significant tremor reduction was observed in two out of three study participants, P2 and P3. Specifically, P2 experienced 39% median tremor suppression at the constant, high-frequency (non-phasic) stimulation setting for the z (non-dominant) axis. On the other hand, P3 displayed 26% median tremor suppression at the 240-degree phasic stimulation setting for the y (dominant) axis. P3 also exhibited significant tremor increase, with 31% and 93% median tremor amplification occurring at the 120-degree setting for the y (dominant) axis and 240-degree for z (non-dominant), respectively. It is important to note that in the sham (no stimulation) condition, there was no significant change in tremor for any of the participants or their axes.

4.3.4. Exploring an example of significant change in tremor

Notably, in P3—the study participant exhibiting a significant suppression in tremor during phasic stimulation during the random search stage—significant suppression in the most frequently dominant axis (y) was accompanied by significant amplification in the second most frequently dominant axis (z). Out of a total of 10 trials at 240 degrees, seven exhibited an inverse relationship between the change in tremor severity across axes y and z. In five trials, tremor was suppressed in x and amplified in z, while in the other two, it was amplified in y and suppressed in z.

Figure 4.9 visually represents, for this participant, the tremor envelope time courses of the y and z axes during these 10 trials at 240 degrees, including the 1 second prior to the onset of stimulation (utilised in the change in tremor severity calculation). In trials 1 and 8, for example, clear changes in the dominant axis during the 10-second phasic stimulation were observed, with the y-axis overtaken by the z-axis.

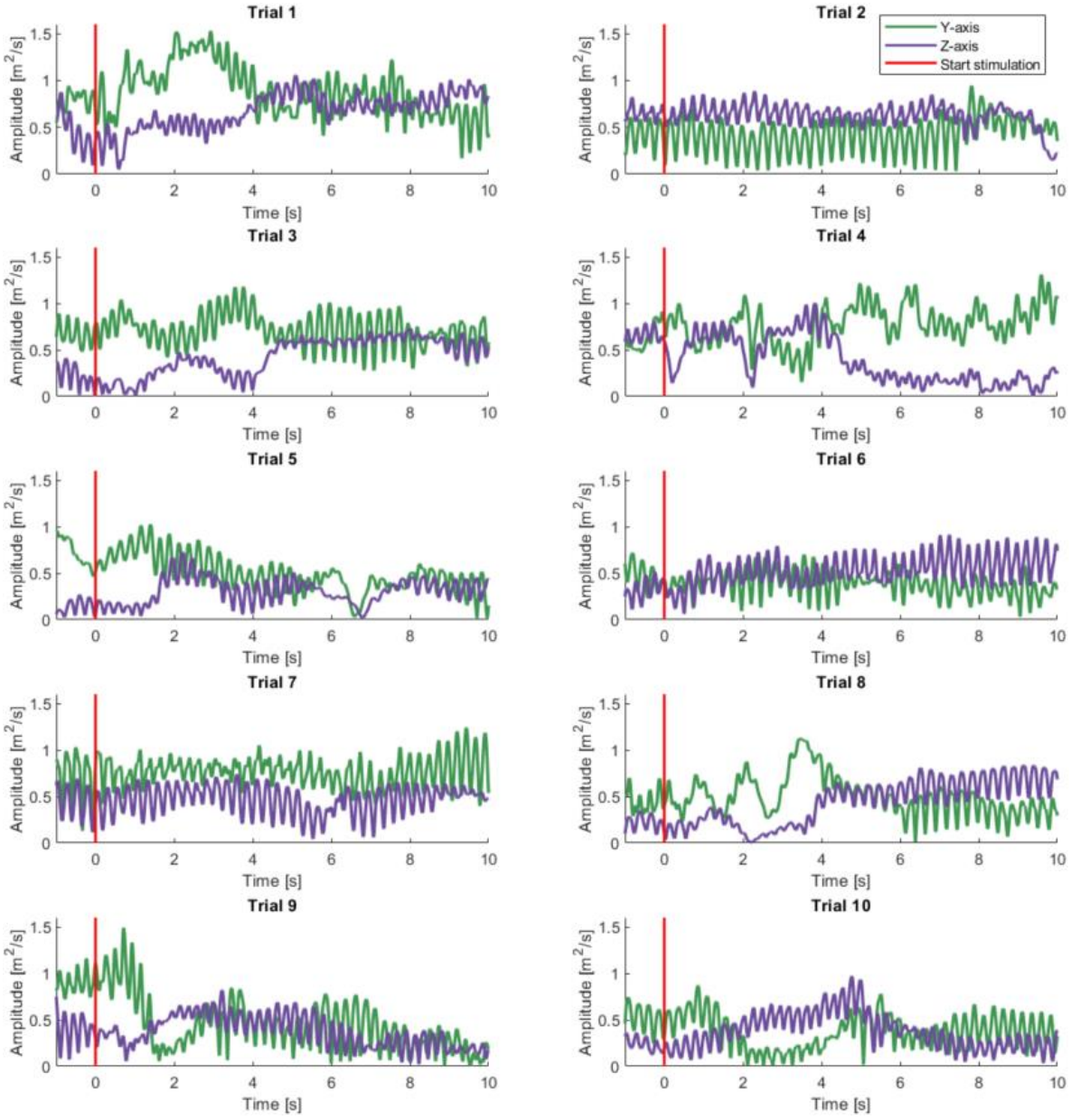


Figure 4.9: Tremor envelope time courses obtained during the random search for P3. *The envelope corresponding to the axis y is illustrated in green and that corresponding to z in purple during all 10-second trials at 240 degrees, in addition to the 1 second prior to the start of stimulation and the subsequent 10 seconds of stimulation.*

4.3.5. Continuous stimulation at the most suppressive state

Continuous stimulation was delivered for 10 minutes at the state identified as the most suppressive one within the axis tracked as dominant during the random search condition. The subject-specific optimal stimulation states, determined online from an envelope approximation (refer to *Section 3.3.5—Calculation of change in tremor severity),* matched, for all three participants, the optimal states computed offline from the Hilbert transform (see *Figure 4.8*). The continuous stimulation states were constant high-frequency (open-loop, non-phasic), phasic at 180 degrees, and phasic at 240 degrees for P1, P2, and P3, respectively.

The impact of continuous stimulation was initially evaluated based on the mean and standard deviation of the most frequent dominant axis's envelope in three segments: the 1-minute recording without stimulation, the final 1-minute of stimulation, and the entire 10 minutes of stimulation, summarised in *Table 4.4*. For P2 and P3, individuals with optimal phasic stimulation states selected, the tremor envelope amplitude increased and remained close to that of the baseline recording when accounting for the standard deviation. Conversely, in P1, exposed to continuous non-phasic stimulation, tremor decreased compared to the baseline recording.

The Wilcoxon rank-sum test was applied to compare the tremor envelope of the 1-minute baseline recording with that of the envelope during the final minute of stimulation, focusing on the most frequently dominant axes. This analysis revealed significant differences across these segments in P1 and P2 ($p << 0.05$ in both cases) but not in P3 ($p = 0.2343$).

Participant	Envelope without stimulation, 1 min (mean ± SD) [g]	Envelope during stimulation, final 1 min (mean ± SD) [g]	Envelope during stimulation, all 10 min (mean ± SD) [g]
1	0.54 ± 0.11	0.29 ± 0.13	0.39 ± 0.12
2	0.19 ± 0.10	0.37 ± 0.15	0.34 ± 0.19
3	0.46 ± 0.21	0.46 ± 0.21	0.50 ± 0.21

Table 4.4: Summary envelope metrics during distinct continuous stimulation segments. *The mean and standard deviation of the tremor envelope are presented for the most frequently tracked dominant axis of each participant during continuous stimulation in three segments: 1 minute without stimulation, the final 1 minute of continuous stimulation, and the entire 10 minutes of continuous stimulation.*

To further explore potential changes in tremor induced by continuous stimulation, the percentages of the stimulated segment that remained below the median of the recording without stimulation were calculated. *Table 4.5* showcases these percentages for the entire 10-minute segment with stimulation and for the segments with each axis tracked as the most frequently occurring (y and z for P1 and P3, y only for P2). It is noteworthy that, for P1, the axis tracking was not relevant for stimulation purposes, as non-phasic stimulation was applied. In P1, the segments consistently remained below the median for the dominant axes, notably for the z-axis, dominant during the random search, where more than 90% of those segments exhibited suppression, as indicated by staying below the threshold. Between the two participants undergoing phasic continuous stimulation, only in P3's z (non-dominant) axis more than 50% of the stimulation segments significantly remained below the median. *Figure 4.10* provides a visual representation of the percentiles and the tremor dominant axis

time courses throughout the continuous stimulation condition for all study participants.

Participant	Axis	Stimulation segment	Duration below median [%]	Wilcoxon rank-sum test, p-value
1	Y	Final 1-min	74	< 0.0001
	Y	10-min	58	0.0168
	Z	Final 1-min	100	0.0258
	Z	10-min	92	< 0.0001
2	Y	Final 1-min	11	0.9637
	Y	10-min	22	< 0.0001
3	Y	Final 1-min	50	0.3147
	Y	10-min	41	0.2079
	Z	Final 1-min	95	< 0.0001
	Z	10-min	39	< 0.0001

Table 4.5: The percentage of segments during the continuous stimulation condition that remained below the baseline envelope's median amplitude for both the final 1-minute of stimulation and the entire 10 minutes of stimulation. *The table also includes the p-values for comparisons, using the Wilcoxon rank-sum test, between the durations of those segments that remained below the median relative to the baseline. Data is presented only for those axes that were identified as dominant during the 10-minute stimulation period. P-values indicating significant differences are highlighted in red.*

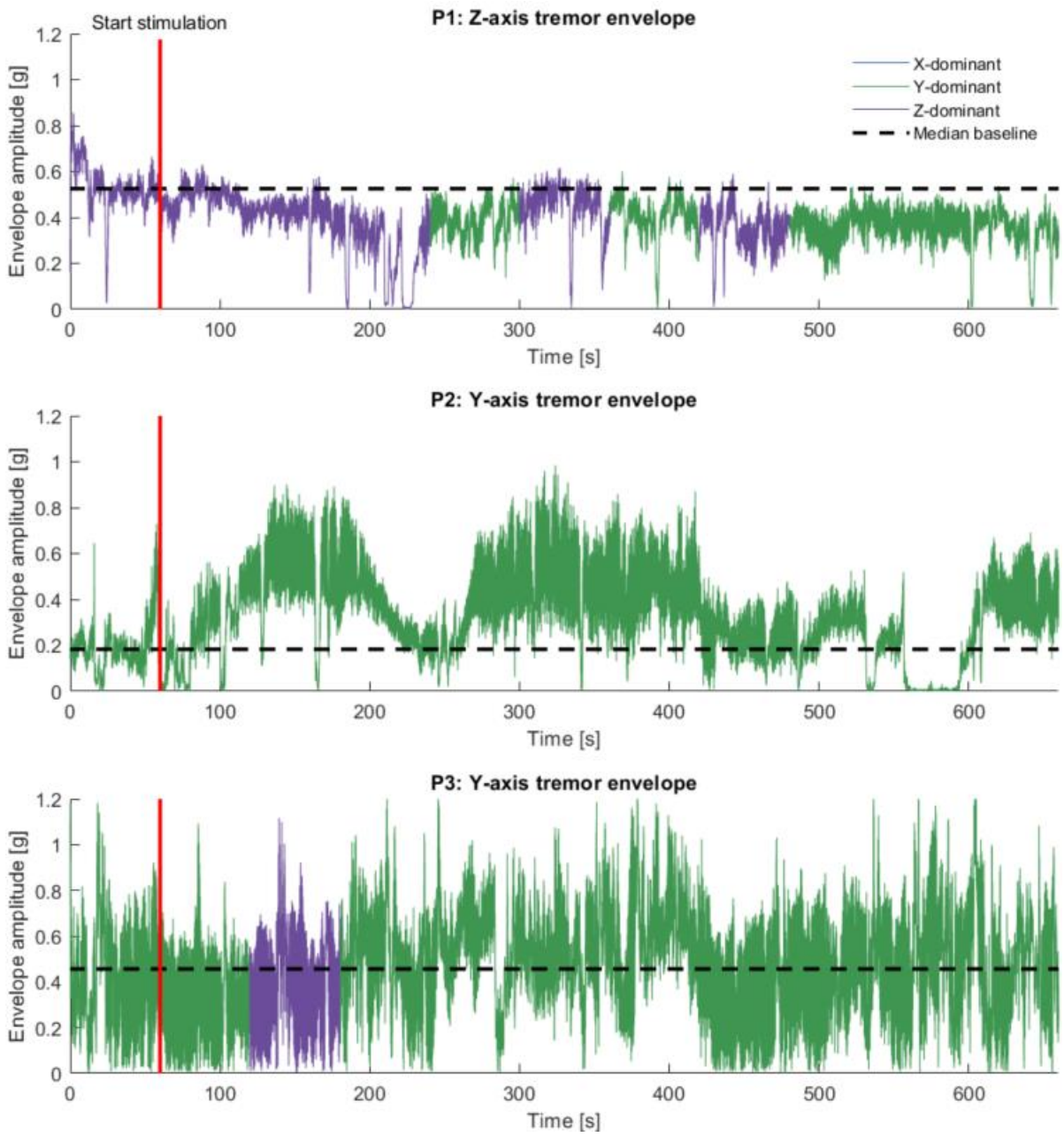


Figure 4.10: Tremor envelope during the continuous stimulation setting for the most frequently tracked dominant axis of each study participant. *Segments in which the dominant axis tracked on-board was x, y or z were plotted in blue, green, or purple, respectively. Continuous stimulation started at the instant indicated with a red horizontal line (after 1 minute of baseline recording).*

4.3.6. Participant feedback

A summary of participant responses, gathered using a 5-point Likert scale questionnaire to assess the sensation experienced during stimulation, is presented in *Table 4.6*. The responses from participants varied, spanning across three distinct items on the scale.

Participant	**1**	**2**	**3**
Likert scale assessment	Strongly agree	Agree	Neither Agree nor Disagree

Table 4.6: Participant responses on the 5-point Likert scale questionnaire. *The Likert scale had the following options: "The stimulation was easily tolerated: A) Strongly disagree; B) Disagree; C) Neither agree nor disagree; D) Agree; E) Strongly agree".*

4.4. Discussion

The wrist-worn system proved to be a robust adaptive tool, effectively estimating Parkinsonian rest tremor in real time, and eliciting significant changes in tremor severity through phasic and non-phasic stimulation. However, the extent to which this system can be considered a viable therapeutic intervention for reducing Parkinsonian tremor remains unknown due to limited number of participants in the validation study.

4.4.1. Phase estimation algorithm validation

The phase estimation algorithm has been validated as a valuable tool for real-time phase tracking of Parkinsonian rest tremor without the need for an a priori band-pass filter, demonstrating performance consistent with that shown in the system verification in *Chapter 3*. This algorithm, previously described for tracking invasively-recorded neural oscillations (McNamara et al., 2022), has now been successfully implemented in a wrist-worn system to work with peripheral oscillations. The occurrence of high error segments (*Figure 4.3*) highlights an expected behaviour of the algorithm: when there is no signal to track, the algorithm outputs random estimates.

Any phase estimation algorithm encounters limitations when the phase reference is lost due to the disappearance of the input signal—an expected scenario in potential therapeutic interventions for tremor. If the tremor is effectively suppressed, the signal will significantly decrease. System designers must then decide how to handle these instances when the tremor disappears. Options include: (i) stopping stimulation (already tested as a stimulation state in the sham condition), (ii) providing constant, non-phasic stimulation (also presented as a possible stimulation state in this protocol), or (iii) our design choice—providing stimulation at random output points. As options (i) and (ii) were tested as stimulation states, we opted for (iii). Another key reason that we opted against stopping stimulation is that, in various studies characterising effects of either peripheral or deep brain stimulation on tremor, stimulation settings are tested against no stimulation, and stopping stimulation typically causes tremor to reemerge (Cagnan et al., 2017; Holt et al., 2016; Isaacson et al., 2020). Other alternatives were not tested to avoid prolonging the protocol duration and the time participants spent in-clinic. However, they may be explored in future studies investigating the effects of phasic stimulation.

4.4.2. Adaptive strategy assessment

The wrist-worn system demonstrated effective adaptability to changes in the dominant tremor axis, a feature that proved essential given the observed shifts in tremor orientation during the recordings, as depicted in *Figure 4.5*. Our approach to dominant axis selection was straightforward, relying on a moving average calculation. An alternative approach, used in other studies, involves computing the tremor vector and estimating its phase (Schreglmann et al., 2021). However, we decided against this method due to several drawbacks: vector calculations can introduce artefacts in the signal, necessitate more intensive filtering, potentially add distortions arising from noise and non-linearities in individual axes, and may not capture the distinct tremor oscillatory patterns that emerge, reflected by changes in the tremor dominant axis (Arruda et al., 2021).

Regarding the selection of the centre tremor frequency, considerable variability was noted in two of the three participants (P2 and P3), as shown in *Figure 4.6*. In these instances, the online frequency selection closely matched the offline criteria—including a replication of the algorithm and the median instantaneous frequency—within 1 Hz for at least 71% of the segments. P1, in turn, displayed a consistent centre frequency. This consistency was mirrored in the frequency selection, with a perfect match between the online and offline data across all segments. This ability to adapt to tremor variability represents an advancement provided by our system and fills a gap left by previous studies, which did not account for such tremor fluctuations (Arruda et al., 2021).

One important consideration for future development is the observed concentration of segments around the 4 to 6 Hz frequency range. Despite segments being centred at all seven tested frequencies, a predominance in this particular range suggests the potential for refining the number of parallel streams considered. By

focusing the frequency selection more narrowly on this range, we could enhance the resolution of the available frequencies and tailor the system more precisely to the most commonly observed tremor frequencies.

4.4.3. Changes in tremor severity upon phasic and non-phasic stimulation

The small size of our participant cohort limited definitive conclusions regarding the potential therapeutic effects of the stimulation. Notably, participant-specific responses did not reveal any conclusive suppressive effects of phasic stimulation. Only one out of three participants exhibited significant instantaneous tremor suppression at a phasic stimulation state, and in this case, the reduction occurred at the dominant axis but was accompanied by significant tremor amplification at the secondary axis. This observation suggests that stimulation may have altered the tremor oscillatory pattern from y-dominant to z-dominant rather than achieving effective suppression (Arruda et al., 2021). This underscores the importance of incorporating adaptive elements in phasic stimulation systems, as distinct tremor oscillatory patterns may be suppressed by different stimulation phases.

Analysing the effects of prolonged, 10-minute-long continuous stimulation, phasic continuous stimulation did not conclusively suppress tremor in P2 and P3, while non-phasic continuous stimulation in P1 exhibited significant suppression—although non-phasic high-frequency stimulation in the random search condition did not produce significant instantaneous changes in tremor for any participant. In P2, the overall effect of phasic stimulation was amplification, with an increase in its dominant axis' mean envelope and significant changes across the baseline and stimulation conditions. Conversely, in P3, no significant effects of phasic stimulation were observed.

The lack of tremor suppression in P2 and P3 during continuous phasic stimulation cannot be solely attributed to a switch in the dominant axis induced by stimulation. This is evident from the fact that the dominant axis remained y throughout the continuous stimulation condition for P2 and during most of it for P3 (*Figure 4.10*). P1, on the other hand, experienced five dominant axis switches during continuous stimulation.

Phasic stimulation demands significantly greater computational resources compared to constant open-loop stimulation. This additional complexity involves real-time phase estimation, optimising stimulation for maximum suppression, and adaptive adjustments to detect and respond to shifts in tremor oscillatory patterns. However, the observed effects of phasic and non-phasic peripheral nerve stimulation on tremor in this study did not reveal any substantial advantage of phasic over non-phasic stimulation.

4.4.4. Limitations and challenges of this study

First, our cohort was notably small, with only three participants. A larger cohort would provide a more robust basis for drawing conclusive observations regarding the potential therapeutic effects of phasic peripheral nerve stimulation on Parkinsonian rest tremor.

Additionally, the selected phase resolution of 60 degrees may be deemed insufficient to precisely capture the participant's optimal suppressive stimulation phase. However, this resolution was a strategic choice aimed at minimising the number of stimulation states to reduce the overall testing duration and thus prevent participant fatigue, especially considering the time spent in-clinic. With a 60-degree resolution, our protocol allowed for the testing of eight stimulation states, including six phasic ones.

The practical need to limit the duration of participants' in-clinic sessions constrained the number of phases we could incorporate into the study. In future studies, particularly those employing a similar system in an ambulatory setting outside the clinic, different settings with finer resolutions could be explored.

The accelerometer's wrist placement may also have limited the system's ability to accurately capture changes in the dominant axis, thereby reducing the usage of the adaptive element in the wrist-worn system. With the sensor enclosed in a self-contained box on the wrist, as opposed to being isolated on the hand knuckle, the constraints on limb movements could lead to a bias in sensed oscillations, favouring sideways movement along the y-axis. While exploring alternative placements, such as incorporating the system into fingerless gloves, was considered, it was deemed less feasible for potential users, and the wrist placement was retained for practical reasons.

Finally, the Likert scale assessment used to gather participant feedback on stimulation may be insufficient to reflect their actual experiences and likelihood of wearing the device. A key limitation in the design of the wrist-worn system and the study was the absence of patient and public involvement (PPI). It is crucial for designers and researchers to ensure that the stimulation is not more discomforting than the tremor it aims to alleviate. A spontaneous comment from a participant during testing highlights this concern: "If I were at home watching TV, maybe I would switch this off." This remark underscores the importance of a comprehensive understanding of user experiences and preferences, which is essential for the acceptability and practicality of the therapeutic approach being proposed.

4.4.5. Future directions

To further assess the potential therapeutic effects of both phasic and non-phasic continuous stimulation and conclusively evaluate whether the additional computational cost of phasic stimulation is justified, prolonged application of both phasic and non-phasic stimulation should be considered. This would involve delivering continuous stimulation at the most suppressive phase and at a constant non-phasic setting for all participants. However, the potential influence of order effects should be considered, as the sequence in which prolonged phasic or non-phasic stimulation is provided might impact the results. Additionally, validation in a larger cohort and inclusion of participants with other movement disorders, such as ET, could contribute to a more comprehensive evaluation of this technology as a potential treatment for pathological tremor. Adapting this system for at-home use, as a continuous therapeutic intervention, could then be considered pending in the results of such studies.

User comfort and safety are key considerations in the application of this or similar technologies for the treatment of pathological tremor. To achieve this, future iterations of the design process should actively involve patients and the public. This integration should include gathering patient feedback on the stimulation experience and the creation of a user interface that is intuitive, responsive to patient needs, and safe for unsupervised use. By embedding PPI more comprehensively into the development cycle, we can better tailor the technology to real-world use.

4.5. Conclusion

In this study, we successfully validated a self-contained wrist-worn system capable of accurately tracking Parkinsonian rest tremor phase on-board and triggering peripheral electrical stimulation at the median nerve. These were the first study

investigating the effects of both phasic and open-loop peripheral nerve stimulation in Parkinsonian rest tremor, and the first system capable of adapting to changes in the dominant tremor axis and centre frequency, thus accounting for the tremor variability. Our findings suggest that phasic stimulation may induce significant changes in tremor; however, the therapeutic efficacy of this technology and its potential advantages over non-phasic stimulation remain subjects of debate. The limitations of our small participant cohort, coupled with challenges in system design, emphasise the need for further exploration in larger cohorts and the refinement of testing strategies to elucidate the feasibility of this innovative approach to treating pathological tremor.

5. General discussion

This chapter synthesises the findings from our preceding studies and explores their broader implications in the context of pathological tremor management, with a particular emphasis on Parkinsonian rest tremor and essential tremor. Through a critical examination of our research methodologies, we reflect on their limitations and consider potential avenues for future research.

5.1. Summarised outcomes

The three experimental chapters of this thesis were dedicated to addressing the goals as outlined in *Section 1.6—Thesis objectives*. To facilitate an understanding of how these objectives were met and the key results that emerged, a comprehensive overview is presented in *Table 5.1*. This table serves as a foundation for the subsequent sections, where we delve into a detailed discussion of these results, examining their implications, and critically assessing their limitations. The insights gained from our studies inform our understanding of the potential and challenges in applying phase-locked peripheral electrical stimulation for the management of pathological tremor.

Chapter	Objective	Core results
2	Exploring the effects of phasic peripheral nerve stimulation at the wrist.	Tremor in the hand involves multiple oscillators, represented by significant differences in tremor amplitude and dominant axis as well as centre frequency. Phase-locked stimulation can significantly modulate Parkinsonian rest tremor, provided that the existence of multiple oscillations is accounted for.
3	Design and bench-top verification of an adaptable, phase-tracking wrist-worn system.	An adaptable and wearable phase-tracking system, the first of its kind accounting for the variability in the tremor, adapting to changes in the tremor dominant axis and centre frequency, was developed and verified.
4	In-clinic system validation in people with Parkinsonian rest tremor.	The custom-built wrist-worn device showed robustness and consistent results with the benchtop verification. Significant but modest tremor modulation occurred in selected individuals and stimulation settings, including phasic and constant high-frequency stimulation.

Table 5.1: Summary of key thesis objectives and experimental chapters' results.

5.2. Tremor modulation by peripheral nerve stimulation

The research presented in *Chapters 2* and *4* explored the use of non-invasive electrical stimulation at the median nerve to modulate Parkinsonian rest tremor. These studies suggested instantaneous tremor modulation following phase-specific stimulation, with significant changes in tremor severity observable within 5- or 10-second intervals.

The initial pilot study, as detailed in *Chapter 2*, lacked an adaptive mechanism to accommodate tremor variability in dominant axis and centre frequency during phase tracking. The variability, however, was captured through cluster division analysis of the data, which revealed distinct oscillation patterns in hand tremor and identified cluster-specific phases producing significant tremor suppression or amplification.

In the subsequent in-clinic study, which incorporated a custom-built device tailored to tremor variability, significant instantaneous tremor modulation was observed in one of the three subjects receiving phasic stimulation. A recurring theme in both studies, however, was the modest level of tremor suppression. The pilot study demonstrated an average significant suppression of 36% among five subjects, while the mean significant amplification was 117% in six subjects. This finding indicates that while optimised phasic stimulation can yield modest tremor reduction, inappropriate phasic stimulation might inadvertently intensify the involuntary shaking.

Chapter 4's in-clinic device validation study further explored phasic stimulation effects. The participant who responded significantly to phasic stimulation showed a 26% reduction in tremor at an optimal phase in the dominant tremor axis. Interestingly, this suppression was accompanied by a 93% amplification at the same phase but in a different axis. As illustrated in *Figure 4.9*, suppressing tremor along one axis at the optimal stimulation phase resulted in amplification along another axis, indicating a shift in tremor orientation upon stimulation. Across the three subjects, extended testing over 10 minutes at the person-specific optimal stimulation state revealed significant suppression only in the subject undergoing constant, open-loop stimulation, as opposed to phasic, closed-loop stimulation, which led to no change or increased tremor envelope amplitude, suggested in *Tables 4.4* and *4.5*.

These observations suggest that while phasic stimulation can significantly affect Parkinsonian rest tremor, its therapeutic efficacy, especially for continuous, long-term stimulation which would be employed in potential at-home settings, remains uncertain.

Comparatively, in a study on essential tremor (ET), phase-locked stimulation yielded only modest tremor modulation, primarily amplification, in about half of the subjects (Reis et al., 2021). By contrast, constant, non-phasic stimulation demonstrated more promising outcomes in a large-scale study involving 263 ET patients, in which at least 50% tremor reduction was observed in 54% of patients, and some improvement noted in 92% (Isaacson et al., 2020). Additionally, investigations into phasic stimulation for ET identified specific patient groups who might experience greater tremor modulation with this approach. One study observed more pronounced modulation in individuals with smaller pre-stimulation tremor amplitudes, while another found greater suppression during peak or trough phasic stimulation of higher amplitude tremor (Kim et al., 2020; Reis et al., 2021). While the pathophysiology of Parkinsonian rest tremor is distinct from ET (less variable and predominantly postural and kinetic), the observations from ET studies suggest that the therapeutic efficacy of phasic stimulation for tremor in general may be limited.

The considerable computational demands and the need for increased processing memory for real-time phase estimation, especially when adapting to the variability of Parkinsonian rest tremor, and for parameter optimisation, coupled with the risks of significant tremor amplification due to incorrect phase identification, pose crucial questions about the practicality and effectiveness of phasic stimulation as a treatment method. These challenges bring into focus the potential advantages of constant, open-loop stimulation, a more straightforward approach, in managing tremor, and warrant further investigation to understand the impacts of phasic and open-loop stimulation in different tremor disorders.

Chapters 3 and *4* introduced a significant advancement in tremor research: a robust, portable phase-tracking tool that innovatively accounts for tremor variability in phase estimation. This development was particularly pertinent given the observed changes in dominant tremor axis and centre frequency, as identified in both the initial pilot study and the subsequent in-clinic system validation. This research tool represents an invaluable opportunity for further investigation into the comparative effects of phase-locked and open-loop stimulation on tremor, potentially leading to more effective tremor management strategies.

5.3. Limitations

In this section, we critically examine limitations at three distinct levels related to our experimental chapters: (i) the inherent limitations of peripheral nerve stimulation as a treatment for Parkinsonian rest tremor; (ii) specific limitations of our experimental protocol design and execution; and (iii) those pertaining to the design of our wrist-worn system.

5.3.1. Peripheral nerve electrical stimulation

A fundamental limitation of using peripheral nerve stimulation for PD treatment is its symptom-specific approach. This modality focuses solely on addressing involuntary upper limb shaking, which, while beneficial for individuals with tremor as the dominant symptom, particularly in early-stage Parkinsonism, does not address the broader spectrum of Parkinsonian symptoms. For many individuals, PD presents with a range of symptoms beyond tremor, including freezing of gait, bradykinesia, postural instability, rigidity, and various cognitive and psychiatric manifestations (Jankovic, 2008; Lenka & Jankovic, 2021; Obeso et al., 2017; Poewe et al., 2017; Riboldi et al., 2022). Thus, while peripheral nerve stimulation can effectively target tremor, its scope is limited in the context of the multifaceted nature of PD.

As such, other treatment options that offer a more comprehensive approach to the condition may provide broader benefits for individuals with PD. This consideration is especially pertinent when evaluating the cost of treatment against the potential improvements in quality of life. For individuals whose Parkinsonian symptoms extend beyond tremor, a treatment approach that encompasses a wider range of symptoms may be more desirable and impactful.

Additionally, a critical question arises regarding the potential adoption of this technology as a wearable system for at-home use: would individuals be willing to regularly wear it? Electrical stimulation of the wrist, even when sub-motor threshold, can be uncomfortable. A key concern is whether the discomfort from the device might outweigh the discomfort caused by tremor symptoms. Interestingly, in our studies, participant feedback on their tolerance to stimulation was mixed. As detailed in *Section 4.4.4—Limitations and challenges of this study*, one participant explicitly communicated an unwillingness to use the technology at home. However, the majority of participants in the study presented in *Chapter 2* reported minimal discomfort, with nine out of 10 marking 1 on a 5-point Likert scale, suggesting that the stimulation was easily tolerated. In contrast, *Chapter 4*, which included the potentially more uncomfortable open-loop stimulation setting, saw a wider range of responses on the Likert scale, covering three options.

The prospect of tailoring stimulation parameters to individual-specific needs and limiting stimulation intensities to lower levels could play a crucial role in reducing discomfort associated with the wearable system. This approach is supported by findings from a large prospective study on essential tremor patients, which evaluated the impact of at-home wrist stimulation using a wearable system (Isaacson et al., 2020). The study reported encouraging patient responses to long-term stimulation. Notably, only 18% of the 263 participants experienced device-related adverse events such as

pain, wrist discomfort, or skin irritation, with most cases being mild to moderate in severity. Furthermore, there was only one instance of a severe adverse event reported.

An interesting aspect of this study was its method of alternating stimulation between the median and radial nerves, synchronised with the individual's tremor frequency. This innovative approach may have contributed to a more comfortable stimulation experience for participants. By integrating such techniques, along with incorporating patient feedback into the design process, wearable systems that utilise electrical stimulation for tremor management have the potential to be well-tolerated for long-term use. Such patient-centred design considerations are vital in ensuring both the effectiveness and the acceptability of these novel therapeutic interventions.

5.3.2. Study design and execution

One of the primary limitations in both in-clinic studies presented in this thesis was the small cohort size. This limited our ability to control for group-level differences in participant characteristics, such as varying medication states during the recordings, which could have influenced tremor behaviour and response to stimulation. In *Chapter 4,* challenges in recruitment and time constraints restricted our cohort to only three participants. While this small sample size allowed us to validate the functionality of our in-house built system and to observe general trends in tremor modulation, it was insufficient to draw comprehensive conclusions about the clinical efficacy of the system.

Furthermore, it is important to acknowledge that all participants in the second cohort were male. Future studies should strive for gender balance in the tested population. This is especially significant considering that gender disparities, particularly affecting women, have been noted in access to tremor treatments, such as deep brain stimulation (DBS) (Memon et al., 2023). Ensuring a diverse and

representative sample is crucial for generalising findings and understanding the full spectrum of potential responses to the treatment across different demographics.

Additionally, the random search setting implemented in our studies, which included 5- and 10-second stimulation blocks in *Chapters 2* and *4* respectively, may not have been long enough to fully capture the effects of stimulation on tremor during the search for the optimal stimulation state. In response to this concern, the duration of these blocks was doubled in the second in-clinic study. However, it is worth noting that other studies in the field typically involve exposing participants to longer-term stimulation, often lasting several minutes (Isaacson et al., 2020; Kim et al., 2020, 2022; Pahwa et al., 2019).

The decision to restrict individual block duration was a balance between the need to avoid overly lengthy in-clinic sessions for participants and the desire to test a variety of stimulation settings. This included six phasic stimulation settings, along with open-loop and sham options, and we also aimed to control for order effects through random presentation of these settings. An ideal research scenario would extend beyond assessing the instantaneous effects of stimulation, exploring the broader tremor dynamics in response to longer-term stimulation across different settings. Such an approach could potentially be realised if a similar system were to be used in out-of-clinic settings, allowing for more extended and naturalistic observation periods.

In contemplating the translation of this system to at-home use, it becomes essential that it operates effectively during a person's daily activities. Action tremor, while a predominant symptom of ET, is also commonly present in PD (Heusinkveld et al., 2018). Our in-clinic studies focused solely on testing tremor at rest, with participants in a consistent stationary position. Expanding the testing to include scenarios where participants engage in various actions would be invaluable for a more

comprehensive characterisation of the system's feasibility as a therapeutic intervention. Integrating action tremor into the testing protocol may bring additional challenges. It would likely necessitate adaptations to the system, particularly in terms of filter settings, which must be rigorously tested in a wide range of movements. These adjustments would be crucial to effectively distinguish between tremor-related movements and other actions, as well as to mitigate gravitational artefacts (Rodger J., 2005).

The number and scope of stimulation settings explored in our studies was also constrained by the necessity to keep the duration of in-clinic protocols manageable. This limitation meant that we could not experiment with a broader range of variables such as different stimulation frequencies, pulse-widths, amplitudes, and duty cycles. These parameters have been explored in studies focusing on ET patients and have shown potential for more personalised stimulation parameter evaluation and optimisation (Kim et al., 2022). Expanding the range of settings tested could have provided a more comprehensive understanding of how various stimulation parameters affect tremor. It could allow for optimising the stimulation more precisely to individual needs, potentially improving the efficacy of the treatment.

Another limitation, related to the constraints of in-clinic testing durations, was our focus on stimulating exclusively the median nerve. While the median nerve is a promising target due to its demonstrated ability to induce spiking activity in the central tremor network (Hanajima et al., 2004; Nowacki et al., 2023), other nerves may also offer significant potential. In particular, the radial nerve has been a focus in various studies investigating tremor treatment, either as a single target or in conjunction with the median nerve (Isaacson et al., 2020; Kim et al., 2020, 2022; Lin et al., 2018; Pahwa et al., 2019). Exploring stimulation of other nerve targets could provide valuable insights into further optimising tremor management strategies. Our present studies'

focus on a single nerve target was also influenced by our hardware choices, which will be further discussed in the section below.

5.3.3. Wrist-worn system design

During the pilot study, when data was stored on a computer, we were not constrained by memory limitations, allowing us to maintain a high sampling rate above 10 kHz. However, when the system was transitioned to a portable format, memory constraints became a significant factor, requiring adjustments to the sampling rate. Consequently, the sampling rate of our in-house built system was set to approximately 208 Hz. While this rate was adequate for capturing oscillations within the tremor frequency range, it also introduced the need for an error margin in phase estimation, as detailed in *Section 3.3.6—Triggering stimulation*.

This compromise was necessary due to the memory limitations of the portable device and resulted in a degree of imprecision in phase estimation. One potential solution to this challenge could involve optimising memory storage, implementing wireless data transmission. However, this approach could increase battery usage and introduce variable processing delays, presenting a new set of challenges to the system's design and functionality.

Regarding phase estimation methods, both the zero-crossings approach used in *Chapter 2* and the simplified state-space model implemented in *Chapters 3* and *4* were based on the assumption of a sinusoidal signal input. However, while Parkinsonian tremor is often described as roughly sinusoidal, it has also been characterised by its non-sinusoidal traits, including higher levels of entropy (Chan et al., 2022; Vaillancourt & Newell, 2000). This complexity is further highlighted by other studies that have pointed out the challenges in phase estimation for Parkinsonian tremor due to the variability in the periods of these oscillations (Saifee et al., 2016).

Despite our phase tracker's ability to adapt to changes in tremor centre frequency, the reliance on a sinewave reference in our wrist-worn device may introduce inaccuracies in phase estimation. This assumption could potentially impact the performance of the phase estimator, particularly when dealing with the non-sinusoidal characteristics of Parkinsonian tremor.

Such discrepancies between the theoretical model and the actual tremor characteristics require a careful consideration of the methods used for phase estimation. Future developments in this area might involve exploring more complex signal models that can better accommodate the irregularities and variability inherent in Parkinsonian tremor, thereby enhancing the accuracy and efficacy of the phase estimation process.

While we successfully transitioned the phase-tracking and protocol control elements to a portable format, the delivery of electrical stimulation in our system still relies on an external, CE-marked device. This dependency on an external apparatus currently limits the system's suitability for at-home use. To move towards a home-use system, significant design modifications are necessary, including the development of an integrated, on-board stimulator. The externalised stimulator setup also limited our ability to deliver stimulation to multiple nerves, as the commercially available device had a single stimulation trigger input and one output, interfacing with a bar electrode. Potential design adaptations will be further explored in the section below, discussing future research directions.

5.4. Avenues for future research

5.4.1. Potential explorations with the current system

For future studies, expanding the cohort size is crucial to enable a more robust and conclusive evaluation of the population-level effects of phase-locked peripheral electrical stimulation on tremor. This approach would allow for a comprehensive assessment of its therapeutic potential, particularly in individuals with PD. A key aspect to explore is the comparative efficacy of open-loop vs. phase-locked stimulation. This could be achieved by testing both open-loop and the most suppressive phasic setting continuously over several minutes. Such an extended duration would provide a more consistent basis for comparing the effectiveness of open-loop and phase-locked stimulation.

The current system and proposed protocol modifications could be leveraged to investigate the effects of stimulation in other tremor disorders, such as ET. In these explorations, it would be beneficial to continue comparing the outcomes of phasic and non-phasic stimulation. This would not only offer insights into the specific modulatory effects of each stimulation type but also help determine whether the optimisation efforts required for phasic stimulation yield significant therapeutic advantages.

Another critical avenue for research involves utilising our system to investigate the central effects of stimulation. Studies have already demonstrated that spiking activity evoked by median nerve stimulation can be detected in the thalamus and subthalamic nucleus (Hanajima et al., 2004; Nowacki et al., 2023). A promising direction for future research could involve using our system to administer both phasic and open-loop stimulation to tremor patients who have undergone DBS surgery, particularly in those with externalised leads or implanted with devices capable of wireless data transmission (Cagnan et al., 2019; Krauss et al., 2021).

Conducting such studies would be invaluable in elucidating the underlying mechanisms of phasic modulation of tremor. A key objective would be to explore whether various tremor modes identified peripherally, each with its unique preferred stimulation phase, correspond to the activities of distinct central oscillators in the brain. This research could reveal if and how these central oscillators are influenced or altered by phasic stimulation, potentially leading to a reduction in pathological oscillations. Determining the direct effects of phasic stimulation on central neural pathways could contribute towards more personalised therapeutic interventions for tremor.

5.4.2. Considerations for at-home use

A primary concern in adapting our system for at-home use is ensuring user safety, particularly when the device operates without the constant supervision of experimenters. One major risk involves the possibility of a user inadvertently holding both poles of an electrode with both hands during stimulation, potentially causing an electrical current to pass through the heart, which could lead to severe or even lethal injury. To mitigate this risk, the system must incorporate a reliable safety mechanism that prevents stimulation unless the device is correctly and securely positioned on the wrist. Additionally, user comfort is essential. This can be achieved by integrating an easily accessible emergency off button, allowing users to immediately disable stimulation if they feel discomfort or simply wish to stop the treatment.

Enhancements of our system for at-home use must incorporate advancements in memory capacity and battery life to support continuous operation throughout a user's daily activities. Incorporating a reliable data transmission system is also required for effective monitoring and analysis. Enhancements in memory could further enable higher recording resolution, which would be beneficial for more precise phase estimation. This could involve integrating more efficient data storage and transmission

protocols, optimising the system's functionality while maintaining its portability and ease of use.

A critical development for our system is the integration of an on-board stimulator capable of delivering stimulation up to 10 mA. Stimulation levels must be adjustable to remain within comfortable limits for the user while maintaining device safety. Adding an on-board stimulator component to the wearable system would open up the possibility of stimulating more than one nerve, as seen in studies that have successfully targeted both the radial and median nerves (Isaacson et al., 2020; Lin et al., 2018; Pahwa et al., 2019). Future iterations of the device could include a custom-designed wristband with more than one electrode, enabling the exploration of multi-nerve stimulation.

A core advantage of at-home testing is that it would facilitate longitudinal recordings and extensive parameter testing, including different stimulation frequencies, pulse-widths, amplitudes, and duty cycles. The key to selecting the optimal parameters for effective tremor suppression could lie in leveraging novel computational approaches, such as time-varying Bayesian optimisation, which can adaptively navigate a wide range of parameters while accounting for time-dependent factors. These factors may include disease progression and circadian rhythms, adding a dynamic layer to the treatment strategy (Fleming et al., 2023). Implementing such techniques could lead to more personalised and effective tremor management solutions, tailored to the evolving needs of each individual over time.

5.5. Concluding remarks

This thesis began with a pilot study investigating the effects of phasic stimulation on PD and progressed to the development and preliminary validation of an

adaptable wrist-worn system for tremor phase estimation. Our in-house built device addressed two critical limitations identified in earlier studies: its portability as a self-contained phase-tracking wearable unit and its adaptability to the variable dominant axis and centre frequency of tremor. This adaptability distinguishes our system as a first-of-its-kind innovation. Our pioneering research in applying phasic stimulation at the wrist to modulate Parkinsonian rest tremor has demonstrated significant suppression and amplification, especially when considering instantaneous changes in tremor severity and multiple tremor oscillation patterns. However, the modest suppression achieved in only half of our participants prompts a critical reassessment of this approach's therapeutic viability. These findings underscore the need for future research to further explore open- and closed-loop stimulation methods, particularly their potential central effects and overall effectiveness as treatment strategies. By addressing gaps in current research and introducing innovative solutions, this thesis represents a step toward the development of personalised non-invasive treatments for tremor, potentially offering more accessible options for a wider population.

6. References

Abosch, A., Timmermann, L., Bartley, S., Rietkerk, H. G., Whiting, D., Connolly, P. J., Lanctin, D., & Hariz, M. I. (2013). An International Survey of Deep Brain Stimulation Procedural Steps. *Stereotactic and Functional Neurosurgery*, *91*(1), 1–11. https://doi.org/10.1159/000343207

Agapaki, O. M., Christakos, C. N., & Anastasopoulos, D. (2018). Characteristics of Rest and Postural Tremors in Parkinson's Disease: An Analysis of Motor Unit Firing Synchrony and Patterns. *Frontiers in Human Neuroscience*, *12*, 179. https://doi.org/10.3389/fnhum.2018.00179

Alberts, W. W., Wright, E. W., & Feinstein, B. (1969). Cortical potentials and parkinsonian tremor. *Nature*, *221*(5181), 670–672. https://doi.org/10.1038/221670a0

Alkhani, A., & Lozano, A. M. (2001). Pallidotomy for Parkinson disease: A review of contemporary literature. *Journal of Neurosurgery*, *94*(1), 43–49. https://doi.org/10.3171/jns.2001.94.1.0043

Arruda, B. S., Reis, C., Sermon, J. J., Pogosyan, A., Brown, P., & Cagnan, H. (2021). Identifying and modulating distinct tremor states through peripheral nerve stimulation in Parkinsonian rest tremor. *Journal of NeuroEngineering and Rehabilitation*, *18*(179). https://doi.org/10.1186/s12984-021-00973-6

Azodi-Avval, R., & Gharabaghi, A. (2015). Phase-dependent modulation as a novel approach for therapeutic brain stimulation. *Frontiers in Computational Neuroscience*, *9*, 26. https://doi.org/10.3389/fncom.2015.00026

Baker, W. L., Silver, D., White, C. M., Kluger, J., Aberle, J., Patel, A. A., & Coleman, C. I. (2009). Dopamine agonists in the treatment of early Parkinson's disease: A meta-analysis. *Parkinsonism & Related Disorders*, *15*(4), 287–294. https://doi.org/10.1016/j.parkreldis.2008.07.004

Ben-Pazi, H., Bergman, H., Goldberg, J. A., Giladi, N., Hansel, D., Reches, A., & Simon, E. S. (2001). Synchrony of rest tremor in multiple limbs in Parkinson's disease: Evidence for multiple oscillators. *Journal of Neural Transmission*, *108*, 287–296. https://doi.org/10.1007/s007020170074

Bezard, E., Brotchie, J. M., & Gross, C. E. (2001). Pathophysiology of levodopa-induced dyskinesia: Potential for new therapies. *Nature Reviews Neuroscience*, *2*(8), 577–588. https://doi.org/10.1038/35086062

Bhatia, K. P., Bain, P., Bajaj, N., Elble, R. J., Hallett, M., Louis, E. D., Raethjen, J., Stamelou, M., Testa, C. M., Deuschl, G., & the Tremor Task Force of the International Parkinson and Movement Disorder Society. (2018). Consensus Statement on the classification of tremors. From the task force on tremor of the International Parkinson and Movement Disorder Society. *Movement Disorders*, *33*(1), 75–87. https://doi.org/10.1002/mds.27121

Blackwood, E., Lo, M. C., & Alik Widge, S. (2018). Continuous Phase Estimation for Phase-Locked Neural Stimulation Using an Autoregressive Model for Signal Prediction∗. *Proceedings of the Annual International Conference of the IEEE Engineering in Medicine and Biology Society, EMBS*, *2018-July*, 4736–4739. https://doi.org/10.1109/EMBC.2018.8513232

Blum, C., & Dambeck, J. (2020). Analytical Assessment of the Propagation of Colored Sensor Noise in Strapdown Inertial Navigation. *Sensors*, *20*(23), 6914. https://doi.org/10.3390/s20236914

Brittain, J. S., Cagnan, H., Mehta, A. R., Saifee, T. A., Edwards, M. J., & Brown, P. (2015). Distinguishing the Central Drive to Tremor in Parkinson's Disease and Essential Tremor. *The Journal of Neuroscience*, *35*(2), 795–806. https://doi.org/10.1523/JNEUROSCI.3768-14.2015

Brittain, J. S., Probert-Smith, P., Aziz, T. Z., & Brown, P. (2013). Tremor suppression by rhythmic transcranial current stimulation. *Current Biology*, *23*(5), 436–440. https://doi.org/10.1016/j.cub.2013.01.068

Brodkey, J. A., Tasker, R. R., Hamani, C., McAndrews, M. P., Dostrovsky, J. O., & Lozano, A. M. (2004). Tremor cells in the human thalamus: Differences among neurological disorders. *Journal of Neurosurgery*, *101*(1), 43–47. https://doi.org/10.3171/jns.2004.101.1.0043

Cagnan, H., Denison, T., McIntyre, C., & Brown, P. (2019). Emerging technologies for improved deep brain stimulation. *Nature Biotechnology*, 1024–1033. https://doi.org/10.1038/s41587-019-0244-6

Cagnan, H., Pedrosa, D., Little, S., Pogosyan, A., Cheeran, B., Aziz, T., Green, A., Fitzgerald, J., Foltynie, T., Limousin, P., Zrinzo, L., Hariz, M., Friston, K. J., Denison, T., & Brown, P. (2017). Stimulating at the right time: Phase-specific deep brain stimulation. *Brain*, *140*(1), 132–145. https://doi.org/10.1093/brain/aww286

Calabresi, P., Picconi, B., Tozzi, A., Ghiglieri, V., & Di Filippo, M. (2014). Direct and indirect pathways of basal ganglia: A critical reappraisal. *Nature Neuroscience*, *17*(8), 1022–1030. https://doi.org/10.1038/nn.3743

Chan, P. Y., Ripin, Z. M., Halim, S. A., Arifin, W. N., Yahya, A. S., Eow, G. B., Tan, K., Hor, J. Y., & Wong, C. K. (2022). Motion characteristics of subclinical tremors in Parkinson's disease and normal subjects. *Scientific Reports*, *12*(1), 4021. https://doi.org/10.1038/s41598-022-07957-z

Chen, L. L., Madhavan, R., Rapoport, B. I., & Anderson, W. S. (2013). Real-time brain oscillation detection and phase-locked stimulation using autoregressive spectral estimation and time-series forward prediction. *IEEE Transactions on Biomedical Engineering*, *60*(3), 753–762. https://doi.org/10.1109/TBME.2011.2109715

Cohen, M. X. (2014). Bandpass filtering and the Hilbert transform. In *Analyzing Neural Time Series Data* (pp. 175–193). MIT Press.

Crutcher, M. D., & DeLong, M. R. (1984). Single cell studies of the primate putamen—II. Relations to direction of movement and pattern of muscular activity. *Experimental Brain Research*, *53*, 244–258. https://doi.org/10.1007/BF00238154

de Lau, L. M. L., & Breteler, M. M. B. (2006). *Epidemiology of Parkinson's disease* (p. 5:525-35). Lancet Neurol. https://doi.org/10.1016/S1474-4422(06)70471-9

DeLong, M. R., Crutcher, M. D., & Georgopoulos, A. P. (1985). Primate globus pallidus and subthalamic nucleus: Functional organization. *Journal of Neurophysiology*, *53*(2), 530–543. https://doi.org/10.1152/jn.1985.53.2.530

Deuschl, G., & Elble, R. (2009). Essential tremor—Neurodegenerative or nondegenerative disease towards a working definition of ET. *Movement Disorders*, *24*(14), 2033–2041. https://doi.org/10.1002/mds.22755

Deuschl, G., Raethjen, J., Baron, R., Lindemann, M., Wilms, H., & Krack, P. (2000). The pathophysiology of parkinsonian tremor: A review. *Journal of Neurology, Supplement*, *247*(5), 33–48. https://doi.org/10.1007/pl00007781

Deuschl, G., Wenzelburger, R., Löffler, K., Raethjen, J., & Stolze, H. (2000). Essential tremor and cerebellar dysfunction. Clinical and kinematic analysis of intention tremor. *Brain*, *123*(8), 1568–1580. https://doi.org/10.1093/brain/123.8.1568

Dideriksen, J. L., Laine, C. M., Dosen, S., Muceli, S., Rocon, E., Pons, J. L., Benito-Leon, J., & Farina, D. (2017). Electrical stimulation of afferent pathways for the suppression of pathological tremor. *Frontiers in Neuroscience*, *11*, 178. https://doi.org/10.3389/fnins.2017.00178

Dorsey, E. R., Constantinescu, R., Thompson, J. P., Biglan, K. M., Holloway, R. G., Kieburtz, K., Marshall, F. J., Ravina, B. M., Schifitto, G., Siderowf, A., & Tanner, C.

M. (2007). Projected number of people with Parkinson disease in the most populous nations, 2005 through 2030. *Neurology*, *68*(5), 384–386. https://doi.org/10.1212/01.wnl.0000247740.47667.03

Dosen, S., Muceli, S., Dideriksen, J. L., Romero, J. P., Rocon, E., Pons, J., & Farina, D. (2015). Online tremor suppression using electromyography and low-level electrical stimulation. *IEEE Transactions on Neural Systems and Rehabilitation Engineering*, *23*(3), 385–395. https://doi.org/10.1109/TNSRE.2014.2328296

Elble, R. J., Shih, L., & Cozzens, J. W. (2018). Surgical treatments for essential tremor. *Expert Review of Neurotherapeutics*, *18*(4), 303–321. https://doi.org/10.1080/14737175.2018.1445526

Escobar Sanabria, D., Johnson, L. A., Yu, Y., Busby, Z., Nebeck, S., Zhang, J., Harel, N., Johnson, M. D., Molnar, G. F., & Vitek, J. L. (2020). Real-time suppression and amplification of frequency-specific neural activity using stimulation evoked oscillations. *Brain Stimulation*, *13*(6), 1732–1742. https://doi.org/10.1016/j.brs.2020.09.017

Fabbri, M., Ferreira, J. J., & Rascol, O. (2022). COMT Inhibitors in the Management of Parkinson's Disease. *CNS Drugs*, *36*(3), 261–282. https://doi.org/10.1007/s40263-021-00888-9

Fahn, S. (1989). Adverse Effects of Levodopa in Parkinson's Disease. In D. B. Calne (Ed.), *Drugs for the Treatment of Parkinson's Disease* (Vol. 88, pp. 385–409). Springer Berlin Heidelberg. https://doi.org/10.1007/978-3-642-73899-9_14

Fishman, P. S. (2008). Paradoxical aspects of parkinsonian tremor. *Movement Disorders*, *23*, 168–173. https://doi.org/10.1002/mds.21736

Gerbasi, M. E., Nambiar, S., Reed, S., Hennegan, K., Hadker, N., Eldar-Lissai, A., & Cosentino, S. (2022). Essential tremor patients experience significant burden beyond tremor: A systematic literature review. *Frontiers in Neurology*, *13*, 891446. https://doi.org/10.3389/fneur.2022.891446

Gilron, R., Little, S., Perrone, R., Wilt, R., de Hemptinne, C., Yaroshinsky, M. S., Racine, C. A., Wang, S. S., Ostrem, J. L., Larson, P. S., Wang, D. D., Galifianakis, N. B., Bledsoe, I. O., San Luciano, M., Dawes, H. E., Worrell, G. A., Kremen, V., Borton, D. A., Denison, T., & Starr, P. A. (2021). Long-term wireless streaming of neural recordings for circuit discovery and adaptive stimulation in individuals with Parkinson's disease. *Nature Biotechnology*, *39*(9), 1078–1085. https://doi.org/10.1038/s41587-021-00897-5

Grado, L. L., Johnson, M. D., & Netoff, T. I. (2018). Bayesian adaptive dual control of deep brain stimulation in a computational model of Parkinson's disease. *PLoS*

Computational Biology, *14*(12), 1–23. https://doi.org/10.1371/journal.pcbi.1006606

Hamid, E., Ayele, B. A., Massi, D. G., Ben Sassi, S., Tibar, H., Djonga, E. E., El-Sadig, S. M., Amer El Khedoud, W., Razafimahefa, J., Kouame-Assouan, A. E., Ben-Adji, D., Lengané, Y. T. M., Musubire, A. K., Mohamed, M. H., Phiri, T. E., Nestor, N., Alwahchi, W. A., Neshuku, S. N., Ocampo, C., … Shalash, A. (2021). Availability of Therapies and Services for Parkinson's Disease in Africa: A Continent-Wide Survey. *Movement Disorders*, *36*(10), 2393–2407. https://doi.org/10.1002/mds.28669

Hanajima, R., Chen, R., Ashby, P., Lozano, A. M., Hutchison, W. D., Davis, K. D., & Dostrovsky, J. O. (2004). Very fast oscillations evoked by median nerve stimulation in the human thalamus and subthalamic nucleus. *Journal of Neurophysiology*, *92*(6), 3171–3182. https://doi.org/10.1152/jn.00363.2004

Hao, M. Z., Xu, S. Q., Hu, Z. X., Xu, F. L., Niu, C. X. M., Xiao, Q., & Lan, N. (2017). Inhibition of Parkinsonian tremor with cutaneous afferent evoked by transcutaneous electrical nerve stimulation. *Journal of NeuroEngineering and Rehabilitation*, *14*, 75. https://doi.org/10.1186/s12984-017-0286-2

Harris, B. D., Nilsson, S., & Poole, C. M. (2015). A feasibility study for using ABS plastic and a low-cost 3D printer for patient-specific brachytherapy mould design. *Australasian Physical & Engineering Sciences in Medicine*, *38*(3), 399–412. https://doi.org/10.1007/s13246-015-0356-3

Hauser, R. A., Ellenbogen, A., Khanna, S., Gupta, S., & Modi, N. B. (2018). Onset and duration of effect of extended-release carbidopa-levodopa in advanced Parkinson’s disease. *Neuropsychiatric Disease and Treatment*, *Volume 14*, 839–845. https://doi.org/10.2147/NDT.S153321

Heusinkveld, L. E., Hacker, M. L., Turchan, M., Davis, T. L., & Charles, D. (2018). Impact of Tremor on Patients With Early Stage Parkinson's Disease. *Frontiers in Neurology*, *9*, 628. https://doi.org/10.3389/fneur.2018.00628

Hirschmann, J., Hartmann, C. J., Butz, M., Hoogenboom, N., Özkurt, T. E., Elben, S., Vesper, J., Wojtecki, L., & Schnitzler, A. (2013). A direct relationship between oscillatory subthalamic nucleus-cortex coupling and rest tremor in Parkinson's disease. *Brain*, *136*(12), 3659–3670. https://doi.org/10.1093/brain/awt271

Holt, A. B., Kormann, E., Gulberti, A., Pötter-Nerger, M., McNamara, C. G., Cagnan, H., Baaske, M. K., Little, S., Köppen, J. A., Buhmann, C., Westphal, M., Gerloff, C., Engel, A. K., Brown, P., Hamel, W., Moll, C. K. E., & Sharott, A. (2019). Phase-dependent suppression of beta oscillations in parkinson's disease patients.

Journal of Neuroscience, *39*(6), 1119–1134. https://doi.org/10.1523/JNEUROSCI.1913-18.2018

Holt, A. B., Wilson, D., Shinn, M., Moehlis, J., & Netoff, T. I. (2016). Phasic Burst Stimulation: A Closed-Loop Approach to Tuning Deep Brain Stimulation Parameters for Parkinson's Disease. *PLoS Computational Biology*, *12*(7). https://doi.org/10.1371/journal.pcbi.1005011

Hurtado, J. M., Gray, C. M., Tamas, L. B., & Sigvardt, K. A. (1999). Dynamics of tremor-related oscillations in the human globus pallidus: A single case study. *Proceedings of the National Academy of Sciences of the United States of America*, *96*(4), 1674–1679. https://doi.org/10.1073/pnas.96.4.1674

Hurtado, J. M., Lachaux, J. P., Beckley, D. J., Gray, C. M., & Sigvardt, K. A. (2000). Inter- and intralimb oscillator coupling in Parkinsonian tremor. *Movement Disorders*, *15*, 683–691. https://doi.org/10.1002/1531-8257(200007)15:4<683::aid-mds1013>3.0.co;2-%23

Hurtado, J. M., Rubchinsky, L. L., Sigvardt, K. A., Wheelock, V. L., & Pappas, C. T. E. (2005). Temporal evolution of oscillations and synchrony in GPi/muscle pairs in Parkinson's disease. *Journal of Neurophysiology*, *93*(3), 1569–1584. https://doi.org/10.1152/jn.00829.2004

Isaacson, S. H., Peckham, E., Tse, W., Waln, O., Way, C., Petrossian, M. T., Dahodwala, N., Soileau, M. J., Lew, M., Dietiker, C., Luthra, N., Agarwal, P., Dhall, R., Morgan, J., Calakos, N., Zesiewicz, T. A., Shamim, E. A., Kumar, R., Lewitt, P., … Pahwa, R. (2020). Prospective home-use study on non-invasive neuromodulation therapy for essential tremor. *Tremor and Other Hyperkinetic Movements*, *10*(1), 1–16. https://doi.org/10.5334/tohm.59

Jankovic, J. (2008). Parkinson's disease: Clinical features and diagnosis. *Journal of Neurology, Neurosurgery and Psychiatry*, *79*(4), 368–376. https://doi.org/10.1136/jnnp.2007.131045

Javidan, M., Elek, J., & Prochazka, A. (1992). Attenuation of pathological tremors by functional electrical stimulation II: Clinical evaluation. *Annals of Biomedical Engineering*, *20*, 225–236. https://doi.org/10.1007/BF02368522

Kalia, L. V., & Lang, A. E. (2015). Parkinson's disease. *The Lancet*, *386*(9996), 896–912. https://doi.org/10.1016/S0140-6736(14)61393-3

Kalman, R. E. (1960). *A New Approach to Linear Filtering and Prediction Problems 1*.

Kaneda, K., Nambu, A., Tokuno, H., & Takada, M. (2002). Differential processing patterns of motor information via striatopallidal and striatonigral projections.

Journal of Neurophysiology, *88*(3), 1420–1432. https://doi.org/10.1152/jn.2002.88.3.1420

Kestenbaum, M., Ford, B., & Louis, E. D. (2015). Estimating the Proportion of Essential Tremor and Parkinson's Disease Patients Undergoing Deep Brain Stimulation Surgery: Five-Year Data From Columbia University Medical Center (2009–2014). *Movement Disorders Clinical Practice*, *2*(4), 384–387. https://doi.org/10.1002/mdc3.12185

Kim, J., Wichmann, T., & Inan, O. T. (2022). Analyzing the Effects of Parameters for Tremor Modulation via Phase-Locked Electrical Stimulation on a Peripheral Nerve. *Journal of Personalized Medicine*, *12*(76). https://doi.org/10.3390/jpm12010076

Kim, J., Wichmann, T., Inan, O. T., & De Weerth, S. P. (2020). A Wearable System For Attenuating Essential Tremor Based On Peripheral Nerve Stimulation. *IEEE Journal of Translational Engineering in Health and Medicine*. https://doi.org/10.1109/JTEHM.2020.2985058

Krauss, J. K., Lipsman, N., Aziz, T., Boutet, A., Brown, P., Chang, J. W., Davidson, B., Grill, W. M., Hariz, M. I., Horn, A., Schulder, M., Mammis, A., Tass, P. A., Volkmann, J., & Lozano, A. M. (2021). Technology of deep brain stimulation: Current status and future directions. *Nature Reviews Neurology*, *17*(2), 75–87. https://doi.org/10.1038/s41582-020-00426-z

Lenka, A., & Jankovic, J. (2021). Tremor Syndromes: An Updated Review. *Frontiers in Neurology*, *12*, 684835. https://doi.org/10.3389/fneur.2021.684835

Limousin, P., & Foltynie, T. (2019). Long-term outcomes of deep brain stimulation in Parkinson disease. *Nature Reviews Neurology*, *15*(4), 234–242. https://doi.org/10.1038/s41582-019-0145-9

Lin, P. T., Ross, E. K., Chidester, P., Rosenbluth, K. H., Hamner, S. R., Wong, S. H., Sanger, T. D., Hallett, M., & Delp, S. L. (2018). Noninvasive neuromodulation in essential tremor demonstrates relief in a sham-controlled pilot trial. *Movement Disorders*, *33*(7), 1182–1183. https://doi.org/10.1002/mds.27350

Lora-Millan, J. S., Delgado-Oleas, G., Benito-León, J., & Rocon, E. (2021). A Review on Wearable Technologies for Tremor Suppression. *Frontiers in Neurology*, *12*, 700600. https://doi.org/10.3389/fneur.2021.700600

Louis, E. D. (2019). Tremor. *CONTINUUM: Lifelong Learning in Neurology*, *25*(4), 959–975. https://doi.org/10.1212/CON.0000000000000748

Louis, E. D., Barnes, L., Albert, S. M., Cote, L., Schneier, F. R., Pullman, S. L., & Yu, Q. (2001). Correlates of functional disability in essential tremor. *Movement Disorders*, *16*(5), 914–920. https://doi.org/10.1002/mds.1184

Louis, E. D., & Ferreira, J. J. (2010). How common is the most common adult movement disorder? Update on the worldwide prevalence of essential tremor. *Movement Disorders : Official Journal of the Movement Disorder Society*, *25*(5), 534—541. https://doi.org/10.1002/mds.22838

Louis, E. D., & Machado, D. G. (2015). Tremor-related quality of life: A comparison of essential tremor vs. Parkinson's disease patients. *Parkinsonism & Related Disorders*, *21*(7), 729–735. https://doi.org/10.1016/j.parkreldis.2015.04.019

Louis, E. D., & McCreary, M. (2021). How Common is Essential Tremor? Update on the Worldwide Prevalence of Essential Tremor. *Tremor and Other Hyperkinetic Movements*, *11*(1), 28. https://doi.org/10.5334/tohm.632

Louis, E. D., Rios, E., & Henchcliffe, C. (2010). How are we doing with the treatment of essential tremor (ET)?: Persistence of patients with ET on medication: Data from 528 patients in three settings. *European Journal of Neurology*, *17*(6), 882–884. https://doi.org/10.1111/j.1468-1331.2009.02926.x

Luinge, H. J., & Veltink, P. H. (2004). Inclination Measurement of Human Movement Using a 3-D Accelerometer with Autocalibration. *IEEE Transactions on Neural Systems and Rehabilitation Engineering*, *12*(1), 112–121. https://doi.org/10.1109/TNSRE.2003.822759

MacErollo, A., Holz, C., Cletheror, D., Vega, J., Moody, J., Saul, G., Paleyes, N., Villar, N., Korlipara, P., Foltynie, T., Limousin, P., Zhang, H., & Kilner, J. (2020). Non-invasive intervention for motor signs of Parkinson's disease: The effect of vibratory stimuli. *Journal of Neurology, Neurosurgery and Psychiatry*, *92*(1), 109–110. https://doi.org/10.1136/jnnp-2020-323427

Macerollo, A., Palmer, C., Foltynie, T., Korlipara, P., Limousin, P., Edwards, M., & Kilner, J. M. (2018). High-frequency peripheral vibration decreases completion time on a number of motor tasks. *European Journal of Neuroscience*, *48*(2), 1789–1802. https://doi.org/10.1111/ejn.14050

Maendly, R., Ruegg, D. G., Wiesendanger, M., Lagowska, J., & Hess, B. (1981). Thalamic relay for group I muscle afferents of forelimb nerves in the monkey. *Journal of Neurophysiology*, *46*(5), 901–917. https://doi.org/10.1152/jn.1981.46.5.901

Maneski, L. P., Jorgovanović, N., Ilić, V., Došen, S., Keller, T., Popović, M. B., & Popovic, D. B. (2011). Electrical stimulation for the suppression of pathological tremor.

Medical and Biological Engineering and Computing, *49*(10), 1187–1193. https://doi.org/10.1007/s11517-011-0803-6

Martin, W. E., Loewenson, R. B., Resch, J. A., & Baker, A. B. (1973). Parkinson's disease: Clinical analysis of 100 patients. *Neurology*, *23*(8), 783–783. https://doi.org/10.1212/WNL.23.8.783

Matsuda, T., & Komaki, F. (2017). Time Series Decomposition into Oscillation Components and Phase Estimation. *Neural Computation*, *29*(2), 332–367. https://doi.org/10.1162/NECO_a_00916

McNamara, C. G., Rothwell, M., & Sharott, A. (2022). Stable, interactive modulation of neuronal oscillations produced through brain-machine equilibrium. *Cell Reports*, *41*(6). https://doi.org/10.1016/j.celrep.2022.111616

Memon, A. A., Gelman, K., Melott, J., Billings, R., Fullard, M., Catiul, C., Miocinovic, S., & Amara, A. W. (2023). A systematic review of health disparities research in deep brain stimulation surgery for Parkinson's disease. *Frontiers in Human Neuroscience*, *17*, 1269401. https://doi.org/10.3389/fnhum.2023.1269401

Meyer, P., Lintingre, P.-F., Pesquer, L., Poussange, N., Silvestre, A., & Dallaudière, B. (2018). The Median Nerve at the Carpal Tunnel … and Elsewhere. *Journal of the Belgian Society of Radiology*, *102*(1), 17. https://doi.org/10.5334/jbsr.1354

Milosevic, L., Kalia, S. K., Hodaie, M., Lozano, A. M., Popovic, M. R., & Hutchison, W. D. (2018). Physiological mechanisms of thalamic ventral intermediate nucleus stimulation for tremor suppression. *Brain*, *141*(7), 2142–2155. https://doi.org/10.1093/brain/awy139

Mo, J., & Priefer, R. (2021). Medical Devices for Tremor Suppression: Current Status and Future Directions. *Biosensors*, *11*(4). https://doi.org/10.3390/bios11040099

Mohammad, M. E., Vizcarra, J. A., Garcia, X., Patel, S., Margolius, A., Yu, X. X., & Fernandez, H. H. (2021). Impact of behavioral side effects on the management of Parkinson patients treated with dopamine agonists. *Clinical Parkinsonism & Related Disorders*, *4*, 100091. https://doi.org/10.1016/j.prdoa.2021.100091

Moll, C. K. E., & Engel, A. K. (2017). Phase matters: Cancelling pathological tremor by adaptive deep brain stimulation. *Brain : A Journal of Neurology*, *140*(1), 5–8. https://doi.org/10.1093/brain/aww308

Monin, J. K., Gutierrez, J., Kellner, S., Morgan, S., Collins, K., Rohl, B., Migliore, F., Cosentino, S., Huey, E., & Louis, E. D. (2017). Psychological Suffering in Essential Tremor: A Study of Patients and Those Who Are Close to Them.

Tremor and Other Hyperkinetic Movements, *7*(0), 526. https://doi.org/10.5334/tohm.338

Moran, A., Bergman, H., Israel, Z., & Bar-Gad, I. (2008). Subthalamic nucleus functional organization revealed by parkinsonian neuronal oscillations and synchrony. *Brain*, *131*(12), 3395–3409. https://doi.org/10.1093/brain/awn270

Nowacki, A., Zhang, D., Wermelinger, J., Abel Alvarez Abut, P., Rosner, J., Pollo, C., & Seidel, K. (2023). Directional recordings of somatosensory evoked potentials from the sensory thalamus in chronic poststroke pain patients. *Clinical Neurophysiology*, *151*, 50–58. https://doi.org/10.1016/j.clinph.2023.03.359

Obeso, J. A., Marin, C., Rodriguez-Oroz, C., Blesa, J., Benitez-Temiño, B., Mena-Segovia, J., Rodríguez, M., & Olanow, C. W. (2009). The basal ganglia in Parkinson's disease: Current concepts and unexplained observations. *Annals of Neurology*, *64*(S2), S30–S46. https://doi.org/10.1002/ana.21481

Obeso, J. A., Stamelou, M., Goetz, C. G., Poewe, W., Lang, A. E., Weintraub, D., Burn, D., Halliday, G. M., Bezard, E., Przedborski, S., Lehericy, S., Brooks, D. J., Rothwell, J. C., Hallett, M., DeLong, M. R., Marras, C., Tanner, C. M., Ross, G. W., Langston, J. W., … Stoessl, A. J. (2017). Past, present, and future of Parkinson's disease: A special essay on the 200th Anniversary of the Shaking Palsy. *Movement Disorders*, *32*(9), 1264–1310. https://doi.org/10.1002/mds.27115

Ohye, C., & Narabayashi, H. (1979). Physiological study of presumed ventralis intermedius neurons in the human thalamus. *Journal of Neurosurgery*, *50*(3), 290–297. https://doi.org/10.3171/jns.1979.50.3.0290

Okwumabua, E., Black, A. C., & Thompson, J. H. (2023). Anatomy, Shoulder and Upper Limb, Nerves. In *StatPearls*. StatPearls Publishing. http://www.ncbi.nlm.nih.gov/books/NBK526056/

Ondo, W. (2016). Essential tremor: What we can learn from current pharmacotherapy. *Tremor and Other Hyperkinetic Movements*, *6*, 356. https://doi.org/10.7916/D8K35TC3

O'Suilleabhain, P., Berry, D. S., Lundervold, D. A., Turner, T. H., Tovar, M., & Louis, E. D. (2023). Stigma and Social Avoidance in Adults with Essential Tremor. *Movement Disorders Clinical Practice*, *10*(9), 1317–1323. https://doi.org/10.1002/mdc3.13774

O'Suilleabhain, P. E., & Matsumoto, J. Y. (1998). Time-frequency analysis of tremors. *Brain*, *121*(11), 2127–2134. https://doi.org/10.1093/brain/121.11.2127

Pacheco, A., Van Schaik, T. A., Paleyes, N., Blacutt, M., Vega, J., Schreier, A. R., Zhang, H., Macpherson, C., Desai, R., Jancke, G., & Quinn, L. (2023). A Wearable Vibratory Device (The Emma Watch) to Address Action Tremor in Parkinson Disease: Pilot Feasibility Study. *JMIR Biomedical Engineering*, *8*, e40433. https://doi.org/10.2196/40433

Paff, M., Boutet, A., Germann, J., Elias, G. J. B., Chow, C. T., Loh, A., Kucharczyk, W., Fasano, A., Schwartz, M. L., & Lozano, A. M. (2021). Focused Ultrasound Thalamotomy Sensory Side Effects Follow the Thalamic Structural Homunculus. *Neurology Clinical Practice*, *11*(4). https://doi.org/10.1212/CPJ.0000000000001013

Pahwa, R., Dhall, R., Ostrem, J., Gwinn, R., Lyons, K., Ro, S., Dietiker, C., Luthra, N., Chidester, P., Hamner, S., Ross, E., & Delp, S. (2019). An Acute Randomized Controlled Trial of Noninvasive Peripheral Nerve Stimulation in Essential Tremor. *Neuromodulation*, *22*(5), 537–545. https://doi.org/10.1111/ner.12930

Pascual-Valdunciel, A., Hoo, G. W., Avrillon, S., Barroso, F. O., Goldman, J. G., Hernandez-Pavon, J. C., & Pons, J. L. (2021). Peripheral electrical stimulation to reduce pathological tremor: A review. *Journal of NeuroEngineering and Rehabilitation*, *18*(1), 1–19. https://doi.org/10.1186/s12984-021-00811-9

Pavlov, D. V., & Petrov, M. N. (2020). Investigation and identification of the spectral composition of noise in the accelerometer channel of the navigation module. *Journal of Physics: Conference Series*, *1658*(1), 012035. https://doi.org/10.1088/1742-6596/1658/1/012035

Paz, R. M., & Murer, M. G. (2021). Mechanisms of Antiparkinsonian Anticholinergic Therapy Revisited. *Neuroscience*, *467*, 201–217. https://doi.org/10.1016/j.neuroscience.2021.05.026

Pedrosa, D. J., Reck, C., Florin, E., Pauls, K. A. M., Maarouf, M., Wojtecki, L., Dafsari, H. S., Sturm, V., Schnitzler, A., Fink, G. R., & Timmermann, L. (2012). Essential tremor and tremor in Parkinson's disease are associated with distinct "tremor clusters" in the ventral thalamus. *Experimental Neurology*, *237*(2), 435–443. https://doi.org/10.1016/j.expneurol.2012.07.002

Peles, O., Werner-Reiss, U., Bergman, H., Israel, Z., & Vaadia, E. (2020). Phase-Specific Microstimulation Differentially Modulates Beta Oscillations and Affects Behavior. *Cell Reports*, *30*(8), 2555-2566.e3. https://doi.org/10.1016/j.celrep.2020.02.005

Perry, V. L., & Lenz, F. A. (1998). Ablative Therapy for Movement Disorders. *Neurosurgery Clinics of North America*, *9*(2), 317–324. https://doi.org/10.1016/S1042-3680(18)30267-5

Poewe, W., Seppi, K., Tanner, C. M., Halliday, G. M., Brundin, P., Volkmann, J., Schrag, A. E., & Lang, A. E. (2017). Parkinson disease. *Nature Reviews Disease Primers*, *3*, 1–21. https://doi.org/10.1038/nrdp.2017.13

Pollak, P. (2013). Deep brain stimulation for Parkinson's disease—Patient selection. In *Handbook of Clinical Neurology* (Vol. 116). Elsevier B.V. https://doi.org/10.1016/B978-0-444-53497-2.00009-7

Prochazka, A., Elek, J., & Javidan, M. (1992). Attenuation of pathological tremors by functional electrical stimulation I: Method. *Annals of Biomedical Engineering*, *20*(2), 205–224. https://doi.org/10.1007/BF02368521

Raethjen, J., Lindemann, M., Schmaljohann, H., Wenzelburger, R., Pfister, G., & Deuschl, G. (2000). Multiple oscillators are causing parkinsonian and essential tremor. *Movement Disorders*, *15*(1), 84–94. https://doi.org/10.1002/1531-8257(200001)15:1<84::AID-MDS1014>3.0.CO;2-K

Rascol, O., Fabbri, M., & Poewe, W. (2021). Amantadine in the treatment of Parkinson's disease and other movement disorders. *The Lancet Neurology*, *20*(12), 1048–1056. https://doi.org/10.1016/S1474-4422(21)00249-0

Reck, C., Florin, E., Wojtecki, L., Krause, H., Groiss, S., Voges, J., Maarouf, M., Sturm, V., Schnitzler, A., & Timmermann, L. (2009). Characterisation of tremor-associated local field potentials in the subthalamic nucleus in Parkinson's disease. *European Journal of Neuroscience*, *29*(3), 599–612. https://doi.org/10.1111/j.1460-9568.2008.06597.x

Reis, C., Arruda, B. S., Pogosyan, A., Brown, P., & Cagnan, H. (2021). Essential tremor amplitude modulation by median nerve stimulation. *Scientific Reports*, *11*(1), 1–10. https://doi.org/10.1038/s41598-021-96660-6

Riboldi, G. M., Russo, M. J., Pan, L., Watkins, K., & Kang, U. J. (2022). Dysautonomia and REM sleep behavior disorder contributions to progression of Parkinson's disease phenotypes. *Npj Parkinson's Disease*, *8*(1), 110. https://doi.org/10.1038/s41531-022-00373-0

Rodger J., E. (2005). Gravitational artifact in accelerometric measurements of tremor. *Clinical Neurophysiology*, *116*(7), 1638–1643. https://doi.org/10.1016/j.clinph.2005.03.014

Rodriguez-Oroz, M. C., Jahanshahi, M., Krack, P., Litvan, I., Macias, R., Bezard, E., & Obeso, J. A. (2009). Initial clinical manifestations of Parkinson's disease: Features and pathophysiological mechanisms. *The Lancet Neurology*, *8*(12), 1128–1139. https://doi.org/10.1016/S1474-4422(09)70293-5

Romanelli, P., Heit, G., Hill, B. C., Kraus, A., Hastie, T., & Brontë-Stewart, H. M. (2004). Microelectrode recording revealing a somatotopic body map in the subthalamic nucleus in humans with Parkinson disease. *Journal of Neurosurgery*, *100*(4), 611–618. https://doi.org/10.3171/jns.2004.100.4.0611

Rousseeuw, P. J. (1987). Silhouettes: A graphical aid to the interpretation and validation of cluster analysis. *Journal of Computational and Applied Mathematics*, *20*(C), 53–65. https://doi.org/10.1016/0377-0427(87)90125-7

Sabari, J., Stefanov, D. G., Chan, J., Goed, L., & Starr, J. (2019). Adapted Feeding Utensils for People With Parkinson's-Related or Essential Tremor. *The American Journal of Occupational Therapy*, *73*(2), 7302205120p1-7302205120p9. https://doi.org/10.5014/ajot.2019.030759

Saifee, T. A., Edwards, M. J., Kassavetis, P., & Gilbertson, T. (2016). Estimation of the phase response curve from Parkinsonian tremor. *Journal of Neurophysiology*, *115*(1), 310–323. https://doi.org/10.1152/jn.00216.2015

Schapira, A. H. V. (2011). Monoamine Oxidase B Inhibitors for the Treatment of Parkinson's Disease: A Review of Symptomatic and Potential Disease-Modifying Effects. *CNS Drugs*, *25*(12), 1061–1071. https://doi.org/10.2165/11596310-000000000-00000

Schreglmann, S. R., Wang, D., Peach, R. L., Li, J., Zhang, X., Latorre, A., Rhodes, E., Panella, E., Cassara, A. M., Boyden, E. S., Barahona, M., Santaniello, S., Rothwell, J., Bhatia, K. P., & Grossman, N. (2021). Non-invasive suppression of essential tremor via phase-locked disruption of its temporal coherence. *Nature Communications*, *12*(1), 363. https://doi.org/10.1038/s41467-020-20581-7

Shalash, A. S., Hamid, E., Elrassas, H., Bahbah, E. I., Mansour, A. H., Mohamed, H., & Elbalkimy, M. (2021). Non-motor symptoms in essential tremor, akinetic rigid and tremor-dominant subtypes of Parkinson's disease. *PLOS ONE*, *16*(1), e0245918. https://doi.org/10.1371/journal.pone.0245918

Soulat, H., Stephen, E. P., Beck, A. M., & Purdon, P. L. (2022). State space methods for phase amplitude coupling analysis. *Scientific Reports*, *12*(1). https://doi.org/10.1038/s41598-022-18475-3

Stowe, R., Ives, N., Clarke, C. E., Van Hilten, Ferreira, J., Hawker, R. J., Shah, L., Wheatley, K., & Gray, R. (2008). Dopamine agonist therapy in early Parkinson's disease.

Cochrane Database of Systematic Reviews. https://doi.org/10.1002/14651858.CD006564.pub2

Stroupe, K. T., Weaver, F. M., Cao, L., Ippolito, D., Barton, B. R., Burnett-Zeigler, I. E., Holloway, R. G., Vickrey, B. G., Simuni, T., & Follett, K. A. (2014). Cost of deep brain stimulation for the treatment of Parkinson's disease by surgical stimulation sites. *Movement Disorders*, *29*(13), 1666–1674. https://doi.org/10.1002/mds.26029

Tambasco, N., Romoli, M., & Calabresi, P. (2018). Levodopa in Parkinson's Disease: Current Status and Future Developments. *Current Neuropharmacology*, *16*(8), 1239–1252. https://doi.org/10.2174/1570159X15666170510143821

Theodosopoulos, P. V., Marks, W. J., Christine, C., & Starr, P. A. (2003). Locations of movement-related cells in the human subthalamic nucleus in Parkinson's disease. *Movement Disorders*, *18*(7), 791–798. https://doi.org/10.1002/mds.10446

Timmermann, L., Gross, J., Dirks, M., Volkmann, J., Freund, H. J., & Schnitzler, A. (2003). The cerebral oscillatory network of parkinsonian resting tremor. *Brain*, *126*(1), 199–212. https://doi.org/10.1093/brain/awg022

Turcano, P., Mielke, M. M., Bower, J. H., Parisi, J. E., Cutsforth-Gregory, J. K., Ahlskog, J. E., & Savica, R. (2018). Levodopa-induced dyskinesia in Parkinson disease: A population-based cohort study. *Neurology*, *91*(24). https://doi.org/10.1212/WNL.0000000000006643

Vaillancourt, D. E., & Newell, K. M. (2000). The dynamics of resting and postural tremor in Parkinson's disease. *Clinical Neurophysiology*, *111*(11), 2046–2056. https://doi.org/10.1016/S1388-2457(00)00467-3

Vitek, J. L., Ashe, J., & Kaneoke, Y. (1994). Spontaneous neuronal activity in the motor thalamus: Alteration in pattern and rate in parkinsonism. *Soc. Neurosci. Abstr.*, *20*, 1498–1513.

Wodeyar, A., Schatza, M., Widge, A. S., Eden, U. T., & Kramer, M. A. (2021). A state space modeling approach to real-time phase estimation. *eLife*, *10*, 1–28. https://doi.org/10.7554/eLife.68803

Wynter, S., & Dissabandara, L. (2018). A comprehensive review of motor innervation of the hand: Variations and clinical significance. *Surgical and Radiologic Anatomy*, *40*(3), 259–269. https://doi.org/10.1007/s00276-017-1898-8

Yamada, K., Takahashi, S., Karube, F., Fujiyama, F., Kobayashi, K., Nishi, A., & Momiyama, T. (2016). Neuronal circuits and physiological roles of the basal

ganglia in terms of transmitters, receptors and related disorders. *The Journal of Physiological Sciences*, *66*(6), 435–446. https://doi.org/10.1007/s12576-016-0445-4

Zhang, C., Ramirez-Zamora, A., Meng, F., Lin, Z., Lai, Y., Li, D., Chang, J., Morishita, T., Inoue, T., Fujioka, S., Oyama, G., Coyne, T., Voon, V., Doshi, P. K., Wu, Y., Liu, J., Patel, B., Almeida, L., Wagle Shukla, A. A., … Okun, M. S. (2020). An International Survey of Deep Brain Stimulation Utilization in Asia and Oceania: The DBS Think Tank East. *Frontiers in Human Neuroscience*, *14*, 162. https://doi.org/10.3389/fnhum.2020.00162

Zrenner, C., Desideri, D., Belardinelli, P., & Ziemann, U. (2018). Real-time EEG-defined excitability states determine efficacy of TMS-induced plasticity in human motor cortex. *Brain Stimulation*, *11*(2), 374–389. https://doi.org/10.1016/j.brs.2017.11.016

Zrenner, C., Galevska, D., Nieminen, J. O., Baur, D., Stefanou, M. I., & Ziemann, U. (2020). The shaky ground truth of real-time phase estimation. *NeuroImage*, *214*. https://doi.org/10.1016/j.neuroimage.2020.116761

Appendix

A.1. Pilot study's supplementary information

A.1.1. Supplementary methods

Tremor oscillation patterns

To determine tremor oscillation patterns (TOPs), principal component analysis (PCA) was applied to the triaxial accelerometer signals from both without stimulation and during peripheral nerve stimulation conditions after signals were divided into 5-second segments. For the peripheral nerve stimulation condition, 5-second segments corresponded to instances when stimulation was delivered at one of the 12 specific phases. For the without stimulation condition, 5-second segments corresponded to consecutive time segments without overlap.

Tremor oscillation patterns and phase-amplitude profiles

To determine whether stimulation delivered at a certain phase of limb acceleration significantly modulated tremor, we compared the change in tremor severity during peripheral nerve stimulation to spontaneous changes in tremor severity during the without stimulation condition. To this end, 50,000 5-second segments were drawn from the without stimulation condition. These segments were used to create a surrogate distribution for changes in tremor severity during the without stimulation condition. As for the peripheral nerve stimulation condition, the change in tremor severity was defined as the difference between the average tremor severity during the last 1 second of the segment (i.e. 4 to 5 seconds) and that during the 1 second prior to segment onset (i.e. -1 to 0 seconds), divided by the average tremor

severity during the 1 second prior to segment onset. It should be noted that some of these segments could partially overlap in time.

In order to determine the interaction between TOPs and phase-amplitude profiles, 5-second segments from the without stimulation condition, which were used to form the surrogate distribution, were concatenated with 5-second segments from the peripheral nerve stimulation condition and subjected to cluster analysis as outlined in *Section 2.2—Materials and Methods*, allowing us to split the surrogate distribution according to TOPs and to compare phase-amplitude profiles from each TOP to a surrogate distribution derived from the same cluster.

A.1.2. Supplementary results

TOPs reflected contributions (i.e. coefficients) of each tremor axis to the first principal component. The median percentage of the total variance that was explained by the first principal component was 91.6 ± 4.8% (mean ± SD) across 5-second epochs derived from the without stimulation condition. In six out of 10 participants, the first principal component accounted for a median of at least 90% of the total variance.

By also taking the second principal component in the remaining four participants, we ensured that over 90% of the total variance of the tremor was captured in every participant. In these four participants, the second component explained 12.2 ± 1.9% (mean ± SD) of the total variance.

Eliminating any clusters which contained less than 10% of the total number of segments from the phase-locked stimulation condition, five out of 10 participants exhibited two clusters in the first principal component. Four participants exhibited two additional clusters in the second principal component resulting in 23 clusters in total.

These clusters were well separated, with a mean Silhouette score of 0.80 ± 0.16 (mean ± SD), and the optimal number of clusters being equal to two for each considered principal component.

	1st principal component						**2nd principal component**					
	Cluster 1			**Cluster 2**			**Cluster 1**			**Cluster 2**		
Participant	X	Y	Z	X	Y	Z	X	Y	Z	X	Y	Z
1	-	-	-	*			-	-	-	-	-	-
2	*			270	240	240	*			*		
3	-	-	-	-	-	-	*			*		
4	*			-	-	-	*			*		
5	-	-	-	-	-	-	-	-	-	-	-	-
6	-	-	-	*			*			*		
7	*			-	-	30	-	-	-	-	-	-
8	330	-	-	120	120	180	*			*		
9	-	-	-	-	-	90	*			*		
10	-	-	-	-	-	270	0	-	-	-	-	270

Table A.1: Phase bins (in degrees) in which significant tremor suppression occurred for each phase-amplitude profile*. Phase amplitude profiles were generated for each study participant, principal component, cluster, and tremor axis. Note that (*) indicates that the corresponding cluster or principal component was not considered in the analysis for that study participant, and (-) indicates that the corresponding cluster or principal component was considered for the analysis, but there was no significant tremor suppression for that phase amplitude profile.*

	1st principal component						2nd principal component					
	Cluster 1			Cluster 2			Cluster 1			Cluster 2		
Participant	X	Y	Z	X	Y	Z	X	Y	Z	X	Y	Z
1	-	-	-	*			-	-	-	-	-	30
2	*			-	-	-	*			*		
3	-	-	-	-	-	-	*			*		
4	*			-	-	-	*			*		
5	-	-	-	-	-	-	-	-	-	-	-	-
6	-	-	150	*			*			*		
7	*			270	90 270	330	330	-	-	-	-	-
8	30 60 120	-	-	30	-	30 150	*			*		
9	30	-	-	-	-	210	*			*		
10	-	-	-	-	-	-	-	60	-	-	-	-

Table A.2: Phase bins (in degrees) in which significant tremor amplification occurred for each phase-amplitude profile*. Phase amplitude profiles were generated for each study participant, principal component, cluster, and tremor axis. Note that (*) indicates that the*

corresponding cluster or principal component was not considered in the analysis for that study participant, and (-) indicates that the corresponding cluster or principal component was considered for the analysis, but there was no significant tremor amplification for that phase amplitude profile.

A.2. Wrist worn system's envelope characterisation

To characterise the filter response of the online envelope approximation, which estimates tremor severity changes onboard, and to compare it with an offline envelope calculation, we conducted a test recording using the wrist-worn system. This recording included approximately 10 seconds of no movement, followed by 30 seconds of oscillations, simulating Parkinsonian tremor movements predominantly perpendicular to the hand dorsum. The system was attached to an experimenter's wrist during these movements.

Figure A.1 depicts the filter response from this test. It shows the raw, unfiltered z-axis signals, the same signals after applying a band-pass filter in MATLAB (second-order Butterworth filter at ±2 Hz around a centre frequency of 4 Hz, using the causal 'filter' function), and the envelopes generated by both the Hilbert transform and the on-board computation of these band-pass filtered signals. Notably, the changes in the envelopes from both Hilbert and on-board calculations occur almost simultaneously, with a minor difference of about 0.23 seconds in their falling times. The falling time was defined as the duration required for the envelope to settle at a new steady state level after a sudden decrease, such as returning to zero once oscillations cease. While the on-board envelope calculation is not identical to the gold-standard Hilbert transform, it serves as a useful and similar approximation.

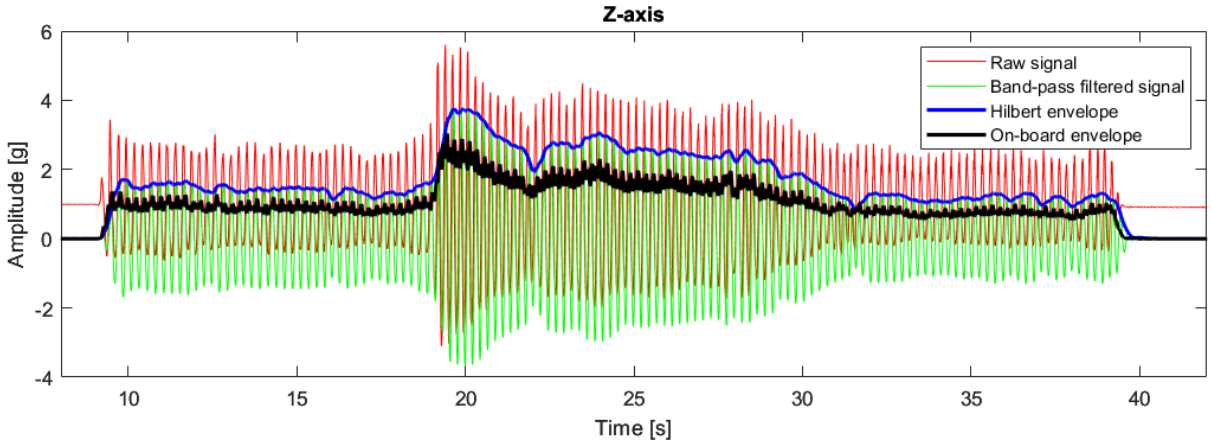


Figure A.1: On-board envelope comparison. *Example filter response, showing the raw tremor signal, band-pass filtered signal on MATLAB, Hilbert-generated envelope, and on-board computed envelope.*

A.3. Wrist-worn system's user interface

The instructions below provide details on how to navigate the wrist worn device's user interface:

(i) To start the random search stage, the experimenter must press Switch 1 for at least 5 seconds. While the switch is pressed, the LED shines blue. If the button press has occurred for at least 5 seconds, the LED shines green, continuously, for 5 seconds. The baseline recording then starts after the green LED turns off. If the memory card is empty, the baseline is 10-minute long (new recording). Otherwise, the baseline is 1-minute long (resumed recording).

(ii) To stop the recording, the experimenter must press Switch 2 for at least 5 seconds. While the switch is pressed, the LED shines red. If the button press has

occurred for at least 5 seconds, the LED shines green, continuously, for 5 seconds. The recording stops after the green LED turns off.

(iii) To resume the recording in the random search stage, the procedure is the same as in (i).

(iv) To start the constant stimulation stage, the experimenter must press Switch 2 for 5 seconds after the recording has already been stopped. While the switch is pressed, the LED shines red. If the button press has occurred for at least 5 seconds, the LED shines green, flashing, for 5 seconds. The recording starts after the green LED turns off.

(v) To access the CLI, after the recording has already been stopped, the experimenter must connect a micro-USB cable to the device and a computer, and open a program such as Putty to interact with the CLI. They must then press Switch 1 and 2 together for at least 5 seconds. While the switches are pressed, the LED shines green. If the button presses have occurred for at least 5 seconds, the LED shines green, flashing, for 5 seconds. The CLI opens after the green LED turns off.

Once the CLI is open, the experimenter can type the following commands:

(i) HELP: to see a list of commands.

(ii) READ: to retrieve the data recorded to the memory card.

(iii) ERASE: to permanently delete all the data from the memory card.

(iv) EXIT: to exit the CLI.

All the information in the CLI can be saved as a '.txt' file, including the data retrieved from the memory card, and then used for subsequent analysis.